Flotation of a UG2 Ore in a Novel Pneumo-mechanical Laboratory Cell

by

Nardus Uys

Thesis presented in partial fulfilment

of the requirements for the Degree

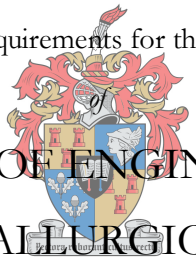

MASTER OF ENGINEERING

(EXTRACTIVE METALLURGICAL ENGINEERING)

in the Faculty of Engineering

at Stellenbosch University

Supervisor
A.J. Burger

March 2018

Declaration

By submitting this thesis electronically, I declare that the entirety of the work contained therein is my own original work, that I am the sole author thereof (save to the extent explicitly otherwise stated), that reproduction and publication thereof by Stellenbosch University will not infringe any third party rights and that I have not previously in its entirety or in part submitted it for obtaining any qualification.

Date: March 2018

Confidentiality

This research project has been executed under a non-disclosure agreement with a mining company and in consultation with the consulting metallurgist of the company.

Abstract

Flotation is regarded as one of the most significant primary separation techniques in the minerals processing industry and most platinum-bearing minerals are separated from their related gangue minerals through froth flotation. The selectivity of the flotation process is influenced by many factors, amongst others, the degree of liberation of the valuable minerals and the size of the particles in the feed slurry. For a specific flotation system – and with all else being equal – the selectivity of the process drops notably below a certain particle size (e.g. 15 μm) due to decreasing efficiencies of particle-bubble attachment and increasing levels of gangue entrainment.

Against this background, conventional mechanically-agitated flotation machines are generally used in the PGM industry, where they are operated to deliver relatively high energy input and high aeration rates. In search of more efficient flotation devices for this industry, a unique flotation machine was designed, built and evaluated in collaboration with a consultant from the PGM industry. In an attempt to achieve both higher valuable mineral recovery and higher concentrate grade, especially in the finer size ranges, the specific design combined the following principles:

- high energy intensity at consecutive (in series) particle-bubble attachment points;
- release of loaded bubbles to a non-agitated calming zone for froth separation.

As such, the flotation unit contained a down-comer (similar to a Jameson Cell™), which was fitted with three internal impellers and subsequent exit ports for the sequential release of aerated slurry. This agitated down-comer represented the high-energy intensity zone for proper particle-bubble attachment, while the outer calming zone provided a non-agitated froth separation environment. The idea behind the sequential release of intensely air-contacted slurry was to establish a concentration gradient within the outer cell in an attempt to improve the concentrate grade at minimal loss of recovery.

The first objective of this study was to utilize the extensive knowledge and know-how captured in literature to design and build a pneumatic flotation cell that enables:

a) multi-stage energy input during aeration for improved overall particle-bubble attachment, in an attempt to maximise recovery;
b) systematic, multi-stage release of the aerated pulp into a non-agitated calming zone for froth separation, in an attempt to maximise grade while minimising recovery losses.

The second objective of this study was to perform a preliminary evaluation of the flotation device, with PGM ore as feed, by characterising the cell's performance in terms of the most prominent

hydrodynamic parameters, such as superficial air velocity, energy input and cell superficial slurry velocity.

These objectives were achieved by answering the following key questions:

- What are the key features of a flotation cell that could potentially produce PGM concentrates with higher grades and similar recoveries than the mechanical cells currently in use?
- How is the flotation efficiency of the newly designed cell (as constructed for this project) typically affected by prominent hydrodynamic parameters such as aeration rate, energy input and recycling rate?
- How does this newly designed cell typically perform with regards to recovery, grade and Cr_2O_3 rejection, compared to mechanical flotation machines used in the PGM industry?

The cell was operated in batch-like mode, with tailings being recycled to simulate multiples of these flotation cells in series. This also enabled some comparison of the test results with flotation data generated in a conventional, mechanically-agitated, laboratory batch flotation cell at an operating PGM flotation plant.

Chemical dosing (*i.e.* activator, collector and frother) and related conditioning times were in accordance to prescriptions from the consultant and similar to recipes used on the PGM plant. A notable difference from the operation at the PGM plant was that low-TDS reverse osmosis permeate was used to prepare the flotation slurry for test work. The operating conditions were: cell superficial slurry velocity (1.8-2.6 cm/s), superficial air velocity (0.8-1.2 cm/s) and mixing intensity (680-1277 rpm in a 36 mm down-comer). The froth depth was maintained at 10 mm and scraping occurred at 8 second intervals.

Within this range of operating conditions and under continuous recycle, promising results could be obtained, similar to batch flotation results from the PGM plant. In a typical run with a high overall 4-element (4E) recovery of 80.8%, the cell produced an overall 4E grade of 76.4 g/t. When the system was operated to improve grade, an overall 4E recovery of 72.6% was achieved at a very high 4E grade of 153.6 g/t. Both these runs produced good chromite rejection.

Opsomming

Flottasie is een van die belangrikste primêre skeidingstegnieke in die mineraalproseseringsbedryf, waar die meerderheid platinum-groep minerale deur middel van skuimflottasie gekonsentreer word. Die selektiwiteit van die flottasieproses word deur 'n menigte faktore bepaal, insluitend die graad van waardevolle mineraal-vrystelling en die partikelgrootte in die voerstroom. Vir 'n spesifieke flottasiesisteem waar alle ander faktore konstant gehou word, verlaag die skeidingseffektiwiteit beduidend wanneer die partikelgrootte kleiner as 'n spesifieke grootte is (bv. 15 μm). Dit volg weens verlaagde partikel-borrel bindingseffektiwiteit en verhoogde slykoordag na die konsentraat.

Teen hierdie agtergrond word hoofsaaklik meganies-aangedrewe flottasieselle in die PGM industrie gebruik waar dit bedryf word met hoë energie insette asook hoë belugtingstempos. In 'n soeke na beter effektiwiteit is 'n unieke flottasiesel ontwerp, gebou en getoets in samewerking met 'n raadgewer vanuit die PGM industrie. Om graad en herwinning te probeer verhoog in spesifiek die kleiner partikelgrootte fraksies, is die volgende eienskappe in die ontwerp vasgevang:

- hoë energie insette by veelvuldige (daaropvolgende) partikel-borrel hegtingspunte;
- vrystelling van gelaaide borrels na 'n nie-gemengde kalm sone vir skuimskeiding.

As sodanig het die flottasiesel 'n afvoerpyp bevat (soortgelyk tot die Jameson Cell™), wat drie inwendige stuwers ingesluit het, met daaropvolgende openinge vir die vrystelling van belugte flodder. Hierdie afvoerpyp met sy stuwers het die hoë-energie gebied verteenwoordig waar effektiewe partikel-borrel hegting kon plaasvind, terwyl die buitenste rustige sone 'n nie-gemengde omgewing verskaf het vir skuimskeiding. Die idee agter die opeenvolgende vrystelling van hoë-intensiteit belugte flodder was om 'n konsentrasiegradiënt te skep in die buitenste rustige sone van die sel in 'n poging om die konsentraat graad te verhoog met minimale verlies aan herwinning.

Die eerste doel van hierdie studie was om die uitgebreide kennis vanuit literatuur te benut vir die ontwerp en bou van 'n pneumatiese flottasiesel wat:

a) veelvuldige energie insette moontlik maak tydens belugting vir verbeterde partikel-borrel binding, in 'n poging om herwinning te verbeter;
b) sistematiese, veelvuldige vrystelling van die belugte flodder na 'n kalm sone te bewerkstellig vir ongesteurde skuimskeiding, in 'n poging om graad te verbeter met minimale verlies aan herwinning.

Die tweede doel van hierdie studie was om 'n voorlopige evaluasie van die flottasiesel te doen deur PGM erts te gebruik as voer, waar die sel se gedrag teen die mees prominente hidrodinamiese eienskappe, soos energie inset sowel as oppervlakkige lug- en flodderspoed, getoets word.

Hierdie doelwitte is bereik deur die volgende sleutel-vrae te beantwoord:

- Wat is die kenmerkende eienskappe van 'n flottasiesel wat potensieel 'n PGM konsentraat kan lewer met hoër graad en soortgelyke herwinnings as met die meganies-gedrewe flottasieselle wat tans gebruik word?
- Hoe word die flottasie-effektiwiteit van die nuut-ontwerpte flottasiesel (soos gebou vir hierdie projek) tipies beïnvloed deur prominente hidrodinamiese faktore soos belugtings-tempo, energie inset en sirkulasietempo?
- Hoe presteer hierdie nuwe flottasiesel met betrekking tot herwinning, graad en Cr_2O_3 verwerping in vergelyking met die meganies-aangedrewe flottasieselle tans in gebruik in die PGM bedryf?

Die sel is bedryf volgens 'n enkelsel benadering, waar die uitskot terug gesirkuleer word na die voer en slegs die konsentraat verwyder word. Dit het dit moontlik gemaak om die resultate van hierdie stel toetse te vergelyk met bedryfsresultate van konvensionele meganies-aangedrewe laboratoriumselle, soos verkry vanaf 'n operasionele PGM flottasie aanleg.

Die dosering van chemikalieë (bv. aktiveerder, skuimmiddel en versamelaar) en die gepaardgaande kondisioneringstye is toegepas volgens die aanwysings van die konsultant en was soortgelyk aan resepte wat gebruik is op die PGM aanleg. 'n Verskil tussen hierdie toetse en dié vanaf die PGM aanleg was dat hierdie toetse gedoen is met tru-osmose water met lae totale opgeloste soute. Die bedryfstoestande was soos volg: sel oppervlakkige flodderspoed (1.8-2.6 cm/s), oppervlakkige lugspoed (0.8-1.2 cm/s) en mengtempo (680-1277 o.p.m. in 'n 36mm afvoerpyp). Die skuimdiepte is by 10 mm gehandhaaf en die skuim is elke 8 sekondes afgeskraap.

Met hierdie verskeidenheid beheertoestande en met aanhoudende hersirkulasie is belowende resultate verkry, soortgelyk aan enkelsel resultate vanaf die PGM aanleg. In 'n tipiese lopie met 'n algehele hoë 4-element (4E) herwinning van 80.8%, het die flottasiesel 'n algehele 4E graad van 76.4g/t geproduseer. Wanneer die sel bedryf is onder toestande om graad te verhoog, kon 72.6% van alle 4E minerale herwin word teen 'n baie hoë algehele 4E graad van 153.6 g/t. Beide hierdie lopies het goeie Cr_2O_3 verwerping gelewer.

Table of Contents

List of Tables

Nomenclature

Symbol	Description	Units
C_a	Air capacity number	Dimensionless
C_i	Circulation intensity	1/s
D	Impeller diameter	m
d_b	Bubble diameter	m
d_p	Particle diameter	m
d_s	Sauter-mean bubble diameter	m
Fr	Froude number	Dimensionless
g	Gravitational acceleration constant	m/s^2
J_g	Superficial gas velocity	cm/s
N_P	Power Number	Dimensionless
N_a	Air flow number	Dimensionless
N_{sa}	Specific Air flow	1/s
P	Power consumption	kW
P_s	Specific Power	kW/m^3
Q	Volumetric flow rate	m^3/s
R	Rotational speed of impeller	1/s
Re_b	Bubble Reynolds number	Dimensionless
St	Stokes Number	Dimensionless
S_b	Bubble surface area flux	1/s
U_b	Velocity of bubble	m/s
U_{ts}	Impeller tip speed	m/s
V_c	Volume of cell	m^3
μ_f	Fluid dynamic viscosity	Pa.s
ρ_f	Density of the fluid	kg/m^3
ρ_p	Density of Particle	kg/m^3
τ	Residence time	1/s

Greek Letters

Symbol	Description	Units
μ_f	Dynamic viscosity	Pa.s
ρ	Density	kg/m^3
τ	Residence time	1/s

Subscripts

Symbol	Meaning
a	Refers to air
b	Refers to the bubble
c	Refers to cell
f	Refers to the fluid
g	Refers to gas
P	Refers to power
p	Refers to the particle
s	Sauter-mean average
ts	Refers to impeller tip speed

Acronyms

Acronym	Meaning
4E	Four elements
CFD	Computational fluid dynamics
LRHI	Long-range hydrodynamic interaction
NFG	Natural floating gangue
PGE	Platinum group element
PGM	Platinum group mineral
PSD	Particle size distribution
TDS	Total dissolved solids
UG2	Upper group 2 (ore reef)
VSD	Variable speed drive

Chapter 1 – Introduction

The froth flotation process came in use during the start of the 20th century. Today it is the most widely utilised separation method for minerals (Ata, 2012). Separation of minerals through froth flotation can only be achieved if there is a difference in the hydrophobicity or wettability of the mineral surfaces. Reagents, namely collectors and depressants are used to selectively alter the wettability of different mineral surfaces. This ensures better separation between the different minerals based on the wettability of their surfaces.

Flotation can be direct, where the valuable mineral is hydrophobic, attaches to the air bubbles and reports to the concentrate or float at the top of the cell. Indirect or reverse flotation is used where the undesired mineral is hydrophobic and the valuable mineral hydrophilic. The undesired mineral will then report to the float while the valuable mineral will report to the underflow of the flotation device. Direct flotation is preferred as the valuable minerals are generally the lower concentration mineral in the ore body. This means that less reagents and energy are required to separate the valuable minerals from the gangue. This study will only focus on direct froth flotation.

Flotation machines are designed to facilitate the interaction between minerals and air in an aqueous environment. Air is supplied to the system through various methods, namely sparging, induced air, dissolved air, electrolysis of the aqueous medium or cavitation. Sufficient energy is supplied to ensure that hydrophobic minerals can transfer from the aqueous slurry to the bubble surface, either through intensive mixing by impellers, pumping or through jets. Energy requirements vary between different minerals, depending on the particle size, density and affinity to water.

Flotation machines are designed with a specific duty in mind with regard to the type of mineral treated. They are also designed according to a specific duty in the process. These duties mainly are the rougher, scavenger or cleaner duty. The rougher flotation machines receive the fresh feed and some recirculation streams. They need to treat large volumes of material at feed grade of the flotation circuit. Good recovery of valuable minerals needs to be achieved while still achieving an improvement in grade to the concentrate stream. The scavenger flotation machines treat the tailings from the rougher circuit, which means that they need to achieve the highest possible recovery from the lowest grade stream in the whole beneficiation process. The cleaner duty flotation machines treat the concentrate stream from the rougher circuit. The cleaner circuit aims to improve the grade of the concentrate stream for further processing.

Since bubbles are used to transport the valuable minerals, there is an upper limit to the size and weight of the minerals that will stay attached to the bubble through hydrophobic attachment while

overcoming gravitational forces in the flotation machine. As flotation machines work on the differences of surface properties of minerals, the valuable mineral surfaces therefore need to be exposed sufficiently through comminution for effective separation.

Crushing and grinding circuits produce a product stream with varying particle sizes. This makes the flotation process more complex, since differently sized minerals require different operating conditions to be separated effectively. The particle size distribution produced by a grinding circuit depends mostly on the desired mineral grain size within the ore to ensure sufficient exposure of the mineral surface for separation (Pease et al., 2010).

Increasing grinding of minerals will generally increase the amount of fines or slimes produced through the grinding circuit. Higher reagent concentrations have to be used with such increase in slimes, since the finer minerals increase the available surface area for these chemicals to attach to (Rubio et al., 2006, Pease et al., 2010). Interestingly, Pease believes that the current flotation technology is sufficient for effective separation of fines, but that the problem lies with effective separation of feed material according to particle size prior to flotation.

The PGM industry favours mechanically agitated flotation machines that are either self-aerating or forced aerated. These machines are chosen due to their higher energy input to ensure attachment of valuable minerals to air bubbles for effective separation (Deglon et al., 2000). The mechanically agitated flotation machines cannot effectively separate minerals with a wide particle size range as the operating conditions vary between fines and large particles (Pease et al., 2010). This study will attempt to design and test a laboratory mechanical flotation machine that can separate minerals with a wide particle size range.

1.1. Objectives of this Study

Objective 1: By utilising the extensive knowledge and know-how captured in literature, design and build a pneumatic flotation cell that enables:

a) multi-stage energy input during aeration for improved overall particle-bubble attachment, in an attempt to maximise recovery;
b) systematic, multi-stage release of the aerated pulp into a non-agitated calming zone for froth separation, in an attempt to maximise grade while minimising recovery losses.

Objective 2: Perform a preliminary evaluation of the flotation device, with PGM ore as feed, by characterising the cell's performance in terms of the most prominent hydrodynamic parameters, such as superficial air velocity, energy input and cell superficial slurry velocity.

1.2. Key Questions

In order to achieve the objectives, the study focussed on answering the following questions:

- What are the key features of a flotation cell that could potentially produce PGM concentrates with higher grades and similar recoveries than the mechanical cells currently in use?
- How is flotation efficiency of the cell affected by the prominent hydrodynamic parameters such as aeration rate, energy input and recycling rate?
- How does this cell perform with regards to recovery, grade and Cr_2O_3 rejection, compared to mechanical flotation machines used in the PGM industry?

1.3. Scope and Limitations

The focus of this study was on the design and preliminary evaluation of an improved flotation device, with special focus on the hydrodynamics of the system. The particle size distribution in the feed slurry was similar to that of typical PGM flotation circuits, with 75% of the particles being smaller than 75 μm. CFD modelling of the different devices in the cell was not performed. The chemistry of the pulp and froth phases were not optimized, but related information from previous studies and information supplied by a PGM separations plant were used. The preliminary characterization of the device only used UG2 reef mining material.

Ore and slurry preparation (including grinding, chemical dosing and conditioning) were based on information provided by the PGM industry. In several cases, limited information was available due to confidentiality within the platinum industry. Therefore, logical comparisons were made as far as possible where information was absent.

This study did not consider optimization of the new flotation device in terms of operating conditions or reagent suite. However, the cell's performance has been demonstrated within selected operating ranges, providing useful core information for further optimisation.

1.4. Methodology

Valuable information was gathered from literature to increase the understanding of fundamental flotation principles and requirements. Operating conditions of industrial flotation machines were investigated where important parameters, that influence the hydrodynamic environment, were discussed. A pneumo-mechanical flotation cell was designed according to information obtained from consultations with a flotation specialist, as well as from the literature. The design aimed at maintaining high recoveries while improving the concentrate grade. Screening runs were conducted to determine the key factors influencing the performance. Three main factors were

selected where a three level analysis on these factors were performed according to a box-Behnken experimental design. The effect of these factors was discussed according to the concentrate grade and recovery of valuable minerals. Water recovery and chromite rejection were also discussed to improve the understanding of factors influencing the concentrate grade. One of the operating condition sets was further investigated in terms of particle size reporting to the concentrate to determine how the new flotation cell separate according to particle size. Some repetitive runs were conducted to show the repeatability of results. A statistical model was constructed based on the data received from the experiments. An optimum in operating conditions – within the selected range of variables – was identified from the model, which were then compared to results obtained from conventional flotation machines.

Chapter 2 – Literature Review

Flotation works in a three-phase medium, which involves a fluid (in most cases water), a solid (the ore being separated) and a gas phase (usually air). The separation method works on the buoyancy principle; when a mineral particle attaches to the surface of an air bubble and the combined bubble-mineral system becomes less dense than the slurry it is suspended in, the mineral can be removed from the slurry by floating to the top and forming a froth that can be collected. Flotation requires enough energy input to allow the mineral particles to break through the streamlines and surface tension of the fluid surrounding the bubbles and then attach to the bubble. This method also requires selective attachment of minerals to the air bubbles to achieve separation between different minerals. Subsequent to such initial attachment, a stable bubble-particle bond needs to develop, which can float to the top of the slurry where a stable froth layer could be formed in order to remove the attached mineral from the slurry, while effectively draining entrained gangue minerals.

In this section, relevant literature on the mechanism of flotation, as well as the fundamentals of achieving stable particle-bubble attachment, are presented. The effect of ore composition and surface chemistry are briefly discussed in order to understand the potential influences thereof during experimental verification of the new flotation cell. A brief overview of the current equipment used in the industry is also offered, highlighting some of the operating parameters influencing the hydrodynamics of these machines. Lastly the different separating principles for selective recovery of fine minerals are summarised. This information could be used in the design of the new flotation cell.

2.1. Typical Ore Used

The Bushveld complex contains a large percentage of the world's palladium and platinum ore deposits. This complex consists of three different ore bodies, namely the Merensky Reef, Platreef and the Chromitite reef (Cawthorn, 1999). The Chromitite reef is further divided into different layers, namely the Upper Group (UG), Upper Group Two (UG2), Middle Group (MG) and the Lower Group (LG). The ore used in this study is from the UG2 reef and the metals of primary interest in this ore type are platinum, palladium, rhodium, iridium, osmium and ruthenium (Cawthorn, 1999). These are the six PGM metals where platinum and palladium are historically the most abundant and economically sought-after metals. Gold is not considered a PGM, but is present in very low grades in the UG2 reef (Vermaak and Van der Merwe, 1999).

The UG2 ore used in this study originated from a site where the main reef consists of chromite. Minerals that are present within the UG2 layer are feldspathic pyroxenite and different forms of

anorthosite. The PGEs are mainly present in base metal sulphides or occur separately in silicates. Below 12% of the PGEs are enclosed in chromite, which is mainly in the form of laurite (Von Gruenewaldt, 1985).

The UG2 ore used was from the same run-of-mine material used by an existing UG2 flotation circuit. This enabled the results from this study to be compared to the laboratory scale mechanical batch cell results from other studies performed on site at the UG2 flotation circuit.

2.2. Surface Chemistry, Water Quality and Frother

Flotation separates minerals from one another based on the physicochemical surface properties of different minerals in heterogeneous mineral particles. Differences in the physicochemical nature of mineral surfaces could be further enhanced by the addition of reagents. Collector reagents are used to further enhance the hydrophobic nature of specific desired minerals, so that they can attach to air bubbles and float to the top and form a mineralized froth phase that can be collected. Depressant reagents further enhance the hydrophilic nature of the bulk or undesired minerals so that they would not attach to air bubbles and remain in the slurry (Glembotskii and Rabinovich, 1963).

Water quality plays an important role in the chemical environment of the flotation process as different ions in the water influences the functionality of the collector, depressant and frother used. It was found that an increase in ionic strength of the water reduces entrainment per unit water recovered, possibly due to changes in mineral surface charge caused by the increased ionic strength of the water. This reduction in entrainment is overshadowed by the increase in froth stability due to the ionic strength increase of the water. The higher froth stability is believed to be caused by an increase in naturally floatable gangue (NFG) present in the froth phase, causing an increase in mass pull and water recovery to the concentrate (Corin, Reddy et al. 2011).

The higher mass pull causes a decrease in concentrate grade, but higher depressant concentrations can reduce the amount of NFG recovered to the concentrate. Higher depressant dosages reduce the mass pull and water recovery to concentrate and it is believed that this is caused by a reduction in froth stability due to a reduction in the amount of NFG in the froth phase (Deglon et al., 2000, Corin et al., 2011). An increase in ionic strength has different effects on the functionality of depressants, depending on the charge density of the specific depressant (Corin and Wiese, 2014).

Froth stability and PGE recovery can also be improved by increasing the frother concentration (Corin and Wiese, 2014, Wiese et al., 2011). Increasing the frother concentration has the same

decreasing effect on bubble size as the increasing ionic strength of the water (Corin and Wiese, 2014). Froth stability can further be improved by increasing the frother strength, which can be done by increasing the chain length of the frother. Increasing the chain length unfortunately results in a decrease in selectivity of the froth phase (Wiese and Harris, 2012). Frother stability is reduced by increased hydrophobicity of collectors, or the addition of copper sulphate as activator. Copper sulphate addition improves PGE recoveries, but reduces concentrate grade through over-activation of gangue minerals (Wiese et al., 2011).

Changing any reagent in the reagent suite of a flotation cell will result in a change in froth stability, which will affect the PGE recovery and grade of the concentrate (Wiese et al., 2011). The effect of an increase in ionic strength of the feed water on PGE recovery and grade can be mitigated by changing the reagent suite. It is important to note that increased ionic strength will increase mass pull to concentrate, thereby increasing recoveries and reducing concentrate grade. This study does not focus on improving the chemical environment of the flotation process or to optimise the reagent suite for a new flotation cell. The reagent suite used can therefore be further optimized to either increase recovery or concentrate grade for the specific application of the new flotation cell design.

2.3. Flotation Process

There are three distinct process phases in froth flotation, namely the slurry, pulp and the froth phase. The slurry (first phase), consisting of the aqueous medium and minerals, are aerated to form the pulp phase, which can be seen as the second phase. If minerals are attached to air bubbles and they rise to the top of the pulp phase, they then enter the froth phase, which predominantly consists of air, water and hydrophobic particles.

There are hydrodynamic limits to particle size in the froth flotation process. Large particles require larger volume bubbles to attach to, to be buoyant enough to rise to the froth phase. If the hydrodynamic environment is too turbulent, then the larger particles can easily detach from the bubbles, reducing their recovery into the froth phase. As the particle size reduces, the probability of attachment to bubbles lowers and the recovery of these small mineral particles therefore also decreases (Song et al., 2001). The hydrodynamic environment should then be more turbulent to improve the probability of attachment for these small mineral particles to bubbles (Ralston & Dukhin., 1999).

There are also physical limits to particle size in flotation which depends on the density difference between the pulp and the particle-bubble system. If the size of a particle increases, the ratio

between particle mass and its surface area increases. As such, if the particle is too big, the volume of air required to render the particle-bubble system buoyant will not have sufficient particle surface area to attach to the particle and the particle will not be able to rise to the froth phase (Gontijo et al., 2007). Therefore, every type of mineral has a maximum particle size where bubbles can attach to the surface and, when combined, be buoyant in that specific mineral slurry.

There is also a minimum particle size to which selective flotation can be applied (if particle size is too small, separation between different mineral types becomes difficult with froth flotation). As the particle size decreases, the ratio between surface area to volume increases and therefore the ratio between particle mass and surface area decreases. The available surface area of the mineral particle is now large enough to attach to a larger volume of air than required to render the bubble-particle system buoyant. The limitation now shifts to a shortage of available bubble surface area as the bubble surface area quickly gets filled with mineral particles. For example, decreasing the particle size from 37 micron to 7 micron increases the surface area fivefold and triples it again when decreasing to a particle size of 2.5 micron (Pease et al., 2010).

This means that more air is needed since the surface area of the bubbles are filled with attached particles without removing the same mass to concentrate, compared to larger sized particles. However, increasing the air flow too much while keeping other factors constant, leads to slugging; the phenomenon when air flow is so high that it overloads the capability of the impeller to disperse the air into smaller bubbles through the volume of the cell. Slugging negatively affects the froth phase since it deposits gangue minerals in the froth phase. It also disturbs the froth phase and increases detachment of valuable minerals from air bubbles in the froth phase and at the pulp-froth interface.

Bubble size has to be reduced in order to prevent slugging and increase the bubble surface area available for attachment. Therefore, in order to float fines, the bubble size needs to be decreased significantly. Unfortunately the rising velocity decreases as bubble size decreases since the density difference between the pulp and the bubble stays the same, but the ratio between volume and surface increases, which means that the surface friction plays a more prominent role. Rulyov (2008) showed that when bubble size decreases below 50 micron, the rising bubble velocity decreases below 8cm/min. This is significant, since the residence time within flotation cells ranges from 3 minutes for coal to 20 minutes for molybdenum. Micro bubbles should therefore be used with caution in cells with large height to diameter ratios while sufficient turbulence should be provided to ensure sufficient attachment energy of smaller mineral particles to air bubbles.

In order to understand the possibility for selective flotation of finer minerals, the mechanisms by which these particles attach to the bubble surface are investigated.

2.3.1. Bubble-particle Collision

When working with larger particles, their attachment to the bubble surface is due to inertial forces. Here the bubble is carried along within the hydrodynamic environment while the particle is big enough to overcome hydrodynamic drag forces and follows a path obtained by inertial forces when exiting the impeller. This allows contact between a bubble and a particle when the particle cuts across the streamline of the bubble and collides with it.

With a decrease in particle size the mechanism of attachment changes. Here the contact is achieved more by surface forces than inertial forces. For two hydrophobic particles to be joined by surface forces in a hydrodynamic environment, their ionic atmospheres need to overlap. This can only happen when the wetted film between them is thinned to a fraction of a micron. The same phenomenon happens with a particle attaching to a bubble surface.

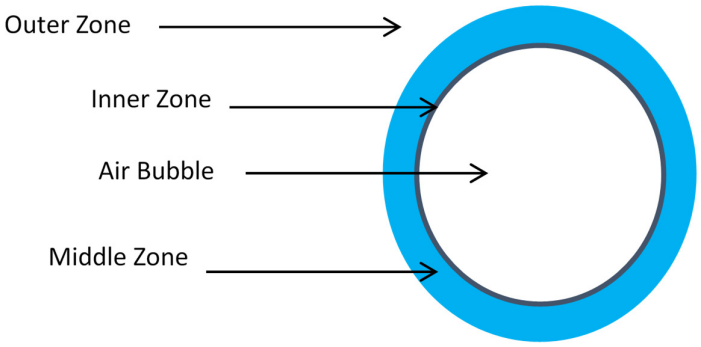

Figure 1: Three zones in the particle-bubble attachment process (Derjaguin and Dukhin, 1993).

The zones around a bubble in a hydrodynamic environment can be separated into three; namely the outer zone, which is the entire liquid body outside the bubble, the middle zone, which is regarded as the diffusion layer and then the inner zone, which is the wetting layer of the bubble surface. For particle attachment to occur, the inner zone needs to be thinned to such an extent that the ionic atmosphere of the mineral particle can attach to the bubble surface. This requires a disjoining action of the liquid layer by the attraction forces between the bubble and the mineral surface as the mineral particle approaches the bubble (Derjaguin and Dukhin, 1993).

When the wetting film is thinned by attraction forces to such an extent that it becomes unstable a contact angle forms between the mineral surface and the liquid-air boundary of the bubble to

ensure a stable attachment of the mineral to the bubble surface (Derjaguin and Dukhin, 1993). This contact angle can be measured to describe the hydrophobicity of mineral surfaces.

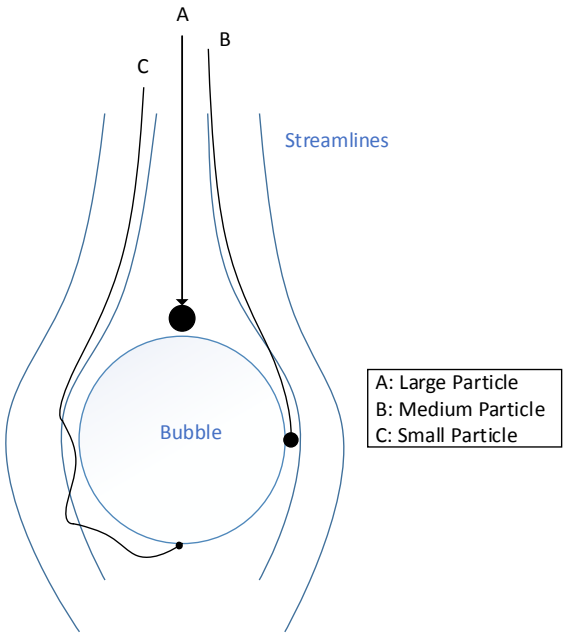

Figure 2: Trajectories of particles and fluid streamlines around a bubble (Ralston et al., 2002).

Attachment cannot occur before the particle is close enough to the bubble for these particle-bubble forces to interact, so that the disjoining action of the inner zone can occur. Figure 2 illustrates the paths different sized minerals follow in order to come close enough to a bubble for attachment to be possible.

There are several forces capable of deviating a mineral particle from the streamlines present in the hydrodynamic environment, including gravitational forces, hydrodynamic drag forces and inertial forces. These forces are more applicable for larger particles, while smaller particles are more influenced by long-range hydrodynamic interaction (LRHI) namely hydrodynamic drag forces and diffusion. This can be seen in Figure 2 where the larger particles deviate from their streamline under inertial forces and follow a near straight collision line towards the bubble. The medium sized particles still follow their streamline, to a certain extent, until the attraction forces, or gravity force diverts it from the streamline and it comes close enough to form an attachment with the bubble. As the particle size decreases, the hydrodynamic drag force becomes larger than the gravitational force and inertial force of the particle, due to the increase in the surface area to volume ratio of the particle. The inertial force and gravitational force will not be able to create attachment to the air bubble. Hydrodynamic interaction forces are the only forces left to create attachment between

the small particle and the air bubble. This means that the smaller particles need to be in a streamline brushing past the surface of the bubble otherwise the attachment is highly unlikely (Ralston et al., 2002).

In order to determine if the particle has enough energy to be able to attach to the bubble surface, the Stokes number needs to be defined. The Stokes number relates the inertial force of the particle to the resistance applied to the particle by the fluid through viscous forces (Ralston et al., 2002).

The Stokes number can be defined as:

$$St = \frac{\rho_p U_b d_p^2}{9 d_b \mu_f} \quad (1)$$

ρ_p: density of the particle,
U_b: velocity of the bubble relative to the fluid,
d_p: diameter of the particle,
d_b: diameter of the bubble and
μ_f: dynamic viscosity of the fluid.

This number shows which forces are dominant to the motion of the bubble rising up through the pulp and the particle moving along the streamlines of the fluid surrounding the bubble. The following information can be obtained from this calculation:

St << 1: The main force acting on the particle is not an inertial force and the particle can be considered to be inertial-free. This means that the particle will not leave the streamline as the streamline bends around the rising bubble.

St≤ 0.1: Inertial forces may be a factor that prevents the particle from attaching to the bubble. Here the inertial forces are so low that the particle may never leave the streamline moving around the bubble.

0.1< St < 1: In this region the collision between the particle and bubble can be described as inelastic. Here the particle loses most of its kinetic energy through the approach to the bubble and the particle only possesses a small amount of energy when the liquid layer between the bubble and particle is formed. Particles are more likely to attach when they fall into this range, making this the most desirable range for the Stokes number in flotation.

St > 3: The inertial forces of the particle with respect to the viscous forces are so large that the particle does not deviate significantly from a straight line. The kinetic energy loss of the particle as

it approaches the bubble is so small that the collision can be considered as a semi-elastic interaction. Here no attachment between the particle and the bubble can be achieved since the particle bounces away from the bubble (Ralston et al., 2002).

The bubble Reynolds number can also be used to determine the type of fluid flow around the bubble. Here only the inertial force of the bubble is compared to the viscous forces of the fluid:

The bubble Reynolds number:

$$Re_b = \frac{u_b \rho_f d_b}{\mu_f} \quad (2)$$

u_b: velocity of the bubble

ρ_f: density of the fluid,

d_b: diameter of the bubble

μ_f: dynamic viscosity of the fluid.

In order to solve the continuity equation (Cengel et al., 2010) for the streamlines around the bubble, either the Stokes flow region or the potential flow conditions should be assumed. The Stokes region exists at bubble Reynolds numbers far less than unity (Schulze, 1992) while the potential flow condition exists at $80 < Re_b < 500$ (Miettinen et al., 2010).

Since flotation generally involves intense mixing with highly turbulent flow processes, it is impossible to solve the continuity equation. It is possible, however, when the Stokes flow region or the potential flow region is assumed. The continuity equation will not be solved here for particle-bubble systems, but the short discussion gives an understanding of the energy requirements of particles to be able to attach to air bubbles.

The froth phase improves the concentrate grade through a few mechanisms, which ultimately result in the rejection of hydrophilic minerals. Discussions on froth phase will be kept to a minimum since characterization of the hydrodynamics within the cell will occur through analysing the concentrate stream. Therefore, the effect of the froth phase has to be minimized in order to really gauge the effect of the hydrodynamic environment on the recovery of valuable minerals as well as rejecting problematic gangue minerals, especially those which contain chrome.

2.3.2 Collision Models for Particle-bubble Attachment

Collision models have been developed in order to better understand the mechanisms involved in the recovery of valuable minerals within froth flotation cells. Many of these models have been

constructed, where different approaches were used in order to quantify recoveries obtained from flotation. Some of these models are listed below:

- The Stokes flow model (Gaudin et al., 1942, Gaudin, 1957)
- Potential flow model (Sutherland, 1948)
- Yoon and Luttrell flow model (Yoon and Luttrell, 1989)
- Generalised Sutherland equation (Dai et al., 1998)
- Rulyov Model (Rulyov, 2001)
- Reay and Ratcliff model (Reay and Ratcliff, 1973, Reay and Ratcliff, 1975)
- Collins model (Collins and Jameson, 1976, Collins and Jameson, 1977)
- Yang et al. model (Yang et al., 1995)
- Nguyen et al. model (Nguyen et al., 2006)

The first five models only consider particle–bubble collision, while the last three include collision as well as attachment. Some also include collision through Brownian diffusion (Miettinen et al., 2010). A new flotation rate model won't be created through this study and therefore existing models won't be discussed extensively.

Favourable flotation cell hydrodynamics are required in order for collision and attachment to occur between particles and bubbles. Flotation cell hydrodynamics are discussed in the next section to obtain a better understanding of the important factors affecting the hydrodynamic environment within a flotation cell.

2.4. Flotation Cell Hydrodynamics

Through the years a significant number of design variations have been made in an attempt to increase the recovery and grade obtained from flotation cells. Some of these designs also incorporate the presence of fines within the slurry, although most flotation machines struggle to achieve their set recovery and grade with the presence of fines. In order to look at these machines, the different bases for comparison should first be defined. These factors are also used for scale up from laboratory scale to the actual size used in the industry, highlighting the important design factors to consider when designing a new cell.

2.4.1. Calculations Used To Compare Different Mechanically Agitated Flotation Devices

The following equations can be used to compare different mechanically agitated cells with one another (Arbiter, 2000, Deglon et al., 2000). Important factors that influence the performance of flotation cells are highlighted in these equations.

Volumetric flow rate through the impeller (Q) is used to compare cells on their mixing capability through the cell, which will have an effect on how many times particles can circulate through the whole flotation cell volume before being removed to tails.

$$Q \sim RD^3 \tag{3}$$

Since impellers have different geometries, the diameter (D) and the rotational speed (R) were taken as the parameter for this analysis. As can be seen from the relation, the same volumetric flow rate can be achieved with different impeller sizes by adjusting the rotational speed.

Power consumption (P) can either be measured by physically measuring the power draw of different cells in operation or by using an empirical correlation that is less cumbersome to use.

$$P \sim \rho_f R^3 D^5 \tag{4}$$

The power consumption can be approximated by the diameter (D) and rotation speed (R) of the impeller (and the fluid density ρ_f). This is not such an accurate approximation, since the impeller design will also play a role in the power consumed by the flotation machine.

The power number is defined to correlate the actual power drawn with the empirically determined power consumption.

$$N_P = \frac{Pg}{\rho_f R^3 D^5} \tag{5}$$

Here the actual power consumption (P) is used and then compared to the density of the fluid (ρ_f), the rotation speed as well as the impeller diameter. This is the comparison between the actual power and the theoretical power consumed. This is in essence a correction factor for the empirical correlation, which incorporates energy transfer efficiencies of different impeller designs as well as operating at different slurry densities.

Power input is also a very important parameter as attachment energy is required for particles to attach to the available bubble surface.

$$P_s = \frac{P}{V_c} \tag{6}$$

Specific power input relates the actual power input (P) to the total volume of the cell (V_C). This parameter allows the power concentration to be calculated and compared to different flotation cells. The weakness of this calculation is that it does not consider the throughput of the cell and therefore a smaller cell will have a higher power concentration, although it may have the same throughput as another cell.

Residence time within the flotation machine (τ) is as important as any other reactor or separator since residence time determines the probability for a particle to attach to the surface of the air bubble. It should be noted that the optimum residence time will be dependent on the minerals being separated, hydrodynamics and particle size of the minerals separated.

$$\tau = \frac{V_c}{Q_f} \tag{7}$$

Residence time is calculated through comparing the volumetric flow (Q_f) of the slurry with the volume of the flotation cell (V_C). It should be noted here that the total volume is used and not just the slurry volume, which will be smaller than the total volume due to the presence of air bubbles in the slurry. Since aeration rates differ between different machine sizes and models, it is better to base the residence time on the total volume of the cell. This also makes the calculations less complicated and easier to determine the throughput of the specific machine.

The Froude number (F_r) can be used to determine the effectiveness of mixing particles within the cell.

$$F_r = \frac{R^2 D}{g} \tag{8}$$

The Froude number relates the inertial force of an element to its gravitational force. Here the inertial force of the particles obtained by the impeller is compared to the gravitational force on the particles. This number can be used in conjunction with the power number to better understand the magnitude of force within the cell.

The air flow number compares the air supplied to the flotation cell with the pumping, or air distribution capabilities of the impeller throughout the cell.

$$N_a = \frac{Q_a}{A_c U_t} \tag{9}$$

The air flow number (N_a) relates the volumetric flow rate of the air (Q_a) to the tip speed of the impeller (U_t) as well as the cross sectional area of the flotation cell (A_C). The impeller tip speed is used since it is an important factor that determines the distribution of bubbles through the cross sectional area of the cell, as well as the bubble size determined through bubble breakup by the impeller.

Air capacity number (C_a) considers the air pumping efficiency through the impeller.

$$C_a = \frac{Q_a}{RD^3} \tag{10}$$

This number is more for self-aerating machines where the air drawn into the machine is determined by the impeller geometry and speed, thus the comparison of the air flow rate to the rotation speed and diameter of the impeller. It should be noted that the air flow here is the actual air flow and not the approximation. The air capacity number can still be used to compare other machine types since it still relates the actual air flow to the approximated air flow through the impeller.

Superficial gas velocity (J_g) relates the air feed ratio to the cross sectional area of the cell. This ultimately describes the air dispersion through the cell cross sectional area.

$$J_g = \frac{Q_a}{A_c} \tag{11}$$

This is a much better parameter to use compared to the actual air feed rate since it is normalised to the cell size and therefore better to use when comparing cell performances with one another. It should be noted that different cells operating at the same superficial gas velocity may not use the same gas flow rate and therefore the air feed requirements should still be taken into account when different cells are considered.

Superficial gas velocity does not measure the available bubble surface area, which will vary between designs according to the bubble size generated. The available bubble surface area effectively determines the collection capacity of the bubbles rising through the slurry. Bubble-surface area-flux (S_b) solves this problem by calculating the rate at which the bubble surface (bubble Sauter-mean diameter: d_S) area moves through the cell.

$$S_b = \frac{6J_g}{d_s} \tag{12}$$

This shows the possible attachment space on the bubble surface for particles and should be calculated with the superficial gas velocity, if possible. This can be used to compare attachment efficiencies through different cells, which can be translated to recovery efficiencies in the pulp phase since bubble surface area is one of the limiting factors in flotation kinetics.

The specific air flow (N_{as}) is similar to the superficial gas velocity although it incorporates differences in the length-to-diameter ratios of different cell designs. Superficial gas velocity only considers the cross sectional distribution of the gas and not the total volume.

$$N_{as} = \frac{Q_a}{V_c} \tag{13}$$

Specific air flow considers the concentration of air through the cell and ultimately the probability for attachment this will give to the cell. Once again this does not incorporate mineral throughput and this should be considered separately.

The impeller tip speed (U_{ts}) is quite an important scale-up criterion, since the tip speed is directly related to the inertial forces of particles and fluid obtained by the impeller. Tip speed also correlates to the particle's speed leaving the impeller and also plays a role in the bubble break up within the mixing process.

$$U_{ts} = \pi DR \tag{14}$$

The circulation intensity (C_i) is a measure of the mixing efficiency as well as bubble contacting within the cell. The reciprocal is also known as the tank turnover time, which is the time it takes to completely replace the fluid volume of a flotation cell.

$$C_i = \frac{Q_f}{V_c} \tag{15}$$

The equations described above serve to compare different mechanically agitated flotation devices without looking at the specific hydrodynamic environments created, or the means of agitation. The circulation intensity compares the volumetric flow rate of fluid through the impeller (Q_f) with the volume of the cell (V_c). It should be noted that most of these parameters can only be used for cells that are agitated by an impeller and not by other agitation methods such as Oscillatory Baffled Columns (OBC), Oscillatory Grid Columns (OGC) or Jameson cells, which utilises different agitation (contact) methods.

What can be noted from these equations is that aeration and air distribution is very important for flotation. This is coupled with bubble size, which affects the collection efficiency of froth flotation. Power input, which is also translated to impeller design and rotation speed is an important factor to determine and compare between cells. Lastly the distribution of particles through the slurry, as well as the residence time within the cell need to be considered when designing a new cell to ensure effective energy transfer as well as improved collision probabilities.

2.4.2. Different Flotation Cell Designs Used in the Industry

The flotation devices mainly used in the industry can be put into three classifications (Nelson and Lelinski, 2000):

- Devices that are agitated mechanically where self-aeration is used: This requires the impeller to be higher up in the tank (such as machines manufactured by EIMCO Process Equipment Co., known as WEMCO™).
- Devices that are agitated mechanically and use external forced aeration: This means the impeller is placed at the bottom of the cell with high circulation of the slurry through the impeller and to provide a good calming zone underneath the froth phase (manufactured by companies such as Outokumpu™, MintecOY™, Metso Minerals™, GL&V/Dorr-Oliver Inc™ and others).
- Columns that use external aeration and do not use any mechanical agitation (flotation columns): These machines are not commonly used in the platinum industry and if they are, it is for cleaner duties.

Mechanically-Agitated Flotation Cells with Forced Aeration

With these flotation cells there are slight differences in the cell's internal design from different companies, but the working mechanisms are roughly the same. Here the slurry is fed into the cell close to the centre and towards the bottom to prevent froth contamination. The basic design of a forced-aerated cell can be seen in Figure 3, which is based on the TankCell™ from Outokumpu (Gorain et al., 2000).

The impeller is placed at the bottom of the cell and is surrounded by a stator. The air is forced through the hollow impeller shaft into the impeller in some designs (illustrated in Figure 3), or the aeration is supplied by a sparger placed at the impeller. The impeller facilitates the air dispersion in the slurry, as well as particle-bubble attachment. The stator and impeller pair also creates a high shear environment for particle-bubble attachment. The stator along with baffles along the tank wall prevents the contents of the whole cell to rotate with the impeller.

Another function of the stator is to control the bubble size leaving the impeller and stator configuration. Bubbles mainly form through cavitation around the impeller. The bubble size created by the impeller and stator depends on the shear rate and cavitation around the impeller. This is one of the reasons why tip speed is so important in the design and scale-up of these machines (Inertial forces of particles leaving the impeller blade is also dependent on the impeller tip speed). By changing the gap between the rotor and stator the fragmentation of bubbles can be controlled. This is also dependent on the rotor and stator design.

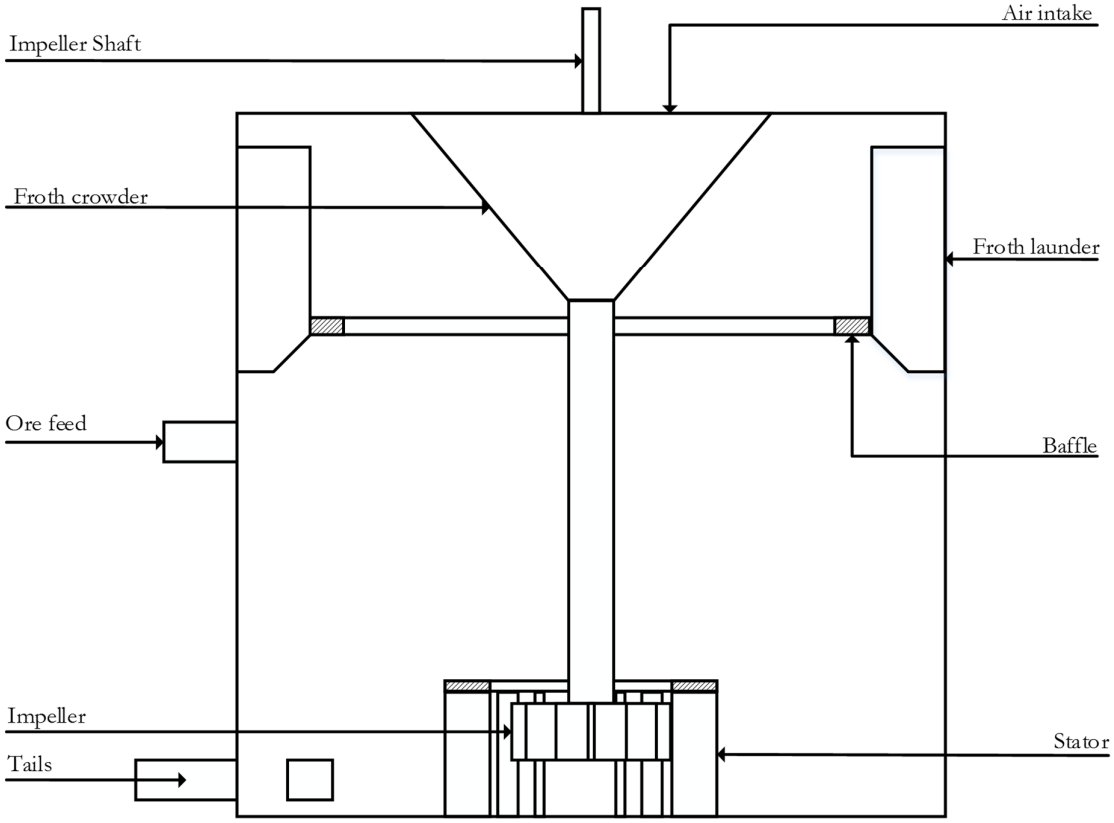

Figure 3: Conventional flotation machine design with forced aeration, showing cell internals (redrawn: Gorain et al. 2000).

This design also forms a circular flow pattern within the cell. The particles are flung to the outside of the flotation cell by the impeller. Here the mechanical mixing creates sufficient force to overshadow all other forces acting on particles. When the slurry reaches the outer walls of the cell, it enters a calmer zone and particles either sink to the bottom, under gravitational forces, or start to rise to the surface due to the density difference between the pulp and the combined density of the particle and the bubble it is attached to. Smaller particles that do not have sufficient inertial forces to exit the circulating bulk fluid motion compared to the larger particles may be sucked back

into the impeller through the bottom. If particles attached to bubbles decouple again, then they will also sink back into the impeller unit. This forced circular motion within the cell will have a higher concentration of aerated particles rising to the surface along the outside of the cell and a higher concentration of decoupled particles sinking back to the bottom towards the centre of the cell.

The circular fluid motion towards the top of the cell is sometimes (for instance RCS machines by Metso) aided by a horizontal baffle strategically placed at a specific height, to force the upward bulk fluid motion at the outer wall of the cell toward the centre of the cell. Here the froth starts to separate from the bulk fluid and rise to the top. The horizontal baffle also aids in providing a turbulent-free environment for particle-bubble decoupling and prevents bubble break-up through turbulence.

The froth launder used here works on the basic principle of a weir, with the froth overflowing over the edge into the froth trough. This makes the slurry depth within the cell an important operating parameter to control the froth height and prevent slurry from being pushed over the weir and into the concentrate. In some cases sprayers or froth washers are added to the top to prevent entrained gangue to be carried over into the concentrate. Washing the froth aims to remove gangue minerals entrained in the froth, but can also cause valuable fine minerals to be washed off the froth bubbles and back into the slurry. Using froth washers also affect the froth stability due to the removal of fine minerals.

As the rotor and stator are situated at the bottom of the cell, aerated slurry needs to travel a significant distance through the pulp in order to reach the froth phase.

WEMCO Working Mechanism

Figure 4 illustrates the design of a WEMCO flotation cell. As stated earlier, the WEMCO flotation cell is a self-aerating device. The addition of air is controlled by vanes situated at the top of the machine while the air drawn into the system depends on how deep the rotor is submerged into the slurry. The slurry feed is situated at the bottom of the cell, below the false bottom. The slurry feed is sucked up through the draft tube to the impeller. Tailings are removed from the cell above the false bottom.

The slurry is sucked up through the draft tube and comes into contact with the air bubbles formed by the impeller. The aerated slurry exits the mixing area in the cell through the disperser where the bulk fluid gets directed downward by the hood. This means that there is flow circulation happening in the lower part of the cell, running up through the draft tube and running down alongside the

cell wall. The circular motion here is in the opposite direction compared to the forced aerated machines discussed earlier.

The particles are flung to the side wall from the centre by the impeller, and these particles sink to the bottom when entering the calmer zone if no attachment occurred. If a particle attached to a bubble, but the buoyancy of the combined particle-bubble system is not sufficient to transfer it to the froth phase, then this particle-bubble system will again be sucked in by the draft tube. This will allow for another opportunity of attachment. The forced downward recycling also ensures that there is sufficient time for detachment of any weak hydrophilic particles that attached to air bubbles before entering the froth phase.

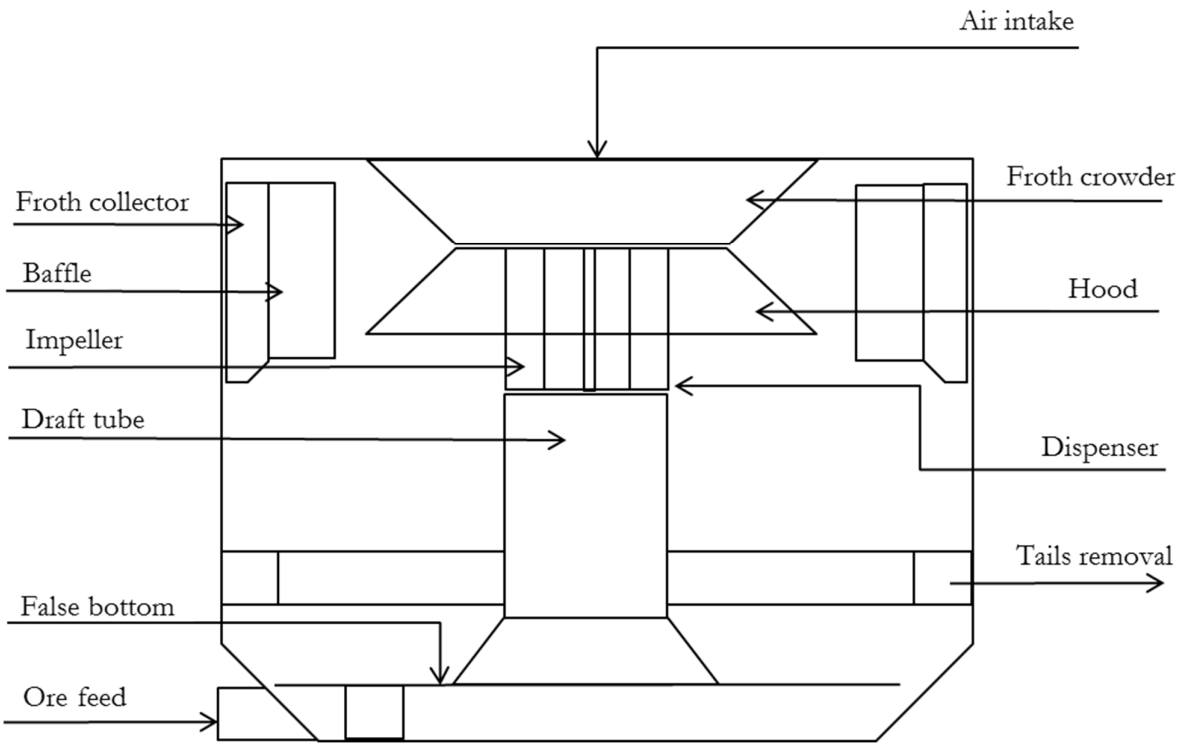

Figure 4: WEMCO self-aerating flotation cell design displaying cell internals (redrawn: Gorain et al. 2000).

The hydrophobic particles that do get attached to the surface of air bubbles will rise to the top, above the diffuser hood. The baffles are placed in such a way to ensure that a calming zone is formed in the slurry just before interfacing with the froth. Here there is also a slight circular flow, since air bubbles move upward along the walls of the vessel while hydrophilic particles move down alongside the froth crowder and the diffuser hood to be joined in the stream exiting the dispenser.

The froth crowder is used to reduce the cross-sectional area as the froth rises to the top, increasing the upward velocity of the froth and pushing the froth to the sides where the froth launder is placed. This minimizes the amount of froth surface exposed to the air that will result in froth break-up. The crowder also helps to reduce the residence time of particles within the froth phase, preventing the collapse of froth, which will typically result in an increase in the drop-back rates of valuable minerals to the slurry.

The impeller is located near the top where the aerated slurry is released to the calm zone of the cell. Travel distance of aerated slurry from the impeller to the froth phase is reduced in this design compared to bottom agitated mechanical cells. Releasing the aerated slurry near the middle of the cell could therefore improve the concentrate grade. The hood ensures a down-flow motion of aerated slurry as it exits the impeller to create a calm zone for the froth and to improve cleaning of the froth. As aerated minerals need to change flow direction, heavier and weak hydrophobic particles can decouple from air bubbles and continue moving downwards in the cell. This could ultimately reduce the recovery of valuable minerals obtained over the cell, making it well suited for cleaning operations. This is due to the fact that cleaning circuits focus on concentrate grade and not on full recovery of all valuable minerals (scavenger circuits operate to recover all valuable minerals possible).

One of the advantages of this cell is that it minimizes short-circuiting in the slurry (with the draft tube) as well as in the froth phase (diffuser hood). A reduction in short-circuiting ensures that the spread around the mean residence time is smaller for all the participating minerals on the residence time distribution curve. The smaller spread in residence time can be translated to increased contacting efficiency within the cell.

Jameson Cell™ Design

The Jameson Cell™ is an adaptation of column flotation. Flotation columns generally consist of long tubular columns where the slurry feed is situated in the middle of the cell while aeration is supplied from the bottom. These columns have a large length to diameter ratios. Here the section below the feed acts as the pulp zone, while the section above the feed is considered the froth zone. The pulp zone should have a high recovery while the froth zone should have high selectivity to the desired mineral for concentration.

Conventional flotation columns have low energy input since no mechanical agitation is used. Therefore the only energy requirement comes from the air blower and pumping the slurry into the cell. Flotation columns work best with fast floating minerals and are also used in soft mineral

industries where the high agitation may result in size reduction of particles. Low energy usage makes column flotation less attractive for the platinum industry as the PGM minerals require a relatively high energy for particle-bubble attachment (Ross 2015, Deglon et al., 2000).

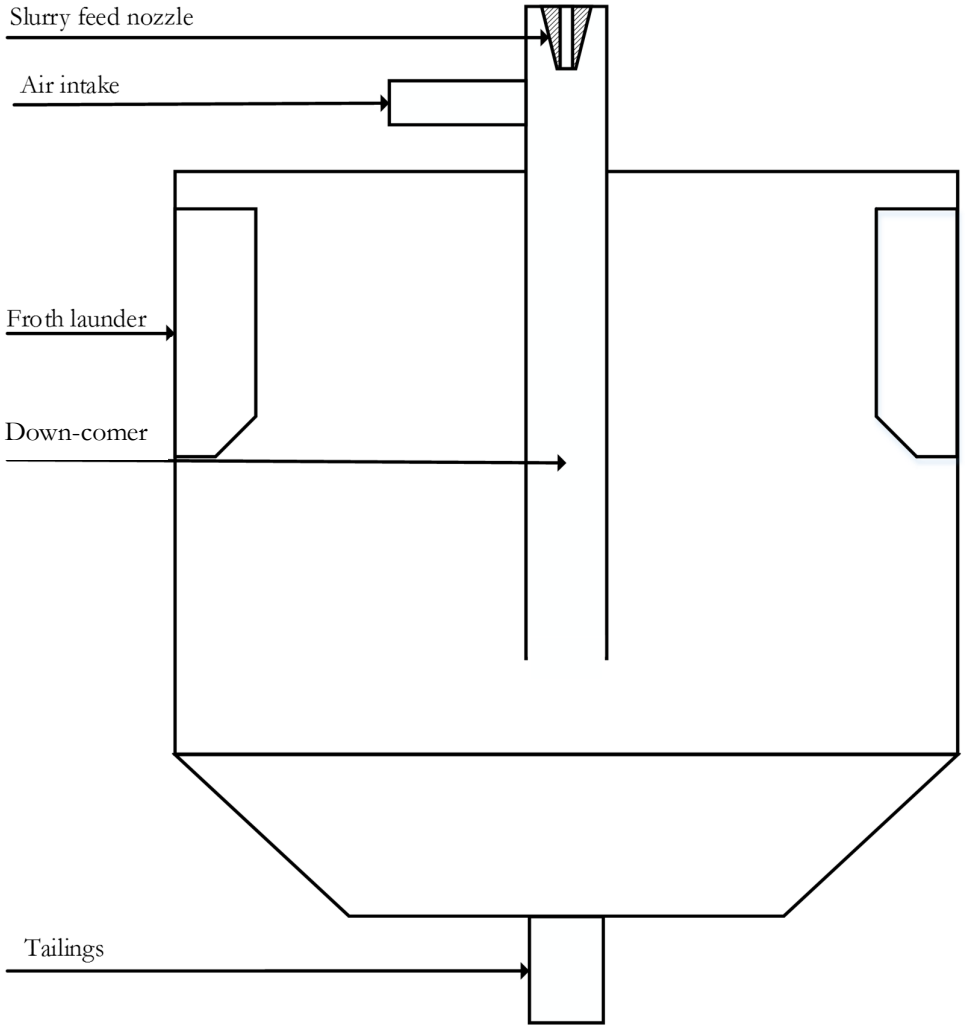

Figure 5: Basic Jameson Cell™ design showing the internals of a Jameson Cell™ (redrawn: Atkinson and Conway, 1993).

Greame Jameson introduced a down-comer in the column which increased the energy intensity within the column, enabling a reduction in overall column size. The Jameson Cell™ uses a nozzle to jet the slurry into the down-comer. Small bubbles are created as this fast moving slurry jet hit the surface of the slurry in the down-comer. Air is drawn into the down-comer, making this a self-aerating machine. Figure 5 shows a basic Jameson Cell™ configuration with only one down-comer within the cell. Many down-comers can be placed into a larger diameter column to increase the throughput of the column.

Jameson cells increase the particle-bubble contact probability compared to conventional flotation columns as well as mechanically agitated flotation cells by significantly reducing bubble size while increasing the volume of air (better dispersion of small bubbles throughout the column) within the column (Atkinson and Conway, 1993).

The Jameson Cell™ separates the high intensity mixing zone from the calm detachment zone. This separation improves the froth interfacial stability to maintain similar froth depths as conventional column cells while still increasing the energy intensity within the column. A Jameson Cell™ is a one pass flotation cell because the slurry feed goes through the down-comer where no recirculation can occur within the cell. This is not the case with self- and forced aerated mechanical flotation cells.

From this discussion it can be seen that there are some significant design differences between flotation cells currently used in the industry. It is affected by the ore type where the most significant factors are density, hydrophobicity and mineral liberation, as well as the application of the flotation cell in rougher, scavenger or cleaner duty. The recovery and concentrate grade of these machines should be compared in different duties in order to better understand the functionality of them in the platinum industry. Unfortunately the platinum industry maintains high secrecy on such information and this is therefore rather difficult to do.

Information with regards to operating conditions is available and will be used to view the design differences of these machines. The operating conditions of the column cells will not be broadly investigated as these machines are not generally used in the platinum industry and will generally not be used in rougher duty.

2.4.3. Operating Parameters of Industrial Flotation Machines

A study done on the flotation cells used in the Platinum industry of South Africa is used to better understand the levels of the different operating conditions for UG2 flotation. Since the operating parameters of the flotation cells greatly depend on the ore being separated, this study will hold more meaning than other studies. This study was done by a research team from the University of Cape Town in 1999, led by D.A. Deglon. It compared the operating parameters of 17 different flotation devices used in different duties at a platinum ore separation plant.

Table 1 shows these 17 different cells with their volume and duty in the separation circuit. Here it can be seen that there is a mixture of different flotation cell types used in conjunction with one another. WEMCO cells seem to be preferred for rougher, cleaner and scavenger duties in

conjunction with other cells. The WEMCO cells used in rougher duty are all modified to increase the energy input to the cell.

Table 1: Details of flotation cell studied (re-used with permission from Elsevier: Deglon et al., 2000).

Cell Type	**Volume (m^3)**	**Cell Duty**
Batemans	3	Cleaner
WEMCO 84 (bank)[1]	4.2	Cleaner
WEMCO 120 (bank)	8.5	Cleaner
OK 8 Tank Cell	10	Rougher
WEMCO Unit Cell	10	Cleaner
OK 16 (bank)	16	Rougher
OK 16	16	Rougher
WEMCO 144L (bank)[2]	16	Rougher
WEMCO 144D	16	Rougher
WEMCO 144D (90)[3]	16	Rougher
SK 500 Flash Cell	23	Flash
WEMCO 164	30	Rougher
WEMCO 164 (F)[4]	30	Scavenger
OK 38	38	Rougher
OK 50 Tank Cell (FF)[5]	50	Rougher
OK 50 Tank Cell (MM)[6]	50	Rougher
Column Cell	60	Cleaner

Note: 1) Bank refers to a number of individual cells used together in a bank (series arrangement). 2) WEMCO™ 144L cells that was fitted with WEMCO™ 164 impellers. 3) WEMCO™ 144D cells fitted with a 90 kW motor. 4) WEMCO™ 164 cells fitted with all-round launders. 5) OK 50 Tank Cell™ fitted with Freeflow™ mechanism. 6) OK Tank Cell™ fitted with a Multimix™ mechanism.

The cell volumes have a significant range from 3 to 60 cubic meters depending on their duty. In general, larger cells are typically used for roughing and scavenging of the tailings, since it is here where the largest quantities of ore need to be treated.

From the note it is clear that there were some custom alterations to these machines to improve their role in recovery of valuables in the specific ore being treated. These changes have an effect on the operating conditions used within these cells, as seen in Table 2:

Table 2: Operating conditions of flotation cells (re-used with permission from Elsevier: Deglon et al., 2000).

Cell Type	**V (m^3)**	**P (kW)**	**R (RPM)**	**D (m)**	**ϱ_f (ton/m^3)**	**Q_a (m^3/min)**
Batemans	3	7	220	0.49	1.15	1.3
WEMCO 84 (bank)[1]	4.2	10	310	0.41	1.12-1.25	2.9-4.1
WEMCO 120 (bank)	8.5	15	220	0.56	1.05	6.4-9
OK 8 Tank Cell	10	-	145-180	0.65	1.09-1.15	0.6-0.8
WEMCO Unit Cell	10	95	-	0.89	1.15	5.3
OK 16 (bank)	16	30	160	0.75	1.2-1.3	9.3-17
OK 16	16	30	160	0.75	1.2-1.3	9.9-16.4
WEMCO 144L (bank)[2]	16	41	170	0.76	1.25-1.35	5.1-8.7
WEMCO 144D	16	41	170	0.76	1.25-1.35	4-7.7
WEMCO 144D (90)[3]	16	82	220	0.76	1.25-1.35	6.7-14.6
SK 500 Flash Cell	23	-	150	0.9	±2	4.2
WEMCO 164	30	23-49	140-180	0.76	1.29-1.32	6-10.8
WEMCO 164 (F)[4]	30	41	170	0.76	1.27-1.3	8
OK 38	38	39-50	150	0.9	1.24	6.9-10.8
OK 50 Tank Cell (FF)[5]	50	49	105	1.05	1.25-1.3	2-4
OK 50 Tank Cell (MM)[6]	50	69	130	1.05	1.25-1.3	2-4
Column Cell	60	-	-	-	1.12	4.2-5.2

The power in Table 2 was estimated by subtracting the amps drawn by the motor, when the flotation cell was running without load, from the current drawn when it was operating under load. This was then multiplied with the volts drawn as well as a power draw factor. (This should only be seen as an estimate.) The rotational speeds of the impellers vary significantly from 105 to 310 revolutions per minute. The ranges given in this table were when a bank of cells was investigated and it was found that they run under different conditions. It should be noted that there is no way to perfectly split a stream according to density, flow rate and particle size, so the operating conditions in a bank will always differ slightly.

The density of slurry treated within these cells ranges from 1.05 to 2 kg/m^3, which is a significant variation with respect to cell size selection and residence time.

The air feed rate also varied significantly from 1.3 to 16.4 m^3/min, which affect the operating cost of these units, but should rather be compared with the specific air input to determine its effect on the collection efficiency.

Table 3: Hydrodynamic data of the flotation cells (re-used with permission from Elsevier: Deglon et al., 2000)

Cell Type	**P_s (kW/m^3)**	**U_{ts} (m/s)**	**N_P**	**Fr**	**$1/C_i$ (s)**	**τ (min)**
Batemans	2.3	5.6	4.4	0.67	7	
WEMCO 84 (bank)[1]	2.4	6.7	5.2	1.12	12	
WEMCO 120 (bank)	1.8	6.5	5.3	0.77	13	7.1
OK 8 Tank Cell		4.9-6.1		0.39-0.6	12-15	5.7-8.8
WEMCO Unit Cell	9.5					
OK 16 (bank)	1.9	6.3	5.4	0.54	14	
OK 16	1.9	6.3	5.4	0.54	14	
WEMCO 144L (bank)[2]	2.6	6.8	5.5	0.62	13	3.2
WEMCO 144D	2.6	6.8	5.5	0.62	13	
WEMCO 144D (90)[3]	5.1	8.8	5.1	1.04	10	
SK 500 Flash Cell		7.1		0.57	13	
WEMCO 164	0.8-1.6	5.6-7.2	5.5	0.42-0.7	23-29	6.8
WEMCO 164 (F)[4]	1.4	6.8	5.5	0	24	
OK 38	1-1.3	7.1	3.4-4.4	0.62	21	2.8
OK 50 Tank Cell (FF)[5]	1	5.8	5.6	0.57	25	10
OK 50 Tank Cell (MM)[6]	1.4	7.1	4.2	0.33	20	10
Column Cell				0.5		11.1

Table 3 indicates that the specific power input is more even throughout the cells with a significant increase in the WEMCO 144D and even more so with the WEMCO unit cell. The power input into these cells is significantly higher than the average inputs in other industries (Deglon et al., 2000). This shows that the South African platinum industry is prone to using higher power inputs to obtain the best separation possible. The average power input ranges between 1 and 2.6 kW/m^3.

In Table 2 it can be seen that there is a significant variation in the rotational speed, as well as the diameter of the impellers. Considering Table 3, the impeller tip speed, calculated from those two parameters, is closer together and range between 4.9 and 8.8 m/s. This is a very important scale-up parameter in flotation cell design.

The turnover time (reciprocal of circulation intensity) is relatively constant between 10 to 13 minutes for most cells, although there is a significant rise in the turnover times of the larger cells which increased up to 29 minutes.

Table 4 shows the specific air flow, the air capacity, the air velocity at the impeller, the Sauter-mean bubble diameter, the superficial gas velocity and the bubble surface area flux of the different flotation cells.

Table 4: Gas dispersion data of flotation cells (re-used with permission from Elsevier: Deglon et al., 2000)

Cell Type	**N_{sa} (min^{-1})**	**C_a**	**Q_a/D^2 (m/s)**	**ds (mm)**	**J_g (cm/s)**	**S_b (s^{-1})**
Batemans	0.43	0.05	0.09	1.8	1.6	52
WEMCO 84 (bank)[1]	0.7-0.98	0.14-0.19	0.29-0.41	1.3-1.5	1.3-1.9	56-78
WEMCO 120 (bank)	0.75-1.05	0.17-0.23	0.34-0.48	1.4-2	1.4-1.8	52-60
OK 8 Tank Cell	0.06-0.08	0.02	0.02-0.03	1.2-1.4	1-1.4	47-62
WEMCO Unit Cell	0.53		0.11	1.7	1.7	59
OK 16 (bank)	0.58-1.06	0.14-0.25	0.28-0.5	1.6-2.4	1.8-2.7	64-77
OK 16	0.62-1.03	0.15-0.24	0.29-0.49	1.6-1.7	1.8-2.2	69-77
WEMCO 144L (bank)[2]	0.32-0.54	0.07-0.12	0.15-0.25	1.3-1.6	1-1.5	47-56
WEMCO 144D	0.25-0.48	0.05-0.1	0.11-0.22	1.3-1.8	1.5-2.1	66-71
WEMCO 144D (90)[3]	0.42-0.91	0.07-0.15	0.19-0.42	1.3-1.5	1.6-2	74-83
SK 500 Flash Cell	0.18	0.04	0.09	1.3	2.1	97
WEMCO 164	0.2-0.4	0.1-0.15	0.17-0.35	1.4-1.6	1.6-1.9	68-72
WEMCO 164 (F)[4]	0.27	0.11	0.23	1.4-1.8	1.7-2	67-77
OK 38	0.18-0.28	0.06-0.1	0.14-0.22	1.9-2.1	1.4-2.2	43-63
OK 50 Tank Cell (FF)[5]	004-0.08	0.02-0.03	0.03-0.06	1.2-1.7	0.7-1.4	32-54
OK 50 Tank Cell (MM)[6]	0.04-0.08	0.01-0.03	0.03-0.06	1.2-1.6	0.7-0.9	33-37
Column Cell	0.07-0.09			2.6-2.7	2.6-2.7	58-63

The specific air flow shows the dispersion rate of the gas inside the cell and can be compared to the power input. These values vary significantly from one another with a range of 0.04 to 1.06 per minute, which can be related to the design of the specific cell and the specific cell duty. This number increases significantly with a decrease in cell size, which shows that the aeration of smaller vessels is much easier than large ones.

The air capacity is a measurement of the actual air flow to the theoretical aeration rate by the impeller, otherwise stated as the relationship between the volumetric feed flow rates of air to the pumping capacity of the impeller. This is an important scale-up criterion since these two factors are independent from one another and yet they work together for better collection efficiency. The air capacity in the analysed cells varies over a range from 0.01 to 0.25 between the cells of different designs and sizes.

Another scaling factor sometimes used to compare flotation cells of different sizes is the air flow velocity at the impeller and is a relation between the volumetric flow rate to the diameter of the impeller (Arbiter et al., 1976). This is used to measure if a specific impeller size will be able to handle the specific air feed rate of the cell. This factor should also be coupled with a factor for impeller design since different designs may result in different capabilities.

The Sauter-mean bubble diameter in all of the cells is also given in Table 4. Here it is illustrated that the mean diameter does not vary too much between different cells. The bubble diameter ranges from 0.7 to 2.7 mm in diameter, although most cells operate between 1 and 1.9 mm diameter (Deglon et al., 2000). This influences the bubble surface area flux within the cell. It should be noted that the mean bubble diameter is influenced by the superficial gas velocity since the higher the superficial gas velocity go, the higher the probability that bubbles will coalesce and form larger bubbles that will rise faster. The superficial gas velocity normalises the volumetric flow rate of gas with the cross sectional area of the cell. Higher values would mean that bubbles will be closer to each other, increasing the probability of coalescence. Generally, when the superficial gas velocity decreases, smaller mean bubble sizes are achieved.

The bubble size has a significant effect on the bubble surface flux as an increase in the surface flux occurs at decreasing bubble size. The range of the bubble surface flux lies between 32 and 97 per second. The bubble surface flux will also change according to the depth of the measurement within the cell, as bubble volume (and diameter) is affected by the vertical pressure gradient within the cell.

These parameters indicate that the flotation machines used in the platinum industry favour high energy input, generally high superficial gas velocities and varying residence times in each cell. The mechanical cells have mostly bottom-feeding positions, but the impellers and aeration release positions vary. WEMCO™ releases the aerated slurry from the top while the conventional flotation cell releases at the bottom. Column cells have a mixture of these conditions, with low energy input. These differences seem to either focus on recovery or grade, which will be affected by the ore type

and particle size. It could be beneficial to have a flotation cell design that incorporates selective release of aerated slurry at different depths to ensure that the most favourable attachment conditions are created for different particle sizes. This could potentially establish a good vertical concentration gradient within the cell which will reduce contamination of mineralized bubbles and the froth phase with gangue fines in the slurry.

While conventional forced air mechanical flotation cells utilize distance between the impeller and the froth interface to obtain a stable froth, WEMCO™ cells use a hood and Jameson cells use the down-comer plus a separate calming zone to effectively create a stable froth layer. The separation of the high energy intensity zone from the calm zone seems beneficial to improve froth phase stability as well as concentration gradient within the cell. This decoupling of the contact zone and the froth zone endeavours to generate a froth phase that is less contaminated with gangue minerals within the slurry while providing sufficient time for drainage of weakly hydrophobic minerals from the froth.

Both conventional forced air flotation cells and the WEMCO™ cell allow internal circulation of minerals while no internal circulation of minerals can occur in the Jameson Cell™. Preventing internal circulation of mineral slurry provides better control of the residence time within the cell. External circulation also ensures that mineral particles of different size have the same opportunity for energy transfer and contacting with air bubbles.

All these observations are valuable to the design process of a new flotation cell to ensure that the most beneficial parameters are combined. Different designs and techniques used to separate and remove fine minerals will be discussed in the next section to incorporate promising concepts in the new flotation cell.

2.5 Studies on Fines Separation

In order to deal with fines, other separation techniques were previously investigated, including size reduction of bubbles, dissolved gas flotation, agglomeration of fines, electro flotation and turbulent micro flotation. Each separation technique is discussed separately.

2.5.1. Bubble-size Reduction

By reducing the bubble size, the bubble surface area is increased significantly. Available bubble surface area is of utmost importance in fines flotation as the surface area of minerals increases with size reduction. It is reported that the collection efficiency is directly related to the inverse of the bubble diameter (Ahmed and Jameson, 1985). Other studies (Jowett, 1980., Reay and Ratcliff,

1973., Reay and Ratcliff, 1975) indicated that the flotation rate is determined by the bubble frequency, irrespective of bubble size. Reducing the bubble size will however increase the bubble frequency. This shows that decreasing the bubble size within a flotation column will increase the collection efficiency of particles as well as the collection rates. Smaller bubbles will have lower rise rates that will reduce the entrainment of larger weak hydrophobic particles.

The negative aspects of using smaller bubble sizes in general flotation circuits are slower bubble rise rates as well as lower carrying capacity per bubble. The slow rise rate of bubbles results in longer residence times within the flotation device, which is not advantageous as larger flotation cells are needed and the bubbles are longer exposed to gangue minerals in the slurry, which can 'contaminate' the froth. Another negative effect of reducing the bubble size is the transport of water through the froth phase (Matis et al., 1993) which increases the water usage of the flotation process as well as the contamination of the concentrate by slimes entrainment.

However, it is evident that reducing the bubble size can be beneficial for fines flotation due to increased flotation rates. Small particles require a smaller air volume to achieve a positive buoyancy for removal to the froth phase. This is due to the fact that the mass of a mineral particle decreases with particle size reduction. Reducing bubble size will also increase bubble surface area flux when the superficial gas velocity remains constant. A greater bubble surface area flux will result in a larger bubble surface area, ensuring that this will not be a limiting factor. The lower rise rate and concern of contamination can be mitigated by reducing the distance that the bubbles need to travel to reach the froth phase. Establishing a valuable mineral concentration gradient through the depth of the cell can also help reduce the risks of contamination. A real concern of bubble size reduction in fines flotation is the contamination of the froth phase with ultra-fine gangue minerals.

2.5.2. Dissolved Gas Flotation

Dissolved gas flotation can be achieved in two ways; firstly by using a vacuum to form bubbles from the naturally dissolved air present in the slurry and secondly by introducing contact between a pressurized gas and the slurry for a long period of time prior to flotation that operates at atmospheric pressure. With the reduction in pressure, the dissolved gas nucleates around any disturbance present in the fluid. This causes bubbles to form around particles and works around the energy requirements of particle-bubble attachment. This process improves the conditions for fine and ultra-fine particle removal as these particle sizes generally do not have enough kinetic energy of their own to attach to bubbles otherwise (Matis et al., 1993).

The negative implication of using this technology is that most fines are removed from the slurry without any selectivity between hydrophobic and hydrophilic surface properties. This is due to the fact that the bubbles nucleate around any disturbance in the surface tension of the fluid regardless of what type of disturbance it may be. This technology have application in water purification were non-selective removal of suspended solids is required.

2.5.3. Electro Flotation

Electro Flotation involves flotation through the electrolysis of water into oxygen and hydrogen. The micro bubbles generated by the electrodes are used to remove suspended solids out of the aqueous medium. Electro flotation have shown some success in water purification, specifically in the removal of suspended heavy metals and emulsified organic compounds (Matis and Peleka, 2010). Some experimental success have been seem in the flotation of mineral salts through electro flotation, but this area still remains a challenge. Electro flotation is generally used in smaller scale and with very low solid loadings, which will require a bigger concentration plant than conventional air flotation plants (Kyzas and Matis, 2016).

2.5.4. Turbulent Micro Flotation

Rulyov (2008) found a way to overcome the limitations of current equipment with regards to the rising velocity of small bubbles. His design (Figure 6) incorporated a long cylindrical tube fitted with static mixers. The slurry and micro bubbles are introduced at the entrance of this tube where a gradual pressure drop occurs as the slurry and bubbles move along in the tube. This means that the bubble size increases as the slurry moves along, increasing the rising velocity of the bubbles. Plug flow is achieved through the tube that prevents early bubble separation from the slurry, ensuring adequate contacting time between suspended solids and the micro bubbles. The content of the static mixer exits into a shallow separation vessel. This ensures that the distance that the bubbles should rise to be collected in the froth is significantly reduced with regards to current flotation vessels (Rulyov, 2001). This allows for smaller volumetric concentrators to be used.

This method has shown promise in some applications due to lower energy requirements as well as increased separation efficiency. Water purification was done successfully by chemically enhancing the agglomeration characteristics of the suspended solids while utilizing turbulent micro-flotation (Rulyov, 1999).

The success of this separation technique relies on the suppression of floatable gangue, successful liberation of the valuable minerals as well as smaller particle size ranges used in the separation process. Contacting time is strictly controlled while sufficient mixing energy is supplied for

increased attachment probabilities. The shallow separator at the end alleviates the negative effect of slow rising velocity of micro bubbles experienced in conventional froth flotation cell designs.

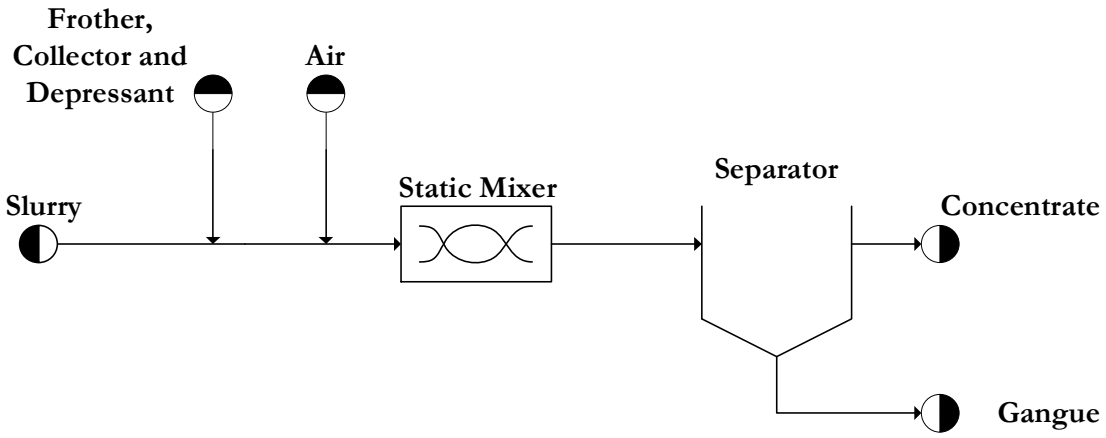

Figure 6: Turbulent Micro Flotation Design (redrawn: Rulyov, 2001).

A highly turbulent environment seems to have merits for fines flotation, as long as a quiet or calm zone is maintained at the froth interface for decoupling of slurry from the froth. Micro bubbles also seem to play a vital role in fines flotation.

2.5.5. Agglomeration of Fines

Agglomeration of fines circumvents the problems of fines in the flotation process by combining individual particles to form a bigger composite particle. The agglomerate is then floated in a conventional flotation device. These agglomerates can be formed through different methods, including hydrophobic agglomeration, selective flocculation and coagulation.

With hydrophobic agglomeration the mineral slurry is treated with the same chemical surfactants as in conventional flotation equipment. These surfactants improve the selective hydrophobicity of the valuable minerals. Thereafter the slurry is heavily agitated to ensure that the hydrophobic particles come into close quarters of each other and possess the required energy to be able to attach to one another as well (Miettinen et al., 2010). There are different methods to achieve the close proximity of the hydrophobic fines, including shear flotation (Warren, 1975), emulsion flotation, carrier flotation and two liquid extractions (Subrahmanyam and Forssberg, 1990).

Coagulation involves the reduction of electrostatic repulsion between valuable mineral particles allowing them to form flocks. This can be achieved by adding electrolytes to the suspension specific to the mineral being coagulated. This method is used in the water purification industry to remove most suspended solids out of the water (Miettinen et al., 2010). Unfortunately this method

does not allow for high separation efficiency, as the electrolytes added are not so specific to the minerals. This causes gangue minerals to be incorporated during the coagulation, which reduces the concentrate grade (Rubio et al., 2006).

Flock flotation also uses chemicals to aggregate minerals together to increase the physical size of the mineral particles (Song et al., 2001). Selective flocculation involves the separation mechanism where surfactants not only render gangue minerals hydrophilic, but also flocculating them to prevent mechanical entrainment of fines (Liu et al., 2006). This allows the purification of fines flotation since this method reduces the amount of gangue fines that contaminate the froth phase and concentrate, but still leaves the valuable mineral hydrophobic and in its original size.

Agglomeration of fines can thus be achieved through a combination of chemically altering the slurry and intense mixing. The reagents or surfactants used in this study will be the same as that used in the industry. Intense mixing can therefore still be investigated in the design of the new flotation cell.

2.6. Summary of Important Design Factors Learned From Literature

Literature indicated that bubble size and gas dispersion plays a significant role in flotation. Small gas bubble creation improves the available bubble surface area for mineral attachment that is important for finer mineral flotation. The energy required to cause attachment between a hydrophobic mineral particle and bubble is directly related to the bubble size and indirectly related to the particle size. Literature further indicates that the platinum industry favours higher energy input compared to other industries. Intense mixing to create a highly turbulent environment for finer particle agglomeration (Section 2.5.5) and attachment to bubbles may therefore be advantageous, especially for the PGM industry.

An evaluation of the current mechanically agitated flotation cells used in the platinum industry, suggests that the vertical position of the impeller and slurry release may have a notable effect on the valuable mineral recovery and concentrate grade. An advantage of the Jameson Cell™ design is that it eliminates internal short circuiting, where any recirculation of slurry can be controlled. The Jameson Cell™ further decouples the turbulent environment from the calm zone. This allows for particle-bubble attachment in the turbulent environment and separation between the froth and slurry in a calm zone. This separation of the turbulent and calm zone also allows for a more stable froth phase.

Chapter 3 – Novel Flotation Device Design

This chapter discusses the chosen design for this study (the detailed manufacturing drawings are shown in Section 8.5).

3.1 Design Introduction

The goal of the design is to achieve high recoveries with higher than conventional concentrate grades from a PGM slurry where 75% of the mineral particles are smaller than 75 µm. The design primarily focuses on establishing an environment of high intensity (or high energy) mixing to create a turbulent environment for particle-bubble attachment. The turbulent environment increases the collision probabilities between air bubbles and hydrophobic particles for selective attachment of hydrophobic mineral particles to the air bubbles. This process is best achieved with focussed mechanical agitation and the high energy input is especially required for PGMs. This high energy mixing is contained in a down-comer to separate the high turbulent environment from the calm outer tank. Figure 7 illustrates the basic cell design with the internal components; the aerator, down-comer and the outer cell (see Section 8.5 for detailed drawings).

The slurry enters the cell through the aeration chamber where air is added to the slurry via a sintered metal sparger with pore sizes of approximately 5µm. The slurry runs perpendicular to the sparger surface, to reduce the bubble size generated by the sparger (see Section 3.4 for more details on the aerator design). The aerated slurry exits the sparger chamber and runs through a narrow channel down the top section of the down-comer to increase the slurry velocity and reduce the possibility of coalescence in the top of the down-comer. The down-comer is sealed at the top to prevent any air from escaping. The down-comer contains three stator-impeller pairs to subject the slurry to sequential high intensity mixing steps prior to release into the calm region of the cell (see Section 3.2 for more details on the down-comer design).

When the particles and air bubbles exit the high intensity mixing down-comer, they enter a calm region (collection zone or outer tank) where gentle separation between the hydrophilic and hydrophobic particles can occur. In this region the hydrophobic particles that attached to air bubbles are able to rise to the surface. The rest of the minerals settle to the bottom of the cell where they can be removed as tailings, or recirculated back to the aeration chamber as slurry feed. Hydrophobic particles that detach from air bubbles in the collection zone can be collected by the stream of bubbles rising up in the cell. This will only be possible if these minerals still possess sufficient energy to break the streamlines surrounding the air bubbles. The hydrophobic minerals

that detach in this region that do not have sufficient energy for re-attachment will settle to the bottom of the cell with the rest of the hydrophilic minerals.

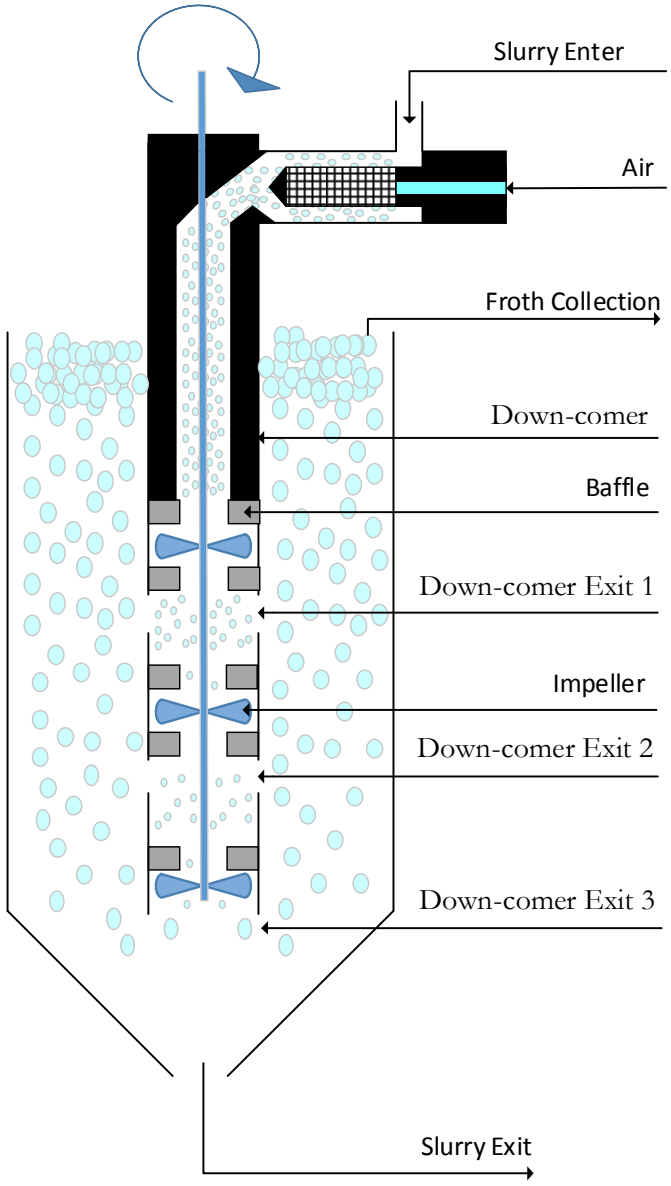

Figure 7: Basic cell design (not to scale)

Figure 8 shows the layout around the cell with the supporting equipment required for operation. Top-up water is added through a weir overflowing vessel to the collection zone in order to regulate the froth depth created in the cell. The tailings are removed and recirculated back to the aerator (feed) to operate the cell under batch conditions.

Table 5: Piping and Instrumentation Diagram equipment descriptions

A-101	C-101	P-101
Slurry, sintered medium aerator	Flotation cell	Pneumatic, positive displacement pump

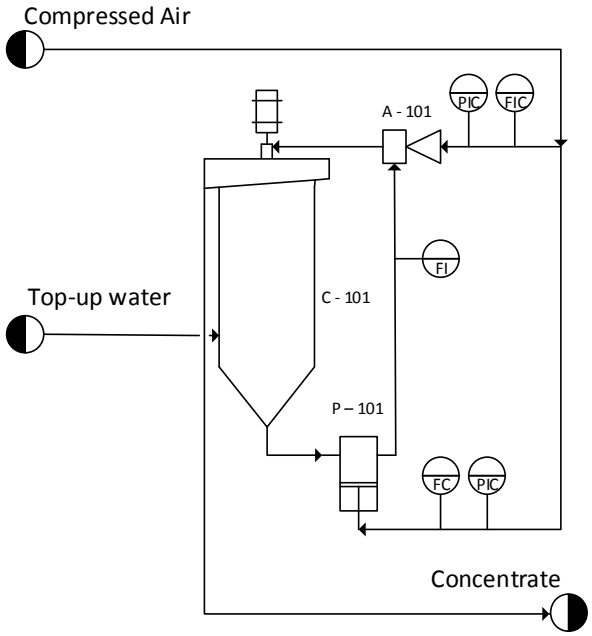

Figure 8: Piping and Instrumentation Diagram of the Novel Flotation Device Design

The slurry volume shows the active slurry volume through the whole system, including the column, cone, down-comer and circulation tubing (see Table 6). The column length was calculated by using the standard Perspex tube diameters available as well as the total slurry volume. The desired length to diameter ratio was greater than 3:1. This would improve the froth interfacial stability as well as the concentration gradient of valuable minerals vertically through the cell. The down-comer submerged depth is the depth from the top of the cell to the bottom of the down-comer. Enough space is left below the down-comer for bubbles leaving the bottom exit to change flow direction and rise to the surface. The active length is the length of the down-comer occupied with stators and impellers. This leaves enough space between the top exit and the froth interface so that the interface would not be disturbed. The impeller diameter was chosen to fit through the stators above and below each impeller for easier assembly. A small gap of 2 mm between the impeller tips and the down-comer wall will help to create a high shear environment in the impeller stations. Only four blades were used per impeller to allow enough open area between impeller blades so that slurry will be able to flow through each impeller without a significant pressure drop.

Table 6: Novel Cell Design Dimension

Parameter	**Dimension**
Slurry volume (L)	8
Column length (mm)	490
Column diameter (mm)	143
Cone depth (mm)	70
Down-comer outside diameter (mm)	40
Down-comer inside diameter (mm)	36
Down-comer submerged depth (mm)	400
Down-comer active length (mm)	270
Distance between exits (mm)	100
Impeller diameter (mm)	32
Impeller height (mm)	10
Number of blades	4
Number of impellers	3

The specifics of the design is handled through four separate headings and attention is focussed on the overall cell design, down-comer design, aerator design and the circulation system design in order to analyse the cell performance in a closed loop.

3.1. Overall Cell Design

The overall design of the cell eliminates short-circuiting of air, water and minerals. This effectively makes the cell a one-pass device with external recycle that enables full control over the number of volume replacements. The cell is designed to have a total active slurry volume of eight litres to be able to directly compare the results with the laboratory mechanical batch cells from an operating platinum plant. Larger cell volumes could also not be utilized since the ore handling capabilities of the experimental facilities were limited.

The overall cell (outer tank) incorporates a length to diameter ratio larger than 3:1 to ensure a concentration gradient throughout the depth of the cell; the concentration of valuable minerals will be highest below the froth while gangue minerals will be concentrated around the bottom of the cell. The depth of the cell also increases the chances of recovering valuable minerals as they move down in the cell. A smaller diameter cell ensures that the whole cell volume actively participates in the flotation process, eliminating dead volume.

The designed operating conditions can be viewed in Table 7. These parameters where chosen to create a desirable hydrodynamic environment within the cell; small bubbles well distributed through the cell, high intensity mixing for bubble-particle attachment and a calm zone for detachment of hydrophilic mineral particles and a stable froth phase. The industrial cells operated with a superficial gas velocity of 0.7-2.7 cm/s with bubble diameters of 1.3-2.7 mm. A superficial gas velocity range of 0.8-1.2 cm/s was chosen to operate in the lower ranges compared to the industrial cells. This would prevent that the slurry are 'blown out' of the cell. The focus will be on creating smaller bubbles than the industrial cells to ensure that the available bubble surface area for attachment would be maintained. Çinar (2007) states that the superficial gas velocity for Jameson Cells is normally around 1 cm/s with bubble sizes around 0.5 mm.

The superficial slurry velocity had to be higher to ensure that the bubbles would not coalesce while moving down the down-comer. A superficial down-comer slurry velocity for coal slime flotation was reported as 18.86 cm/s (Hacifazlioglu and Toroghu, 2007), while another study (Harbort et al., 2002) operated a value of 27.4 cm/s. As the platinum industry favours higher energy input, a superficial slurry velocity of 27.8 cm/s was chosen as the lowest starting point. The higher superficial slurry velocities were also needed to prevent coalescence of the smaller bubbles in the turbulent down-comer. Risk of coalescence within the down-comer could possibly be eliminated if the cell size is increased. The superficial slurry velocity in the bottom of the cell ranged from 1.76 to 2.64 cm/s due to the down-comer superficial slurry velocities, maintaining the length to diameter ration above 3 and keeping the cell total volume 8 litres. The combined superficial gas and slurry velocity at the top of the down-comer equates to 39.4-59.1 cm/s.

The theoretical power calculation (equation 4, Section 2.4.1) was used to determine the power consumption of the new flotation cell. The impellers had to be small to fit into the down-comer on lab scale, which meant that the impeller speed had to be high to achieve similar power input obtained through the industrial flotation cells. The highest attainable rotation speed in this cell is 1277 rpm without causing damage to the equipment. This was used as the upper limit and 680 rpm as the lower limit on mixing intensity that gave an impeller tip speed range of 1.14-2.14 m/s. This translates to a low theoretical power input of 0.06-0.41 W (calculated for the top impeller) that could not be confirmed with actual power measurements as the difference in current draw was insignificant on the 0.75 kW motor used. This power input is just for the impellers and not for the pumping power added to recirculate the slurry externally.

The mixing intensity and recirculation rate was adjusted during the initial runs to obtain better down-comer characteristics and a more stable froth interface. The values given in Table 7 are the final operating ranges used in the experimental run.

Table 7: Operating Conditions of the Novel Cell Design

Parameter	**Range**
Superficial gas velocity, J_g (cm/s)	0.8 – 1.2
Down-comer superficial slurry velocity, $J_{s,down\text{-}comer}$ (cm/s)	27.8 – 41.6
Cell superficial slurry velocity, J_s (cm/s)	1.8 – 2.6
Down-comer max. velocity ($J_g + J_s$: cm/s)	39.4 – 59.1
Theoretical Power (W, equation 4)	0.06 – 0.41
Theoretical impeller specific energy input (J/kg)	0.17 – 0.76
Total theoretical impeller power input (Wh/kg)	0.0052-0.0343
Impeller tip speed (m/s)	1.14 – 2.14
Aeration rate (L/min)	7.1 – 10.7
Recirculation rate (L/min)	17 – 25.4
Tank volume replacement time (s)	19 – 28
Mixing intensity (rpm)	680 – 1277

3.2. Down-comer Design

The down-comer is fitted with three stator and impeller stations to actively control the energy input and distribution through the cell. These stations ensure that the aerated slurry is subjected to high intensity mixing as it moves through the down-comer (refer to Table 7 for values). The high intensity mixing ensures a higher probability of particles having sufficient kinetic energy to break the bubble surface tension and attach to the air bubbles. A down-comer design was chosen to ensure that the high energy mixing zone is separated from the calm zone. The calm zone is required to ensure the detachment of gangue minerals and that a concentration gradient can be achieved vertically through the cell. The down-comer also ensured that no short circuiting of slurry is possible within the cell.

Smaller particles tend to follow the fluid lines around objects (Section 2.3.1), therefore high shear rates are needed to create eddies so the fluid lines are disturbed around the bubbles in the slurry. High shear rates are achieved between the stators and impeller in each impeller station by keeping the gap between them small. The higher shear rates also aid in bubble break-up to prevent coalescence within the down-comer. A stator is placed directly above and below each impeller in

every impeller station to further improve the shear rates generated within the down-comer by utilising both the top and bottom impeller edges. The stators also prevent slurry from spinning with the impellers inside the down-comer as this will decrease the effectiveness of the impellers to transfer kinetic energy to the slurry.

Since hydrophobic particles have a higher probability of attaching to bubbles, the down-comer design incorporates stage-wise release of aerated slurry out of the down-comer and into the calm zone of the cell. The stage-wise release helps to increase the concentration gradient of valuable minerals throughout the cell (in the ideal case) and prevents the contamination of mineralized bubbles before they reach the froth layer. This was another driving factor to have three stator and impeller stations, so that mineralized bubbles could be released to the calm zone as soon as possible.

Particles that did not attach to air bubbles in the first impeller and stators station can either exit at the top down-comer exit or move down the down-comer to the second impeller and stators station. It was found that the air bubbles tend to exit the down-comer as soon as possible, creating a crowding effect around the top exit and limits the amount of slurry that exits with the air bubbles. The second impeller and stator station provides another chance for particles to attach to the air bubbles. If weak hydrophobic particles attach to bubbles, they will be removed from the bubbles by the second impeller station that makes bubble surface area available for stronger hydrophobic particles to attach. Air bubbles and slurry have another chance to leave the down-comer below the second impeller station. The bubbles from the different down-comer exits gather to the same froth phase in the calm zone.

Smaller bubbles are entrained further down the down-comer because of their lower rise rates. These bubbles pass through the third impeller station to exit at the bottom of the down-comer. The third impeller and stators station acts as the stripping section of the down-comer, recovering all possible valuable minerals that could attach to the air bubbles.

The first down-comer design incorporated the down-comer exits in the impeller and stator stations, in line with the impeller. These exits were moved to below the impeller and stator stations through the initial trial runs to prevent jetting of the aerated slurry out of the down-comer into the calm zone (refer to Figure 9). These jets disturbed the froth interface and caused poor distribution of aerated slurry vertically through the cell. An insert was also installed in the top of the down-comer to improve the flow direction change from the aerator into the down-comer. The insert also reduced the amount of coalescence that occurred in the top of the down-comer.

The smallest possible hole size on the down-comer exits is four millimetres, ensuring that bubbles can leave the down-comer without any hindrance. Four millimetres was selected as the bottom limit since the largest bubbles created within the system is estimated at a maximum of two millimetres in diameter. Minimized hindrance to bubble movement ensures that bubbles will not coalesce, or that the minerals attached to the bubble surface will not be removed through contact with surfaces.

The open area at each down-comer exit was also calibrated through the initial trial runs to improve the stage-wise release of the slurry through the whole down-comer. The open area below each down-comer exit was adjusted experimentally at the mid-point operating conditions for good vertical distribution of aerated slurry. Changing the operating parameters within the cell affected the distribution of aerated slurry release from the down-comer to the calming zone.

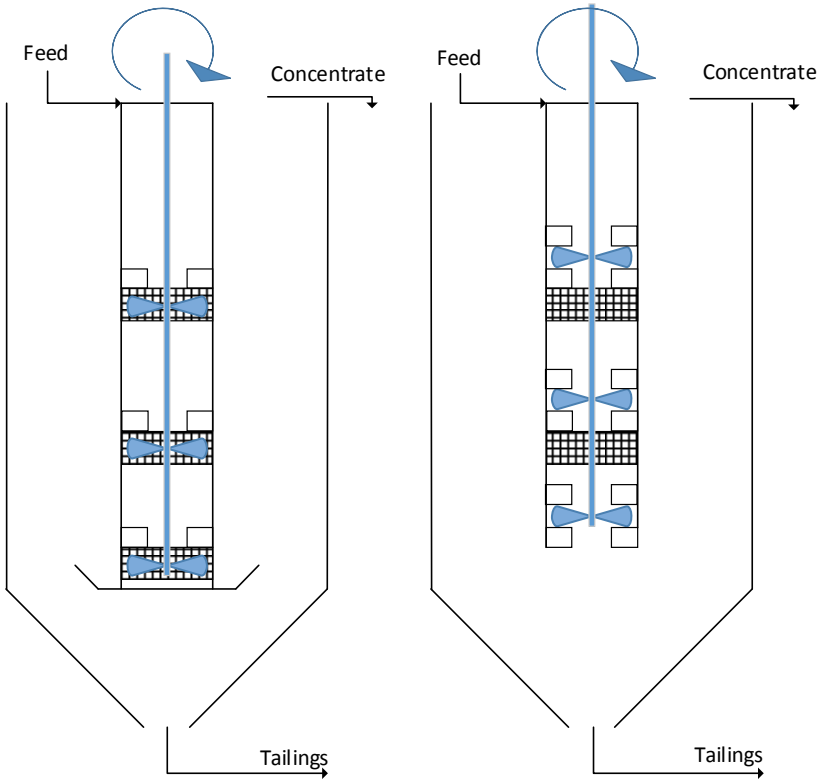

Figure 9: Initial Design (left) and Final Design (right) of the Novel Flotation Device

Quite a few down-comer designs could still be tested. The down-comer length, open area below each impeller station, distance between the impellers as well as the number of impellers can further be optimized. The feed position can also be changed to be from the bottom and re-aerating the slurry could also be investigated. Different impeller designs can be tested as well as the number of

stators used. The results of this design would give a good indication if the design should be further investigated or discarded. The hydrodynamics within the down-comer was greatly affected by adjusting the mixing intensity (680-1277 rpm), the superficial gas velocity (0.8-1.2 cm/s) and the down-comer superficial slurry velocity (27.8-41.6 cm/s). The down-comer design should be optimized after initial testing to improve hydrodynamics for the most favourable operating conditions.

3.3. Circulation Design

To effectively compare this cell's performance with laboratory bench tests of other mechanical cells, a closed system had to be implemented. This called for external circulation of the slurry, from the tailings back to the feed to operate the cell under batch conditions. Recirculation also reduced the amount of ore that had to be supplied and ensured that the ore handling capabilities of the specific laboratory was not surpassed.

Down-comer superficial slurry velocities between 27.8 and 41.6 cm/s were required in order to have sufficient velocity through the down-comer for air bubbles to stay in suspension and to prevent coalescence at the top of the down-comer. A pneumatic diaphragm pump was found to be the best option, capable of pumping high solids loading slurries at a wide range of flow rates. The recirculation rate could be controlled well by regulating the pressure and flow rate of the air feed to the pump. This allowed great flexibility in recirculation flow rates achieved through the cell. The diaphragm pump caused significant pressure pulsation in the system due to the nature of the pumping mechanism which was not feasible for the aerator.

A suction pulsation damper was installed in front of the pump. It consisted of an orifice, followed by an internally reinforced silicone hose to absorb the pulses. An externally reinforced silicone hose (reinforced by coiled wire around it) was also installed downstream of the pump, with an orifice at the end. This was found to be a simple solution to effectively dampen the low pressure pulsations of the pump without creating dead volume within the system. This method did not add significant volume to the system if compared to commercial suction stabilizers and pulsation dampers, although it worked on the same principle as a diaphragm or bladder pulsation damper. The pulsation dampers significantly reduced the pulsation in the recirculation system where no visible pulsation could be detected in the down-comer, or on the froth phase.

Half inch tubing was chosen for the recirculation system to minimize the volume occupied by slurry outside of the flotation cell. Average velocity within the pipes was above two metres per

second, preventing particles to settle out of suspension. Higher velocities within the pipes also ensured that particles of different size had the same approximate residence time within the system.

A flow meter was installed in the recirculation stream to monitor the recirculation rate since a stable, constant flow rate was crucial for the bubble generation in the aerator. Due to the abrasive nature of the slurry and the blocking effect of the particles, a non-intrusive flow meter was selected. The two options on these criteria were either an ultrasonic or magnetic field (mag) flow meter. Accuracy on the ultrasonic flow meters was very low due to the high solids loading of the slurry as well as the variance in mineral composition within the slurry.

The mag flow meter was chosen since it could handle the high solids loading while still maintaining high measurement accuracy and long term stability in the measurement. The accuracy of this specific flow meter type was 0.35% of the flow rate between 3-100 L/min.

Eliminating dead volume throughout the laboratory scale flotation system was very important. All of the ore in the system had to be circulated to ensure accurate representation of the cell performance with the typical low grades of UG2 feed ore being used. This influenced the way the system was loaded and evacuated. Valves with their connections created too much dead volume; therefore a simple 'T' piece valve was manufactured to drain the system after each run. Eliminating dead volume also had a significant influence on the aerator design process.

3.4. Aerator Design

Effective aeration of the slurry plays a significant role in the flotation process. Generated bubbles should have a small size and should be constant throughout the process. Bubble generation had to be separated from the mixing intensity and recirculation in order to effectively study the effect of aeration on the flotation cell performance. This called for an external aerator with forced aeration.

The venturi is often used in the industry for aeration of slurries, but its performance is affected by changes in slurry flow rates. The low volumetric flow rates would require a very small venturi which would cause a significant pressure drop. Different venturis would be needed for aeration at different recirculation rates. This could introduce more variables in the system that could introduce regulation problems.

A sintered (porous) metal aerator was used which is not as dependent on recirculation rate or mixing intensity. The pore size is around 5 μm which was still significantly larger than the slimes

in the slurry. This introduced blockage problems of the sintered metal while the system was loaded with slurry as the air feed to the sinter would be cut during this procedure.

Bypassing the aerator is not an option as the bypass cannot be flushed clean of minerals during operation. This meant that the slurry had to flow through the aerator at all times. The aerator body was designed in such a way that the sintered metal could be removed from the slurry during the loading process without creating any dead volume. When the loading of the cell is complete, the aerator can then be pushed back into the system to aerate the slurry (see Figure 10).

The sintered area exposed to the slurry was maximised to decrease the bubble size generated by the aerator. Slurry will flow on the outside of the sintered metal with air moving through the porous metal in order to achieve this. The gap between the sintered metal and the aerator body was also minimized to increase the cross flow of slurry over the sintered metal for bubble size reduction. The aerator exit was also attached directly on the entrance to the down-comer to minimize coalescence of the micro bubbles through the recirculation process and to ensure that the bubbles size reaching the down-comer was as small as possible.

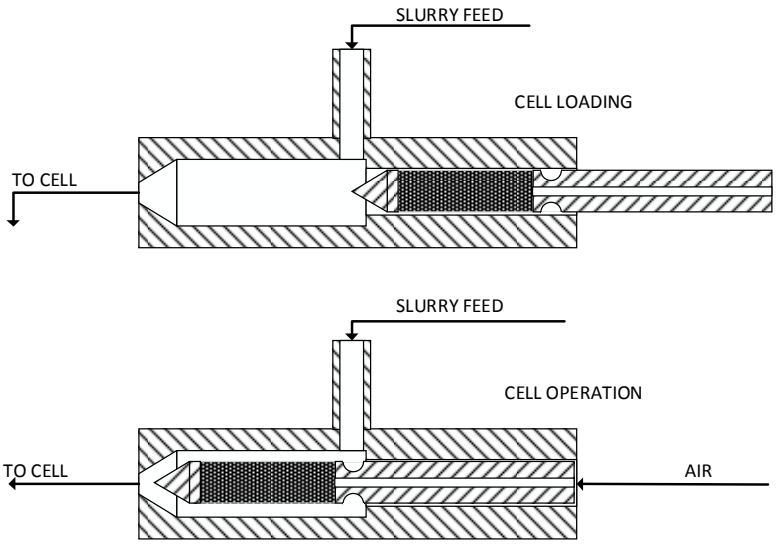

Figure 10: Aerator design: Cross section through the aerator while loading the cell and while the cell is in operation

The gap between the sintered metal and the aerator body were kept constant, which did not allow for expansion of the flow chamber as the slurry was aerated. This caused the flow rate of the aerated slurry to increase as it moved over the sintered metal, which ideally should be kept constant

to reduce pressure drop over the aerator. No expansion in the flow chamber was introduced since variable air and slurry flow rates will be investigated and a specific expansion may negatively influence one set of operating conditions while being beneficial to another.

Through initial testing it was discovered that there was a significant pressure drop over the aerator, especially with a combination of high air and slurry flow rates. Bubbles expanded as they exit the aerator which caused bubble coalescence. This would be the case with any aerator design used due to the placement of the external aerator. It was found that the first station in the down-comer effectively reduced the bubble size again, which made the aeration mechanism successful. Increasing the gap between the sinter and the aerator body proved to reduce the pressure drop through the aerator.

Blocking of the sinter in the aerator occurred after repeated use. A cleaning technique was developed to clean the sinter (Section 8.4). This blockage proved that the available surface area of the sintered metal was more than enough for the aeration requirements by the system. This could be seen by the pressure difference between the slurry and the air through a clean sinter aerator.

The air flow to the aerator had to be controlled and monitored to ensure that the aeration rate stayed constant throughout the experimental run, which ensured high accuracy when quoting superficial gas velocities. A rotameter with a magnetic pick-up was bought from Yokogawa. The measurement accuracy rating of this specific rotameter was class 4 according to the relevant accuracy directive VDI/VDE 3513 sheet 2. This relates to a 4% full-scale range measurement error. The magnetic pick-up ensures that the flow meter body can be manufactured out of stainless steel to be able to endure the process pressure of 8 bar (g), while still providing an accurate dial display. The flow meter also provided a 4-20 mA output for possible automation purposes in the future.

The operating pressure of the flow meter was at 1 bar (g) where the flow could be controlled with a needle valve on the flow meter feed. Since this was above the slurry pressure within the aerator, a pressure gauge was fitted after the flow meter, followed by a needle valve. The second needle valve was used to choke the air flow to the aerator and ensured the flow meter operated at the calibrated pressure to give a reading as accurately as possible on the air flow to the cell.

Adding a pressure regulator on the air flow to both the air pump and the air supply to the aerator ensured that the pulsation effect from the air pump could be eliminated in the aerator.

Chapter 4 – Experimental Methodology

The experimental methodology is discussed according to the following process steps: preparation of the ore, preparation and dosing of chemicals, operating variables under investigation, sampling and sample preparation for analysis.

4.1. Ore Preparation for Flotation

The correct milling times and solids loading in the mill had to be established in order to obtain 75% particles with <75 µm size. This was achieved by firstly varying the water content while keeping milling time constant. A mill solids loading of around 68% (w/w) gave the best results. The milling time was then varied to obtain the required passing rate.

The froth flotation cell had to be operated at a solids loading of 30% (w/w) to obtain the same solids loading used in the PGM industry. Liberation characteristics in the laboratory mill may have been different from the full-scale plant milling circuit, due to different mill dimensions, loading and run times. Unfortunately, specifics regarding liberation and the mass fraction valuables in different size ranges could not be compared to industry data, due to limited availability of such data. Figure 11 illustrates the percentage solids passing 75 µm against the milling time. A time of 225 minutes resulted in at least 75% passing 75 µm.

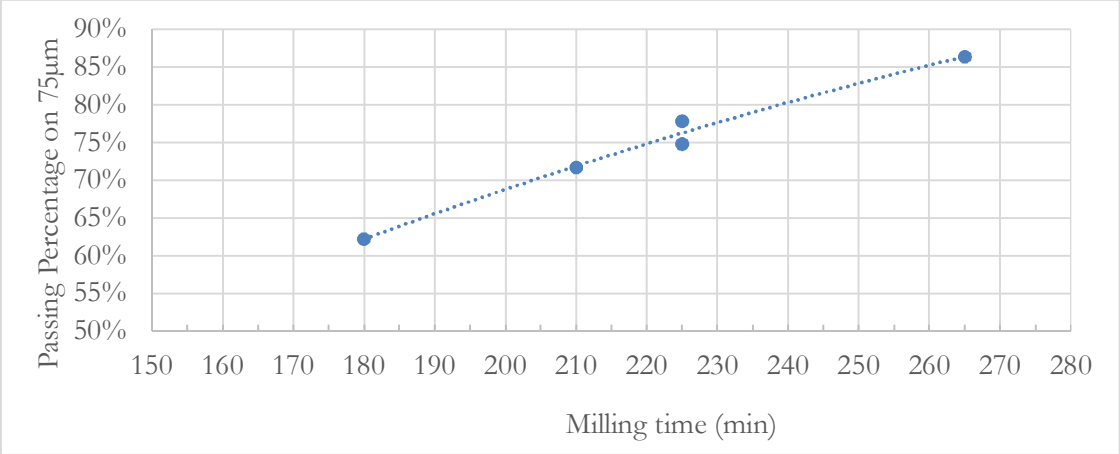

Figure 11: Milling curve of the laboratory rod mill to establish sufficient milling time in order to enable 75% solids to pass 75 µm.

Figure 12 illustrates the particle size distribution (PSD) of the slurry after milling. The finer (-38 µm) fraction created by the mill was just below 35% of the total solids, which may have had a negative effect on the flotation behaviour of the cell. Finer particle sizes are more difficult to separate due to inertial force effects explained earlier (Section 2.3).

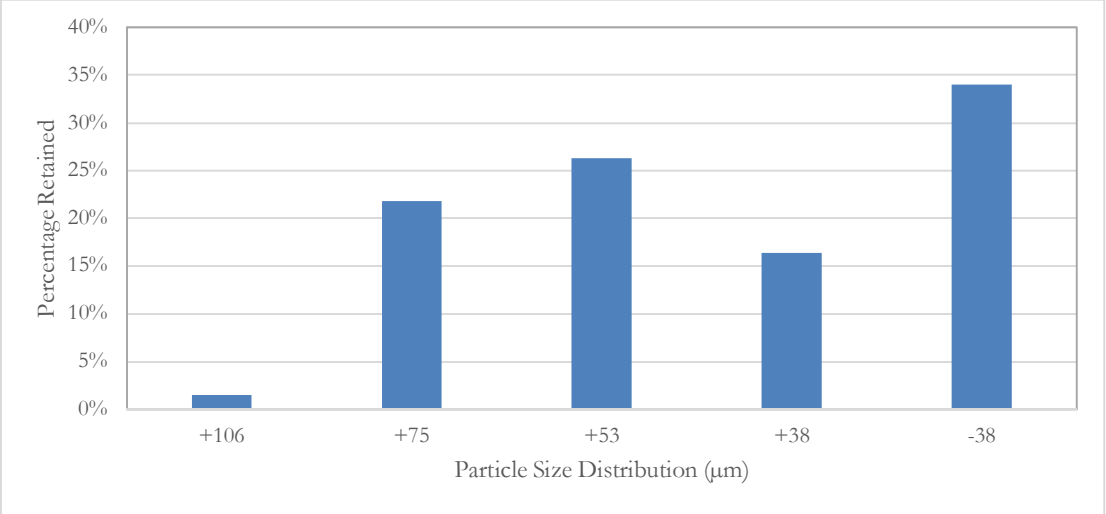

Figure 12: Particle Size Distribution after milling, showing the mass percentage retained on each sieve size

The mill was loaded with 2961 grams of ore and water was added to obtain a solids loading of 68% (w/w) in the mill. The mill was stopped after 225 minutes and an additional 100 ml of water was added to improve cleaning of the mill. The mill was then switched on for another minute to help cleanse the rods. Here the whole mill was transferred to the flotation cell, decanted and the mill contents were washed out. The mill design (Appendix D) allowed good cleaning of the mill to ensure that all the mineral slurry was transferred to the flotation cell. Detailed ore preparation procedures are shown in Appendix D.

4.2. Preparation and Dosing of Chemicals

Reagents were prepared by dissolving the correct amount of each specific reagent in a set volume of water. A specific volume of this solution for each reagent was then added to the flotation machine so that the flotation cell could operate at the same reagent concentrations used in the PGM industry. The reagents used in this study, compared to that in industry, can be seen in Table 8 where the copper sulphate acts as an activator, the Norilose is a Carboxy Methyl Cellulose (CMC) depressant, the sodium n-propyl xanthate (SNPX) is the collector and the Senfroth 200 is a frother. The copper sulphate was supplied by Merc™ and the collector, depressant and frother was donated by Senmin™.

Table 8: Reagent concentrations used in this study compared to industry, as well as the addition residence time used for each reactant before initialising the experiment

	Copper Sulphate	Norilose 8058	SNPX	Senfroth 200
Typical industrial reagent dosage (g/t)	40	60	150	22
Experimental reagent dosage (g/t)	40	60	150	33
Residence time (minutes)	5	2	2	1

Through initial slurry runs it was found that the frother concentration was too low to sustain a stable froth for effective mass pull to the concentrate. This could be due to the fact that the water used in the experiments were reverse osmosis water, while the plant batch tests ran on water with more dissolved solids. The reverse osmosis water was chosen to remove any effects that different salts will have on the flotation process and froth creation. As the new flotation cell was used in the rougher duty, the focus was mainly on improved recovery followed by high grades and chromite rejection. Literature have shown that increasing ion concentrations will improve recovery and froth stability, while increasing water recovery and decreasing the recovery of naturally floated gangue (discussed in Section 2.2). As the laboratory tap water was significantly different to the tap water used in the batch cell tests at the PGM plant (which was also different from the plant water), reverse osmosis permeate was chosen - simulating relatively poor recovery conditions for the cell. As this study did not focus on improving the chemical environment within the cell, this was thought to be a good starting point that could also be repeated elsewhere.

Since reverse osmosis permeate was used, the frother concentration was increased to improve the mass pull to concentrate and thereby obtain higher recoveries of valuable minerals (refer to Table 8). The 50% increase in frother was also based on the fact that this was a one pass system where most of the frother was removed from the cell within the first few minutes.

This cell was tested with only a specific amount of frother used. Therefore the total amount of frother is dosed with the other reagents at the beginning of the experiment. The top-up water contains no frother or any other reagents and the frother and reagents are therefore diluted over time by the water addition. With no frother addition the cell is analysed as a bank of cells in series where the tailings from the one cell flows directly into the next cell. This choice was made in order to highlight the effect of combined conditions within the cell; if mixing intensity is insufficient then the frother will be removed from the cell without a high recovery of valuable minerals or if aeration is too high the frother will be removed from the cell without a high recovery. These effects will not be seen when additional frothers are continuously added to the system. Dosing water with

a specific frother concentration also adds more frother to the cell that would result in differences in the total amount of frother dosed for every run as each run will have different water carry-over characteristics. Frother addition also improves the recovery of the cell and therefore the worst conditions are tested when frother addition does not occur.

Reagents were added to the froth flotation cell by means of a small tube built into the recirculation stream to ensure that the reagents will be mixed throughout the cell as quickly as possible. The slurry volume was increased to around 7.8 litres after the cell was loaded with milled ore by adding water through the froth level control vessel. The reagents were then added in a specific order with different residence times which was developed by industry. The order and residence times before the flotation separation commences can be seen in Table 8.

When the residence time for the reagent mixing completed, the air to the aerator was opened while the sintered medium of the aerator was pushed into place. The last few millilitres of water was then added to the cell to ensure that a froth depth of maximum 10 mm are created by continuously adding water to the level control vessel. The control vessel had a weir overflow that regulated the froth depth by only adding water to the cell if the froth depth increased above 10mm.

4.3. Operating Variables under investigation

There are a significant number of factors that can be influenced to improve the recovery of valuable minerals to the concentrate, as well as the concentrate grade. However, this study focused on designing a new cell primarily to improve the hydrodynamic environment for fines flotation. The design of the cell focussed on increasing separation and valuable mineral recovery to concentrate by utilizing a specific down-comer and aerator design. This down-comer and aerator design attempted to focus the energy input (i.e. high shear rates at point of aeration) on consecutive points in the down-comer, with subsequent systematic release of air bubbles into a calming zone at different heights below the froth. As demonstrated during initial verification runs, the operating parameters that influenced the operation of the down-comer system most were the mixing intensity (energy input), superficial gas velocity and the recirculation rate (superficial slurry velocity in the down-comer and in the bottom of the cell).

A Box–Behnken factorial design was used to evaluate these three factors at three different levels. Table 9 shows the levels at which the different factors were tested. The mixing intensity was controlled by varying the electrical frequency of the mixer motor between 35 and 65 Hz. The relationship between frequency and RPMs were not perfectly linear, causing the intervals on RPM to be slightly skewed.

Table 9: Box-Behnken experimental design with the different levels tested in the new cell

Run Identifier	**Mixing rpm**	**Cell Superficial Air Velocity (cm/s)**	**Recirculation Rate (litre/min)**
1	680	0.8	21.2
2	680	1.0	17.0
3	680	1.0	25.4
4	680	1.2	21.2
5	975	0.8	17.0
6	975	0.8	25.4
7	975	1.0	21.2
8	975	1.0	21.2
9	975	1.0	21.2
10	975	1.2	17.0
11	975	1.2	25.4
12	1277	0.8	21.2
13	1277	1.0	17.0
14	1277	1.0	25.4
15	1277	1.2	21.2
16 (frother increase)	975	1.0	21.2

A randomized run order was used to minimize the effect of systematic errors during the experiments. Table 9 shows the number identifier for each run in order to facilitate easier discussions. These numbers were allocated according to increasing mixing intensity and superficial gas velocity. Table 10 converts the factor levels given above to more useful conditions within the cell; mixing intensity was converted to theoretical power input, recirculation rate was converted to the down-comer and cell superficial slurry velocity at the different factor levels. However, recirculation rate, superficial gas velocity and mixing intensity will also still be used to refer to operating conditions within the cell, as these factors were directly manipulated in the experiments.

Table 10: Correlations between mixing intensity and theoretical power as well as recirculation rate, down-comer and cell superficial slurry velocity.

Factor Level	Mixing Intensity (rpm)	Theoretical Power Input (W)	Recirculation Rate (litre/min)	Down-comer Superficial Slurry Velocity (cm/s)	Cell Superficial Slurry Velocity (cm/s)
Low	680	0.06	17	27.8	1.8
Medium	975	0.181	21.2	34.7	2.2
High	1277	0.41	25.4	41.6	2.6

The mid-point operating conditions were repeated through the experimental design (runs 7, 8 and 9) and these results were used to determine the experimental confidence interval. The effect of frother concentration on the operation of the cell was also demonstrated under these conditions. This was done by increasing the frother dosage by 20% in one run (run 16) to show the related effect on recovery and grade due to higher mass pull. All other factors were kept constant at the mid-point conditions similar to runs 7-9.

Another set of experiments was performed to evaluate the ability of the cell in separating fines effectively. Four experiments were done as a set at the same factor levels, in order to produce enough concentrate mass in each size fraction for analytical purposes. Table 11 shows the factor levels where each set were completed.

Table 11: Independent factor levels used for fines separation experiments

Standard Run (No)	Mixing (RPM)	Superficial Gas Velocity (cm/s)	Recirculation Rate (L/min)
40	975	1	17
20	975	1	21.2
30	975	1	25.4

All the concentrate samples from each experimental set were combined according to the sample number. In other words, all four one-minute samples, all four three-minute samples and so on, were combined. The combined sample was then screened in a laboratory sieve set, with aperture sizes of 75, 53 and 38 micrometres to determine the mass split in the concentrate per size fraction. All the minerals that were retained by a sieve were washed out into a specific tray and dried. The tray mass was recorded beforehand and the dried mineral mass was recorded after the drying process.

All concentrate samples with a low mass was combined according to their size ranges in order to achieve an analysable sample mass. Samples were only analysed alone if all of the samples across the different concentrate sample times (1, 3, 8 and 15 minutes) had a high enough sample mass to be analysed alone. This was mostly the case for all the samples below 38 μm, as each sample at the respective time interval had a significant number of particles below this size.

It should be noted that the runs in Table 9 was only done once, with no combinations between different runs. Only the runs in Table 11 were repeated to obtain enough mass for recovery analysis per particle size.

All these experiments contributed to the evaluation of the froth flotation cell's performance with regards to concentrate mass pull, concentrate grade, valuable mineral recovery as well as the recovery of valuable minerals with regards to particle size

4.4. Sampling and Sample Preparation for Analyses

The time of the separation experiment started the moment the first mineral froth overflowed the cell weir into the concentrate collecting vessel. Froth was then continuously scraped off to prevent froth bubble coalescence and bursting. Bursting bubbles flings the attached minerals in any possible direction. Scraping the whole froth interface in one sweep was impossible due to the placement of the down-comer in the centre of the cell. For scraping purposes, the froth surface was divided in four and scraped every eight seconds on average. Sample containers were removed at specific intervals in order to study the recovery and grade of the samples over time. The first concentrate collection tray was removed after one minute, followed by the others at three, eight, 15 and 30 minutes. These time intervals were chosen to match the time intervals generally used in batch cell tests and to split the collected mass as evenly as possible between the collection trays.

The collection launder was carefully flushed with water (by spray bottle) prior to each collection tray's removal. The wet mass of each collection tray was recorded, as well as the mass of water used to spray the trough. At completion, the whole froth flotation cell was drained of slurry and rinsed, thereby forming the tailings portion of the experiment. The tailings were de-watered through a filter press before the tailings and the concentrate samples were dried in an oven.

Dried concentrate sample masses were recorded before being bagged and labelled for analysis. The dried tailings cake was carefully broken up and thoroughly mixed before a representative sample of 200-300 grams were collected by the following sampling technique. The whole sample was spread out on brown paper and mixed thoroughly by using a systematic and repetitive fold-over

method. The final sample was then collected from eight spread-out points and this representative tailings sample was bagged, labelled and sent for analysis.

Chapter 5 – Results and Discussion

This chapter provides a systematic evaluation of the performance of the flotation cell, bearing in mind that an extensive set of flotation test results was not produced. After consideration of the statistical model results as well as the repeatability of test results, the mass pulls to the concentrate for both solids and water at various test conditions are discussed. Thereafter, the recoveries of valuable minerals and chromite to concentrate, as well as concentrate grades are presented. These results are subsequently used to show how the cell created an effective hydrodynamic environment for froth flotation.

5.1. Statistical Evaluation of the Experimental Results

A significant number of runs with varying factors need to be completed in order to establish the performance of the cell. By using an experimental design, some sensible characterization can be done with far less runs at different conditions. The risk of using a statistical model on minimal data lies in the accuracy of the prediction and that the model cannot necessarily show peaks and minima in between the points tested.

The evaluation was completed using a box-Behnken experimental design. This design can formulate an experimental model with the least amount of information provided. Against this background, after design and construction of the cells, this study only entailed an early evaluation of the cell's performance and it therefore did not produce absolute results over the full range of operating conditions. Rather, it offered preliminary insight into the cell's behaviour over sensible ranges of the three operating factors. The model therefore should only be used to predict general trends and it should also be noted that results from a box-Behnken design cannot be extrapolated outside the area that was tested. The test points are displayed as blue circles on the surface plots of the model prediction, as showed in subsequent graphs.

The final mass pull to concentrate, water recovery, valuable metal recovery, grade and chromite recovery is used in this statistical analysis to analyse the performance of the cell.

From the analysis (see Section 8.3 for analysis results) it is evident that superficial gas velocity and recirculation rate had a meaningful impact on mass pull and water recovery. Interestingly there appears to be no linear interactions between the manipulated variables, but the analysis suggests that there are higher order interactions between mixing intensity and superficial gas velocity, as well as between superficial gas velocity and recirculation rate.

The analysis also indicates that there are no significant correlations between any of the manipulated variables and chromite recovery. From the quadratic ANOVA analysis, it follows that some interaction between mixing intensity and chromite recovery is evident, although this effect is most probably not too significant.

The 4E recovery is notably influenced by the recirculation rate, but no other manipulated variable seem to have a significant effect on recovery, not even at higher order interactions. At this point it must be stressed again that these predictions cannot and should not be extended outside the test ranges of manipulated variables. For example, in the extreme case it is evident that a zero rate of aeration should deliver zero recovery, which means that there will indeed be aeration rates that may influence 4E recovery notably.

The 4E grade can be influenced by all three manipulated variables, where a higher order interaction seems to exist between mixing intensity and recirculation rate.

These interactions are unavoidable in the design of the cell, as the combination of slurry recirculation rate and superficial gas velocity will influence the velocity and retention time in the down-comer. The velocity in the down-comer determines the residence time of the aerated slurry in the high intensity mixing zones created by the impellers. The energy transferred from the impellers to the slurry is therefore dependant on the residence time of the slurry in the various mixing zones, as well as on the impeller speed. The magnitude of this effect should be investigated further in future studies.

5.1.1. Valuable Metals (4E) Recovery Analysis

This cell was tested with the same feed as for the rougher circuits on an industrial PGM plant. In these circuits high recovery is the most important factor for optimization, since the grade and chromite rejection can be improved via the upgrading cleaner and scavenger circuits. The results are compared by plotting the recovery prediction against recirculation rate (litre/min) and the superficial gas velocity (cm/s). The mixing intensity (rpm) is changed from low to high in Figure 13 to Figure 15 respectively. The profiles of the recovery zones in Figure 13 and **Error! Reference source not found.** are very similar, although recovery values of each zone are slightly higher at medium mixing intensity.

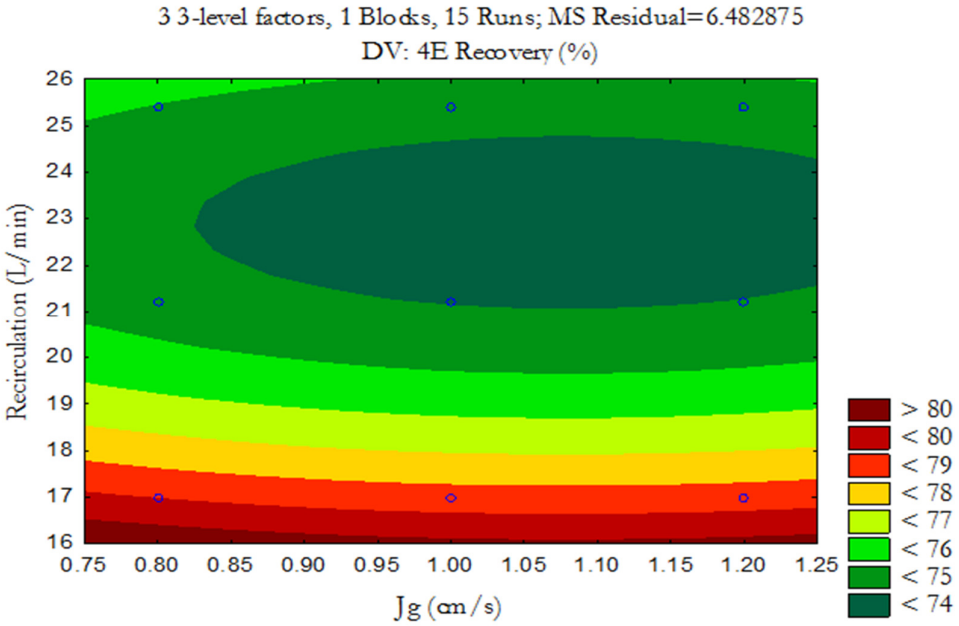

Figure 13: 4E Recovery surface with varying recirculation rate (l/min) and superficial gas velocity (cm/s), while maintaining a constant mixing intensity (680 rpm)

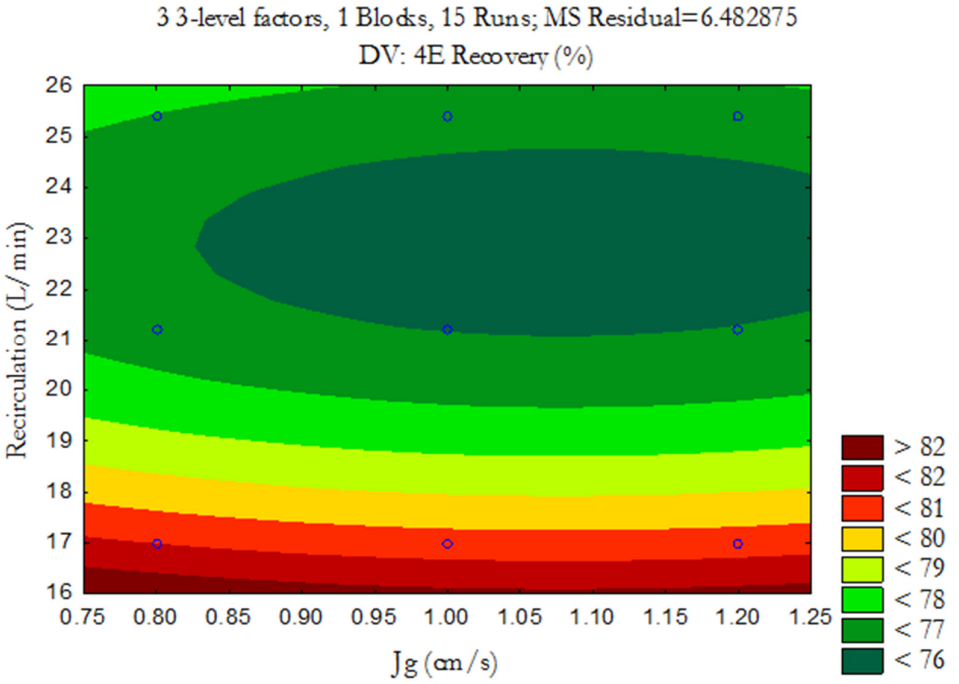

Figure 14: 4E Recovery surface with varying recirculation rate (litre/min) and superficial gas velocity (cm/s), while maintaining a constant mixing intensity (975 rpm)

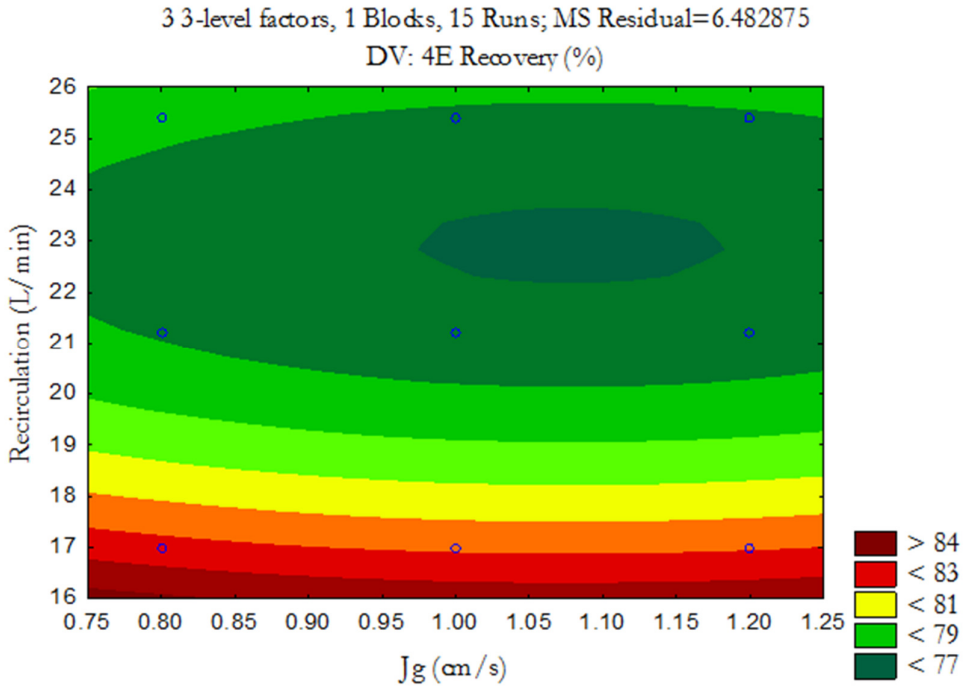

Figure 15: 4E Recovery surface with varying recirculation rate (litre/min) and superficial gas velocity (cm/s), while maintaining a constant mixing intensity (1277 rpm)

The recoveries from Figure 15 show an increase compared to the lower mixing intensities, with a decrease in the profile of lower recoveries. Figure 13 to Figure 15 confirms visually that only recirculation rate plays a significant role in the recoveries within the range tested. A 6% increase in recovery can be achieved through decreasing the mixing intensity from 23 litre/min to 16 litre/min in most cases.

These figures show a minima around a recirculation rate of 23 litre/min, where an increase in recovery can be achieved by either increasing or decreasing the recirculation rate. Since an increase in recirculation rate means higher energy input as well as an increase in total flotation cell volume (to achieve sufficient residence times), it will therefore be more feasible to decrease the recirculation rate for higher recoveries. The mean squared error of the valuable metals recovery is around 6.5, which decreases the confidence in the actual values displayed.

5.1.2. Valuable Metals (4E) Grade Analysis

The 4E grades in the concentrate of rougher circuits are optimized after an acceptable recovery is achieved and grades are generally sacrificed to achieve acceptable recovery. However, obtaining operating conditions in the cell where a high recovery can be obtained together with a high grade, would be considered an ultimate success. The mean squared error of the model for 4E grade prediction is 250 ($g^{0.5}/t^{0.5}$), indicating that the model could not predict the concentrate grade

accurately. This is most likely due to significant noise in the data and more data points are needed to improve the prediction.

5.1.3. Chromite Recovery Analysis

Chromite forms an inactive layer at the bottom of the furnace (spinel), reducing the furnace capacity and ultimately reduces the furnace campaign life (Barnes, Newall 2006). The furnace campaign life is reduced as a result of utilizing higher power intensities to physically mix the chromite within the furnace in order to remove it from the furnace. The higher energy input increases the refractory wear within the furnace, causing the refractories to fail prematurely. A decrease in chromite recovery in the rougher circuit means that the chromite rejection load on downstream processes or circuits can be reduced, with the possibility of reducing the chromite content in the smelter feed material.

The test results are compared by plotting the chromite recovery prediction against recirculation rate (litre/min) and the superficial gas velocity (cm/s). The mixing intensity (rpm) is varied from low (Figure 16) to medium (Figure 17) to high (Figure 18).

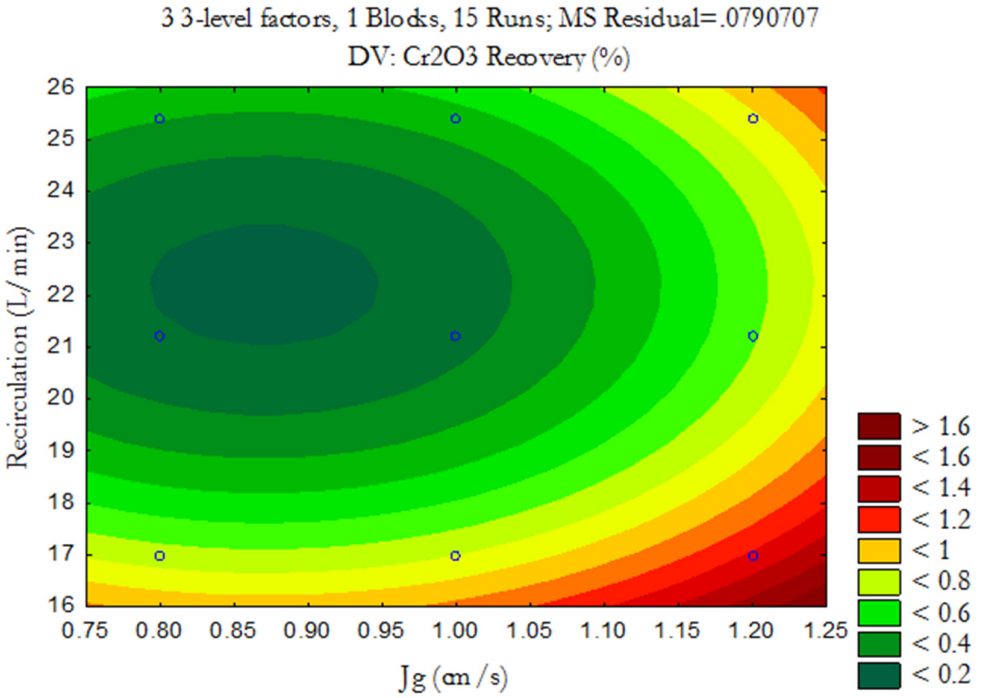

Figure 16: Chromite recovery surface with varying recirculation rate (litre/min) and superficial gas velocity (cm/s), while maintaining a constant mixing intensity (680 rpm)

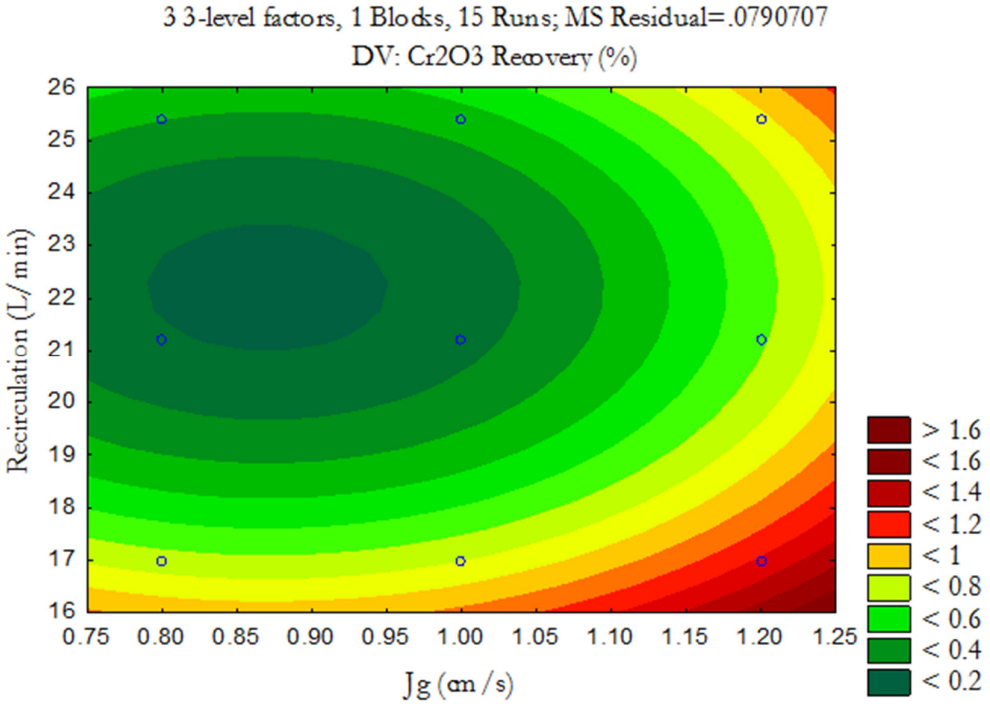

Figure 17: Chromite recovery surface with varying recirculation rate (litre/min) and superficial gas velocity (cm/s), while maintaining a constant mixing intensity (975 rpm)

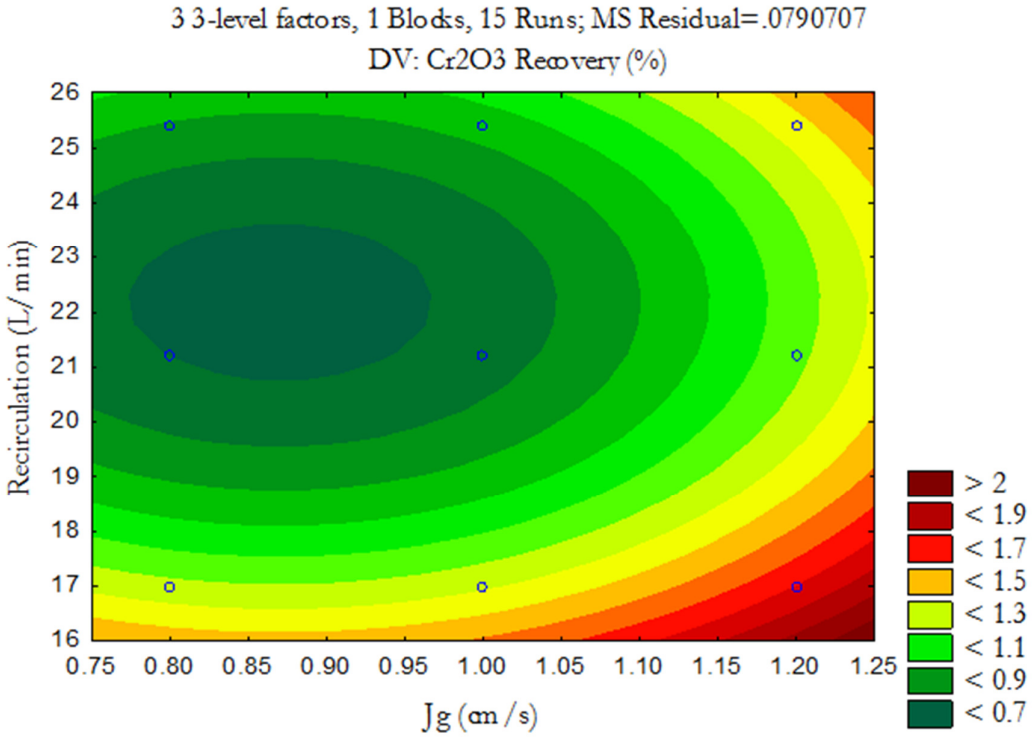

Figure 18: Chromite recovery surface with varying recirculation rate (litre/min) and superficial gas velocity (cm/s), while maintaining a constant mixing intensity (1277 rpm)

Figure 16 to Figure 18 show that the mean squared error of the chromite recovery estimate is small, implying that the model prediction is relatively accurate over the selected range. It should be noted that the statistical evaluation of the data indicates that none of the manipulated variables had a significant effect on chromite recovery. A slight increase in chromite recovery can still be seen with an increase in mixing intensity from medium (Figure 17) to high (Figure 18), although the position of the minima stays the same with respect to recirculation rate and superficial gas velocity.

The model predicts that the best operating conditions for chromite rejection is around a recirculation rate of 22.3 litre/min with a superficial gas velocity of 0.85 cm/s, where the mixing intensity can be between 680 and 975 revolutions per minute.

Combining the results from the 4E recovery as well as the chromite recovery predictions, the optimum conditions can be established. Assuming that, in a rougher circuit, 4E recovery is more important than chromite rejection, the conditions were chosen in this order of importance.

The model predicts that valuable metal grade and recovery are at the exact opposites of the energy input, where high recoveries are achieved at high energy input and low recirculation rates (i.e. by increasing the residence time and unit energy input to the aerated slurry in the down-comer, as well as by decreasing downward drag forces in the cell). Conversely, high grades are achieved by low mixing intensity with high recirculation rates (i.e. by reducing the residence time and unit energy input within the down-comer, as well as by increasing the downward drag forces in the cell). The best chromite rejection overlaps slightly with the high valuable metal grade and can still be achieved with a slightly lower recirculation rate and slightly higher mixing intensities.

The superficial gas velocity had an optimum point between 0.9 and 0.95 cm/s irrespective of the mixing intensity. As such, a good point for initial operation seems to be at this superficial gas velocity with medium mixing intensity and a recirculation rate between 17-18 litre/min. The closest runs to these conditions were run 5 and 13 (the operating conditions are summarized in Table 12). This operating point will achieve a sufficient initial valuable metal recovery, while still maintaining sufficient 4E grade and good chromite rejection. It should be noted that this operating point assumes the whole rougher circuit runs at these conditions. Better conditions can still be achieved by optimizing all the operating conditions related to the cell performance.

Ultimately the final decision will rest on an economic analysis where the capital cost of the whole separation circuit is weighed against related operating cost and production performances. Achieving an initial high 4E grade concentrate with low chromite grade in the rougher circuit

means that the resultant concentrate stream could potentially bypass some cleaner circuits. This may unfortunately affect the size of the scavenger circuits, which are required to achieve an overall high recovery. If a high 4E recovery is obtained through the rougher circuit then the cleaner circuit will have to be larger in order to handle the larger throughput of rougher concentrate and to obtain a sufficient chromite rejection.

Table 12: Optimum operating conditions determined through the initial evaluation of the flotation cell

Parameter	**Value**
Mixing Intensity (rpm)	975-1277
Superficial gas velocity (cm/s)	0.8-1.0
Recirculation rate (litre/min)	17
Superficial slurry velocity in bottom of cell (cm/s)	1.76
Down-comer superficial slurry velocity (cm/s)	27.8
Total theoretical power input (Wh/kg)	0.0153-0.343

5.2. Repeatability Analysis of the Flotation Cell

Tests at mid-point operating conditions were repeated twice in accordance with the box-Behnken experimental design. The results from these runs could also be used to indicate the repeatability of the experiments. Although care was taken to reproduce the run conditions, small variations still occurred through the loading process and in maintaining the froth depth of the cell, especially in the first three minutes of operation. The start time of the experiment was recorded when the first froth started to overflow to the concentrate. Since these runs experienced slow initial froth build-up, the delay between the recorded start time and the time when the air was opened will be different between these runs, having an effect on the recovery obtained in the first minute. The effects of these changes reduced as the run continued towards 15 minutes.

Figure 19 shows recovery-grade profiles for mid-point repeat runs. The recovery obtained in the first minute seems to have an effect on the total run recovery. Run 7 had the highest initial recovery as well as the highest total recovery while run 9 was the complete opposite. The rate of change for run 7 is different from the rest, where the initial grade should have been higher to have similar trends to runs 8 and 9. This is the result of a too shallow initial froth (due to a slow froth build-up).

The repeatability improved as the runs continued. The initial (close to start of run) accuracy was ±4.3% for 4E recovered to concentrate, but it improved to ±2.65% at the end of the runs. The

initial accuracy for concentrate grade was ±34.6 g/t, but it improved notably to ±4.15 g/t at the end of the run. These results illustrate the sensitivity of the cell to changes in froth depth, small loading variations and dosing of the chemicals, especially at the beginning of the experiments. The statistical 95% confidence interval was calculated from these three mid-point runs using t-statistics and plotted as error bars in the figures. The confidence interval was calculated for all the time intervals and plotted accordingly. The 95% confidence interval is quite wide and may have been narrower if more repeats of the mid-point conditions were considered. The process could also be further automated to remove noise created by small operational variations. Furthermore, this measured sensitivity could be partly due to the fact that the flotation cell performance was not measured under steady state, but rather through batch-like operation, including a combination of high-grade (start of run) and low-grade (end of run) feed conditions.

The averaged results of these three mid-point runs compare well with the individual results from run 8. As such, runs 7 and 9 can be seen as two possible extremes, with run 8 generating a median result.

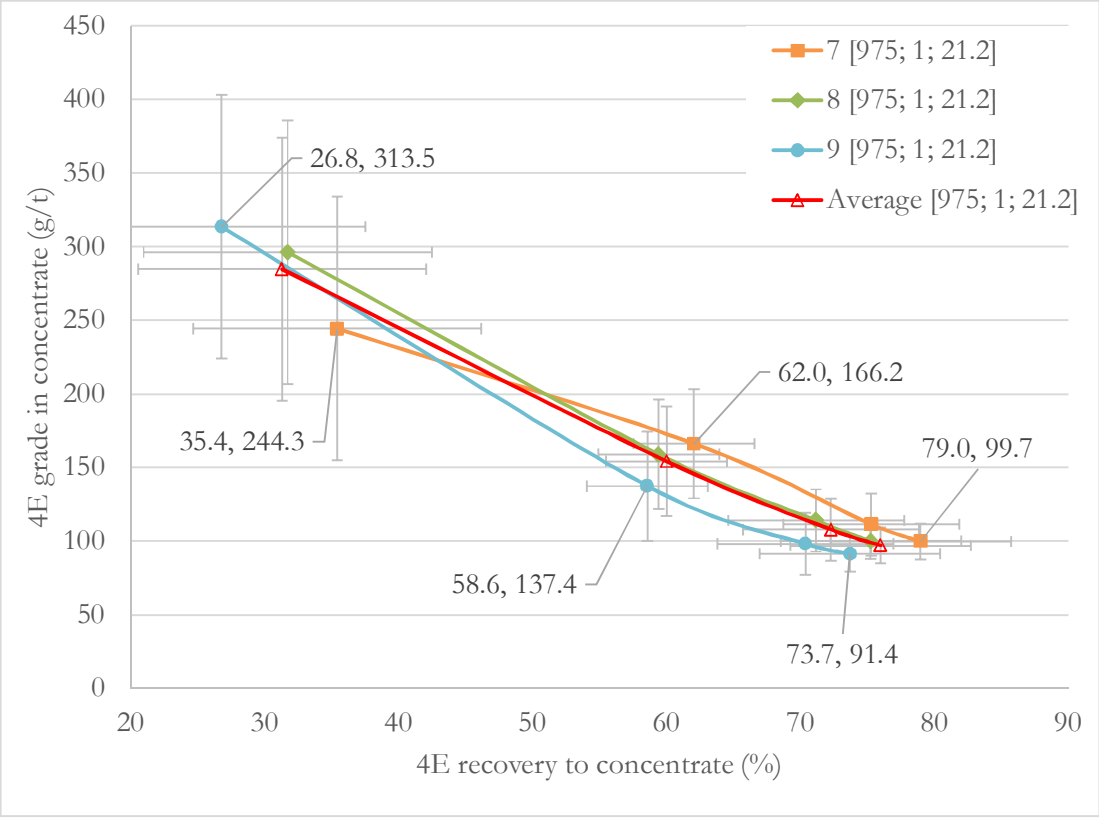

Figure 19: 4E grade vs. recovery for mid-point repeats; where the mixing intensity (rpm), superficial gas velocity (cm/s) and recirculation rate (litre/min) was kept constant. The legend indicates run number [rpm; cell superficial gas velocity; recirculation rate].

Chromite and water recoveries for these three runs are shown in Figure 20. Initially runs 8 and 9 have very similar water recoveries, but they deviate from one another as the runs progress. The initial water recovery of run 7 is significantly higher than in runs 8 and 9, due to the shallow froth layer. Chromite recoveries of runs 8 and 9 are very similar, while such recoveries are constantly higher in run 7. Since the initial water recovery was higher in run 7, the higher chromite recovery can be explained through entrainment at the lower froth height (explained in Section 5.4.4). The repeatability for chromite recovery was constant throughout the runs at ±0.054% while the repeatability for water recovery worsened from ±35.4 to ±47.3 g. It should be noted that the accuracy for water recovery could also be lower due to the addition of spray water to the launder (although this volume was subtracted again afterwards).

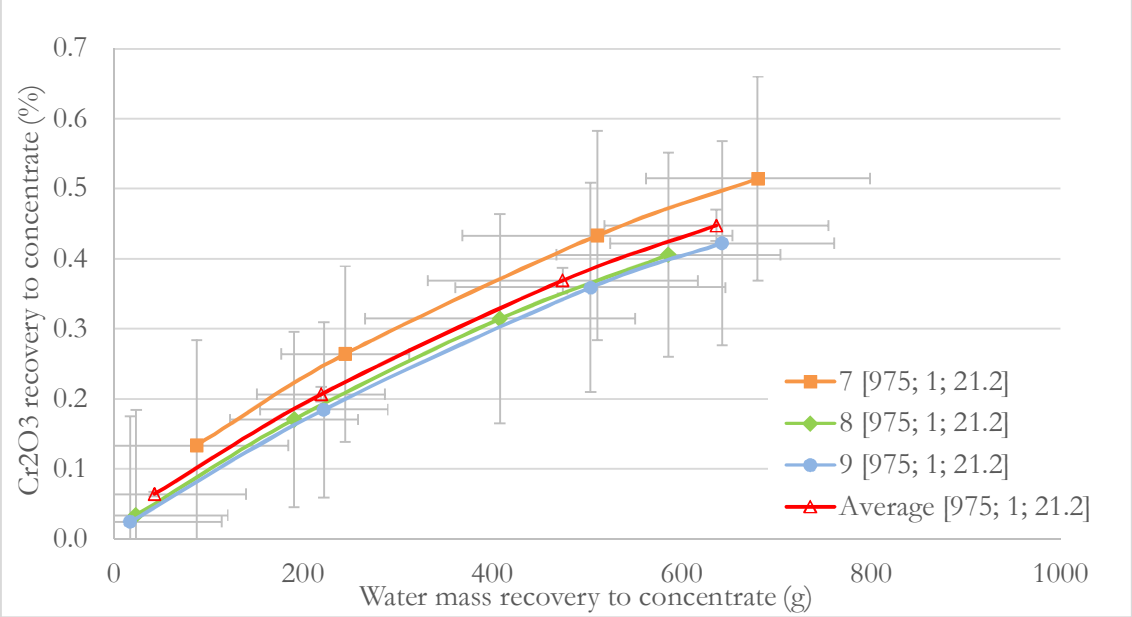

Figure 20: Chromite vs. water recovery for mid-point repeats; where the mixing intensity (rpm), cell superficial gas velocity (cm/s) and recirculation rate (l/min) was kept constant. The legend indicates run number [rpm; cell superficial gas velocity; recirculation rate].

It is believed that the differences between runs 7, 8 and 9 were primarily the result of variations in froth depth, froth build-up and the loading method of the cell. However, small dissimilarities in measured flow rates, ore characteristics, temperatures, etc. could also have played a role. To truly see the repeatability of the cell's performance, these factors should be kept exactly the same, which was rather difficult in the manually operated (and relatively large) laboratory cell. These runs should also be repeated multiple times to improve the evaluation of confidence interval of the results.

5.3. Overall Mass Pull Performance

An evaluation of the mass pull of solids and water to the concentrate provides a useful overview of the cell's general performance, and provides indicators with regard to the potential grade and recoveries achievable with the cell. As such, mass pull data give some indication of the hydrodynamic behaviour within the cell.

Figure 21 gives a good overview of the range of solid mass transferred to the concentrate in the different experimental runs. The spread in final values in Figure 21 indicates that the independently controlled variables used in this study had a noticeable effect on the solid mass recovery. Clearly, and as could be expected, the hydraulic operating conditions had a significant impact on the performance of the cell.

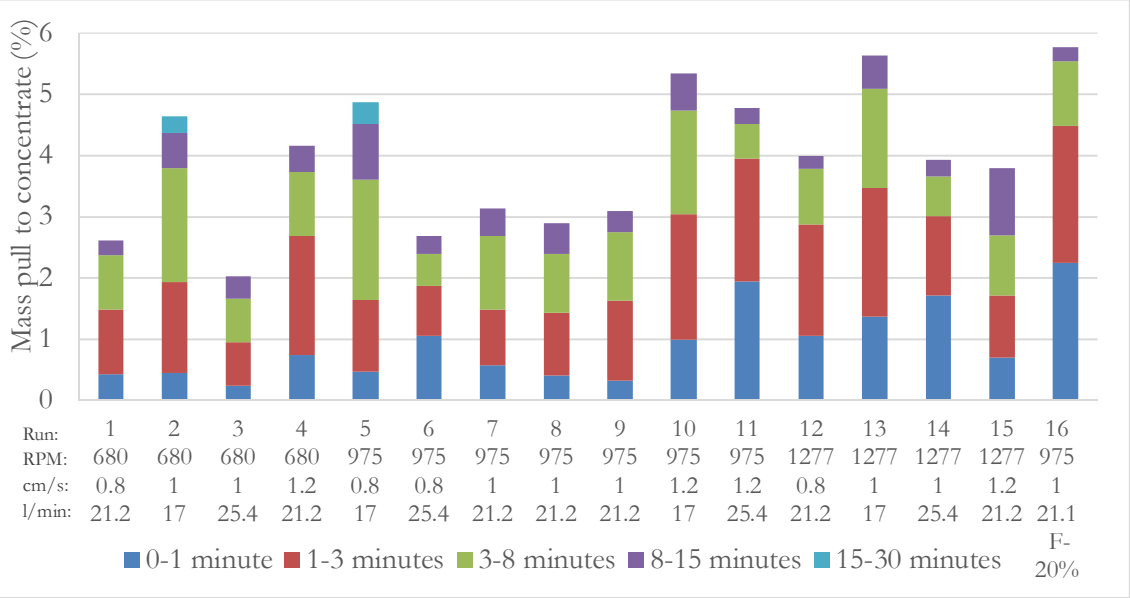

Figure 21: Percentage of ore mass transferred to concentrate within the time interval. Each run is identified by the run number followed by the mixing intensity (rpm), superficial gas velocity (cm/s) and recirculation rate (litre/min).

All runs, except runs 2 and 5, completed within fifteen minutes; where the end of the run was caused by depletion of the frother, generating 15 mm bubbles that carry minimal minerals. Run 2 was done at the lowest mixing intensity and recirculation rate with a medium superficial gas velocity, while run 5 was at the lowest recirculation rate and superficial gas velocity with a medium mixing intensity. The froth phase was visually more stable during these runs, since smaller bubbles were generated than in other runs. It is theorised that the bubble loading efficiency was higher in these runs (with lower superficial gas velocity and recirculation rates), also decreasing the rate at which frother overflowed to the concentrate (frother depletion) and allowing a stable (more

loaded) froth layer to exist past fifteen minutes. The presence of naturally floating gangue could potentially improve froth stability that would also cause a stable froth phase to exist past 15 minutes.

It is interesting to see from Figure 21 that solid mass pull favoured a low to medium superficial gas velocity (0.8-1.0 cm/s) with low recirculation rate (17 litre/min). This could be due to a longer residence time within the down-comer that could possibly translate to increased energy input (0.17-1.14 J/kg) as the slurry particles remains longer within the high intensity mixing down-comer. The highest recirculation rate had the lowest mass pull in each mixing intensity level. This could be due to lower residence time within the down-comer and impeller stations which reduced energy transfer (0.12-0.76 J/kg) to the slurry compared to the lower recirculation rates.

The 1-3 minute time interval on average contributed the most to total solids mass pull, followed by the 3-8 minute interval. In these intervals the froth phase was well established and the frother concentrations high enough to ensure sufficient mass pull. The lower mass pull in the first minute can mostly be attributed to the slow froth build-up that most runs experienced. The low mass pull from 8 minutes onwards would have been due to reduced frother concentrations, and/or the absence of solids in the froth that prevented a stable froth phase, and/or the relatively low floatable mass remaining in the cell. As explained in Chapter 4, a constant amount of frother (except for run 16 where the effect of mass-pull on a higher frother concentration was investigated) was added to the cell through all the experiments to highlight the combined effects of the hydrodynamic environment within the cell on the mass pull and separations efficiency.

Figure 22 illustrates the percentage ore mass recovered to the concentrate at low mixing intensity, while varying the superficial gas velocity and the recirculation rate.

The amount of slurry sequentially released through the various exit ports of the down-comer depends on the pressure drop over the whole down-comer (pressure difference between aerator feed and calm zone of the cell). This pressure drop depends – amongst other – on the mixing intensity and the down-comer slurry velocity (combined flow of aeration and recirculation rates). A combination of high mixing intensity and down-comer slurry velocity produced pressure drops as high as 0.47 bar, while a low mixing intensity and recirculation rate produced pressure drops around 0.13 bar.

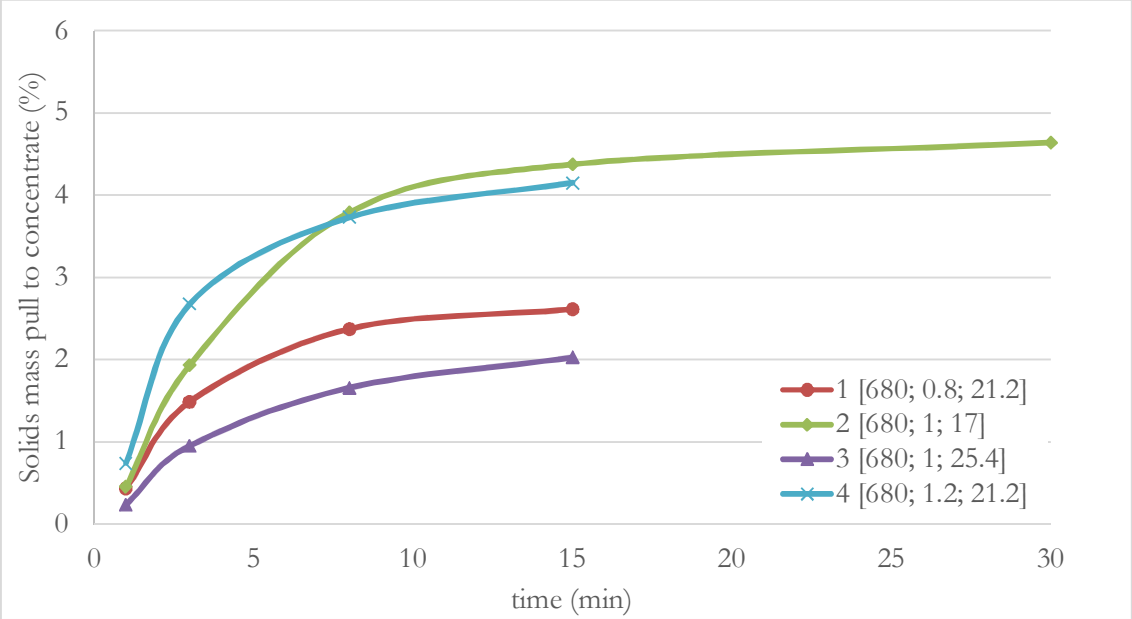

Figure 22: Solid mass transferred to concentrate at low mixing intensity while varying superficial gas velocity and recirculation rate. Each run is identified by the run number followed by the mixing intensity (rpm), superficial gas velocity (cm/s) and the recirculation rate (litre/min) given in square brackets.

A higher pressure drop increases the resistance to slurry flow through the down-comer. A significant portion of the slurry will therefore exit with the air bubbles through the first down-comer exit port. With a low pressure drop, the slurry (following its forward momentum) tends to flow straight through the down-comer towards the lower exit port, while a larger percentage of the air still favours the first exit port. This was confirmed visually through the different runs. Run 3 (from Figure 22) had a low mixing intensity combined with a higher flow velocity through the down-comer (combined flow of circulation and aeration supply), causing the slurry and air bubbles to flow further down the down-comer towards the lower exit. However, one should take note of the fact that the recycle rate was relatively high in run 3 (but the air-flow was low), thereby also implying a potential larger downward drag force in the calming zone with not enough upward air-flow to counter the effect. Furthermore, low mixing intensity and relatively low air addition could have minimised particle-bubble interaction and thereby reduced the floating mass. Therefore, the significant down-flow tendency (in both the down-comer and the calming zone), combined with potential poor particle-bubble attachment conditions, most probably contributed to the fact that run 3 produced the lowest flotation rate of all the experimental runs.

Figure 23 illustrates the percentage solids mass transferred to the concentrate at medium mixing intensity, while varying the superficial gas velocity and the recirculation rate. Run 11 (from Figure

23) had the fastest flotation rate of all the experiments completed with the same frother concentration. Run 11 was performed at the highest superficial gas velocity and recirculation rate with medium mixing intensity, creating favourable conditions for high mass pull rate to the concentrate. The mixing intensity of run 3 (from Figure 22) was just too low to achieve favourable conditions in the down-comer for high mass pull. It should be noted that the recirculation rate and superficial gas velocities have, statistically, a more significant impact on mass pull than mixing intensity.

Both run 2 in Figure 22 and run 5 in Figure 23 produced a stable froth layer beyond 15 minutes of operation. In both these runs the conditions were such that the total energy input into the system (energy added through mixing intensity, aeration as well as recirculation rate) was not too much, and in good relation to one another, to prevent disturbance of the froth phase. The rate of mass pull to concentrate for run 2 and run 5 was sustained more evenly through the run compared to other runs from Figure 22 and Figure 23. The mass-pull rates from these runs point towards the effectiveness of particle-bubble attachment and discharge rates at some optimum combination of air flow rate and recycle rate with a probable influence from mixing intensity.

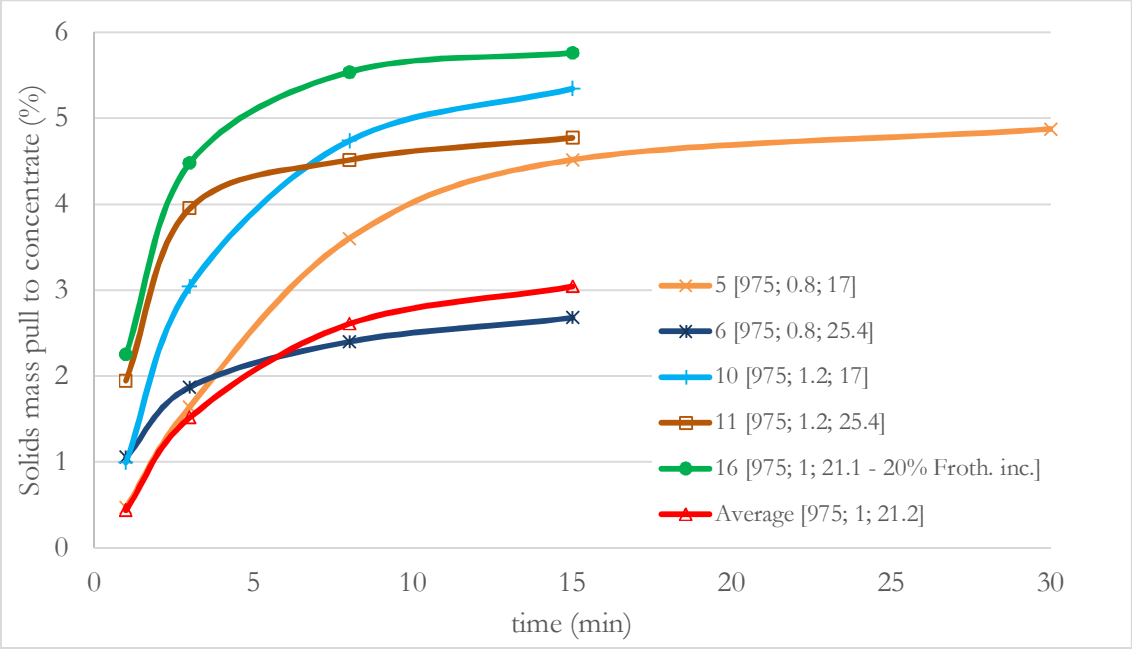

Figure 23: Solids mass transferred to concentrate at medium mixing intensity while varying the superficial gas velocity and recirculation rate. Each run is identified by the run number followed by the mixing intensity (rpm), superficial gas velocity (cm/s) and the recirculation rate (litre/min) given in square brackets.

Reagent concentrations (especially frother) can be tweaked to improve separation and recovery of minerals for different cell designs. This study did not optimize the chemistry for this specific flotation cell design. However, a frother concentration change was made in order to gauge how this could affect the separation and collection efficiency of the cell.

Unsurprisingly, a 20% increase in frother concentration had a significant impact on the mass pull performance of the cell. The frother increase (run 16 in Figure 23) was done with the same mixing intensity, superficial gas velocity and recirculation rate than runs 7-9. Figure 23 shows the average result for these three runs, as well as the mass pull with 20% frother increase. The higher frother concentration increased the initial rate of recovery of solids significantly, but the rate then decreased significantly after three minutes to values very similar to the average of runs 7-9. This may indicate that the overall particle-bubble attachment of run 16 was similar to that in runs 7-9, but that the higher frother concentration only supplied more bubble surface area for such attachment. The higher bubble surface area was generated by maintaining sufficient frother concentration for a longer period within the cell to facilitate flotation, compared to the runs with lower frother concentration. This confirms observations from literature in Section 2.2.

Figure 24 illustrates the mass percentage of ore recovered to the concentrate at high mixing intensity, while varying the superficial gas velocity and the recirculation rate.

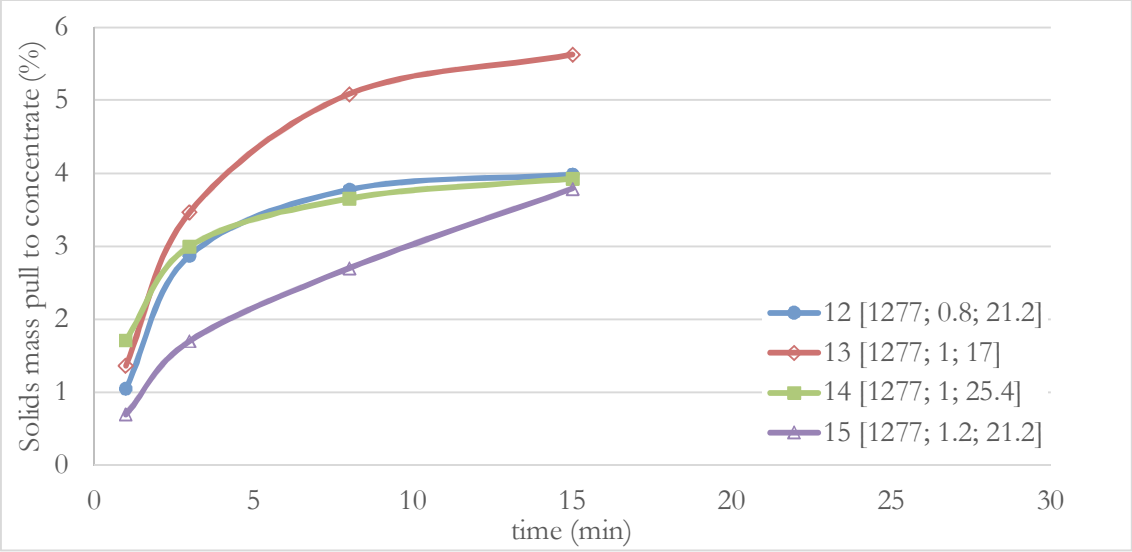

Figure 24: Solids mass transferred to concentrate at high mixing intensity while varying the superficial gas velocity and recirculation rate. Each run is identified by the run number followed by the mixing intensity (rpm), superficial gas velocity (cm/s) and the recirculation rate (litre/min) given in square brackets.

The initial froth created in the flotation cell (first scrape) in runs 12-15 did not have a high solids loading. This was most probably the result of start-up conditions within the cell, i.e. when the air supply was opened it created a disturbance where most of the air exited through the first down-comer exit port, creating froth bubbles without significant particle attachment. The conditions stabilised again and flotation continued, but a small fraction of frother was wasted without effective recovery of minerals to the concentrate. This loss was not quantifiable through these experiments, but should not occur during continuous operation of the cell.

Interesting behaviour is observed by considering the mass pull of run 15 (see Figure 24), where the slope does not gradually decrease with an increase in time. In this run, the mass pull rate was constant from three minutes onwards and the froth phase was depleted before 15 minutes, thereby ending the run. This was the effect of an increased froth depth (35 millimetres) at the beginning of the run with a subsequent decrease of froth depth to 10 millimetres (just after the three minute sample was removed). This highlights the significant effects of froth depth on mass pull.

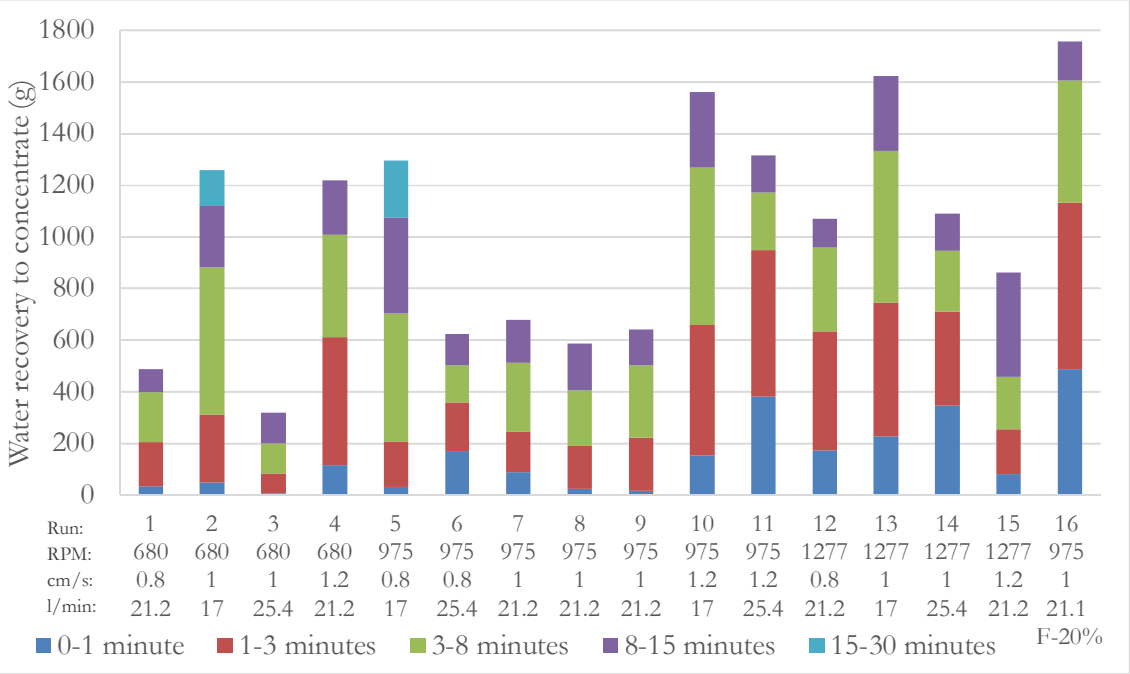

Figure 25: Mass of water reporting to concentrate per time interval for each run. The runs are identified by the run number followed by the mixing intensity (rpm), superficial gas velocity (cm/s) and recirculation rate (litre/min).

There is a relationship between the solids recovery and water recovery, which varies with the froth stability and bubble coalescence in the different runs. However, Figure 25 shows that the variations in water recovery are larger than that of the solids recovery (Figure 21). The difference is quite

significant, i.e. a four percent (118 grams) increase in ore recovery corresponds with an increase in water recovery of over 1200 grams (compare run 3 in Figure 21with run 13 in Figure 25).

Water recovery gives an indication of the froth stability within the cell. Smaller bubbles will transport more water to the concentrate. Grades will have an inverse relationship to water recovery due to the possible entrainment of slimes. It is therefore likely that runs corresponding to higher water recovery will have lower grades than the runs with a lower water recovery.

The mass pull, as well as the water recovery results from runs 7 to 9, correlate quite well with one another (see Figure 21 and Figure 25). The slight differences are a result of imperfect duplication of operating conditions, mostly in terms of controlling the froth depth as well as slight variations in the loading times of the flotation cell.

Figure 26, 27 and 28 illustrate the recoveries of water to the concentrate at low, medium and high mixing intensities respectively, while varying the superficial gas velocity and the recirculation rate.

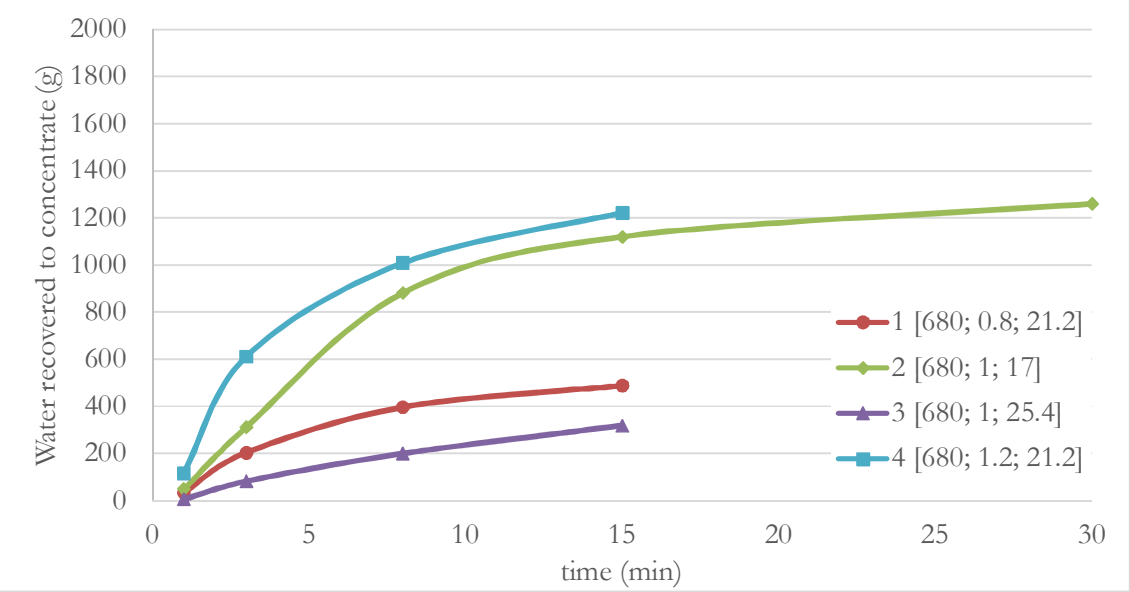

Figure 26: Mass of water reporting to concentrate at low mixing intensity, while varying the superficial gas velocity and recirculation rate. Each run is identified by the run number followed by the mixing intensity (rpm), superficial gas velocity (cm/s) and the recirculation rate (litre/min) given in square brackets.

Figure 27 illustrates a good variation in final water mass recoveries to concentrate as superficial gas velocity and recirculation rate were varied from high to low, and combined with the medium mixing intensity. The water recoveries of runs 10, 11 and 16 had a high initial rate, suggesting that a rather stable froth phase was formed.

The change in slope from the solids mass pull of Figure 22 through to Figure 24 correlates well with the slope change of the water recoveries of the same runs (see Figure 26 to Figure 28).

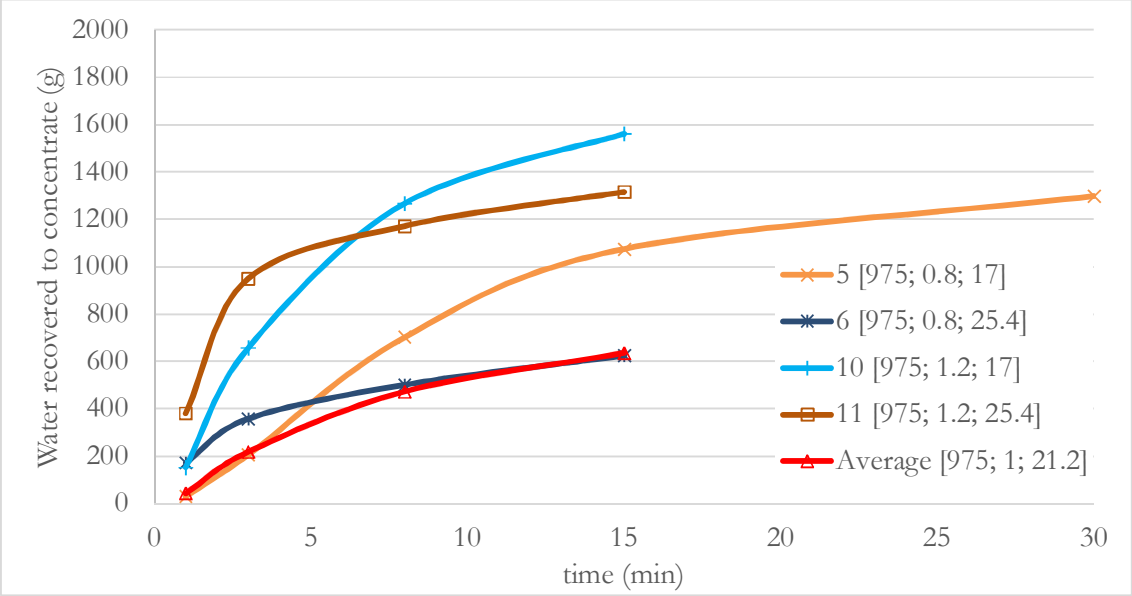

Figure 27: Mass of water reporting to concentrate at medium mixing intensity while varying superficial gas velocity and recirculation rate. Each run is identified by the run number followed by the mixing intensity (rpm), superficial gas velocity (cm/s) and the recirculation rate (litre/min) given in square brackets.

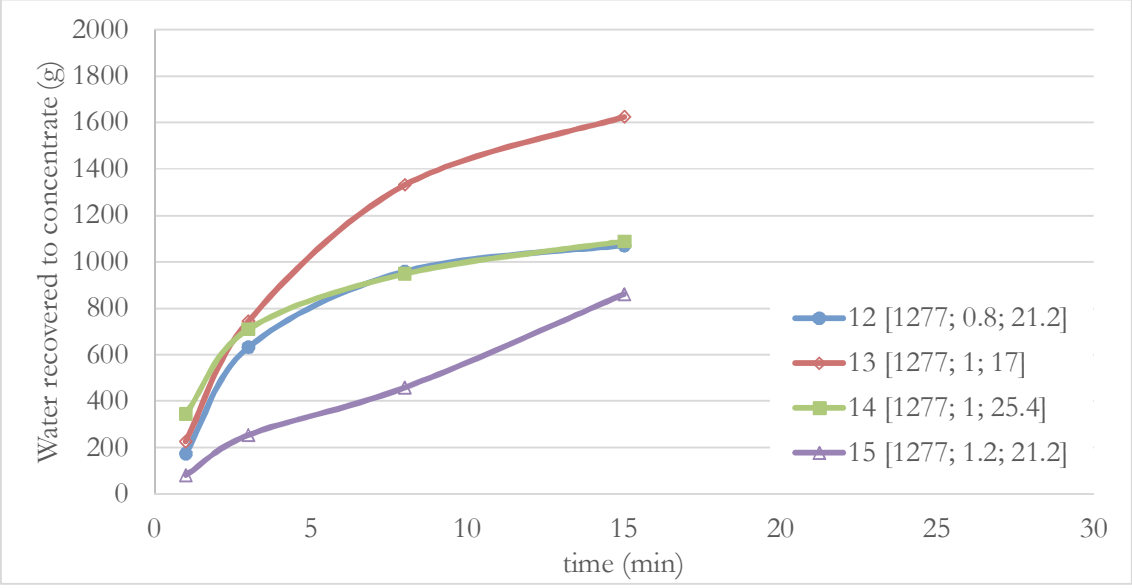

Figure 28: Mass of water reporting to concentrate at high mixing intensity while varying superficial gas velocity and recirculation rate. Each run is identified by the run number followed by the mixing intensity (rpm), superficial gas velocity (cm/s) and the recirculation rate (litre/min) given in square brackets.

Significant variance occurred in the water recoveries of the different runs (Figure 26 to Figure 28). The manipulated variables therefore had a notable effect on the water recovery by influencing solids loading in the froth phase, froth stability, froth coalescence, water drainage through the froth phase and also the rate of frother carry-over to concentrate.

5.4. Grade and Recovery Analysis

The samples were all analysed for the four main metals, platinum, palladium, rhodium and gold as well as for the gangue mineral chromite. The four element analysis (4E) of the valuable metals can be used to compare the collection efficiency of this cell to the performance of other froth flotation equipment.

5.4.1. Valuable Metals (4E) Recovery

Achieving a high valuable mineral recovery through the flotation unit – at an acceptable grade – is an important goal, as this could potentially reduce the number of flotation cells in series needed for maximum possible recovery. A high overall recovery is clearly necessary to maximise profitability.

Figure 29 illustrates the 4E recovery to concentrate per time interval. The total recovery achieved with the cell ranged from 70% to just above 80%. It was possible to increase this total recovery to above 85% with a higher frother concentration at the same mid-point conditions of runs 7-9. Within the first minute of flotation, the 4E recovery ranged from below 30% to above 50%, despite the fact that the highest mass pull rates did not occur in the first minute (see Figure 21).

In the 1-3 minute time interval, the valuable mineral recovery increased, on average, by an additional 20% (Figure 29). After that, the rate of recovery dropped notably. Typically, the runs with relatively low recoveries during the first minute (runs 2, 3 and 7-9) mostly improved their recoveries during the 1-3 minute interval. It is theorised that the low initial mass pull and recovery in these runs were the result of slow froth build-up. Related recoveries improved once a steady froth phase was developed.

The frother increase (run 16) did not produce the highest recovery in the 1-minute interval, but increased the overall recovery significantly when considering the results of runs at the same hydraulic operating conditions (runs 7-9). As such, the increased frother concentration had the most significant effect in the 1-3 minutes time interval.

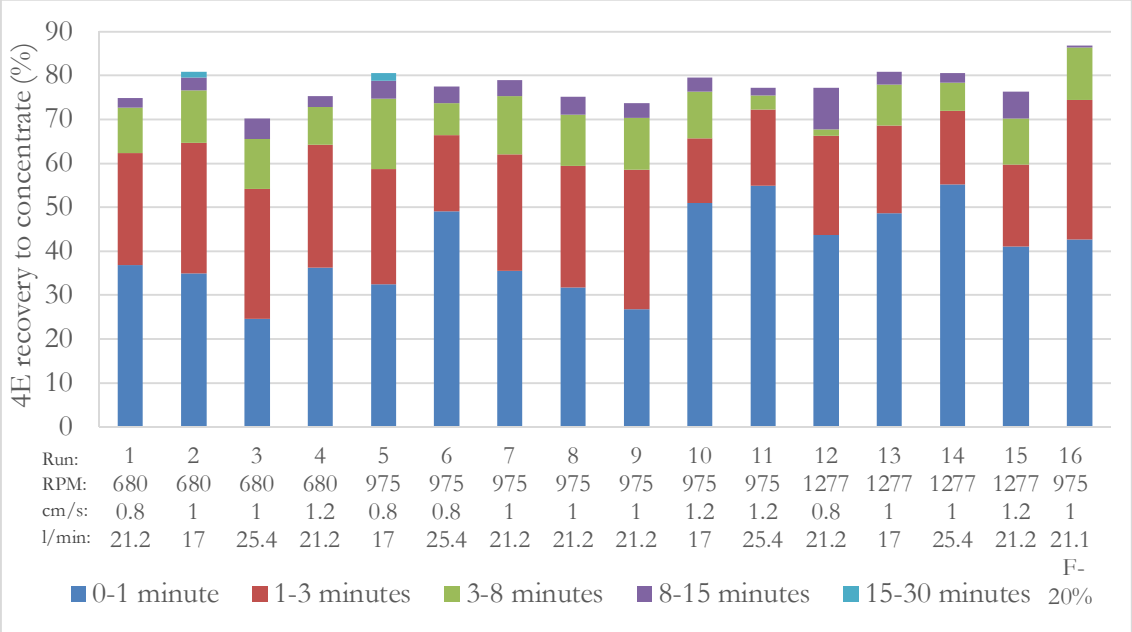

Figure 29: 4E Recovery to concentrate per time interval while varying mixing intensity (rpm), superficial gas velocity (cm/s) and recirculation rate (litre/min). Each run is identified by the run number, mixing intensity (rpm), superficial gas velocity (cm/s) and the recirculation rate (litre/min).

Figure 30, 31 and 32 illustrate 4E mineral recoveries to concentrate at low, medium and high mixing intensity respectively. At each mixing level of intensity, the superficial gas velocity and the recirculation rate were varied.

Figure 30 (low mixing intensity) shows that medium superficial gas velocity coupled with medium recirculation rate, produced the best overall recovery and recovery rate (run 2). These conditions created a very stable froth interface with minimal disturbance in the calming zone of the cell. At medium mixing intensity (see Figure 31) the best recovery was obtained with a low recirculation rate and low superficial gas velocity (run 5). This was followed closely with a low recirculation rate, but a high superficial gas velocity (run 10).

These operating conditions enabled longer residence times within the down-comer that could possibly resulted in good attachment of minerals to bubbles (i.e. the energy input per unit mass slurry was relatively high). The lower recirculation rate (statistically the more significant factor) and low superficial gas velocity also caused the mineralized bubbles to leave the down-comer earlier, with a smaller fraction moving down to the bottom of the down-comer (compared to high recirculation rates). This could possibly mean that the shorter travel distance from the first exit to the froth phase, compared to the third exit to the froth phase, does not allow sufficient time for bubble break-up or mineral detachment from bubbles, resulting in a higher grade concentrate.

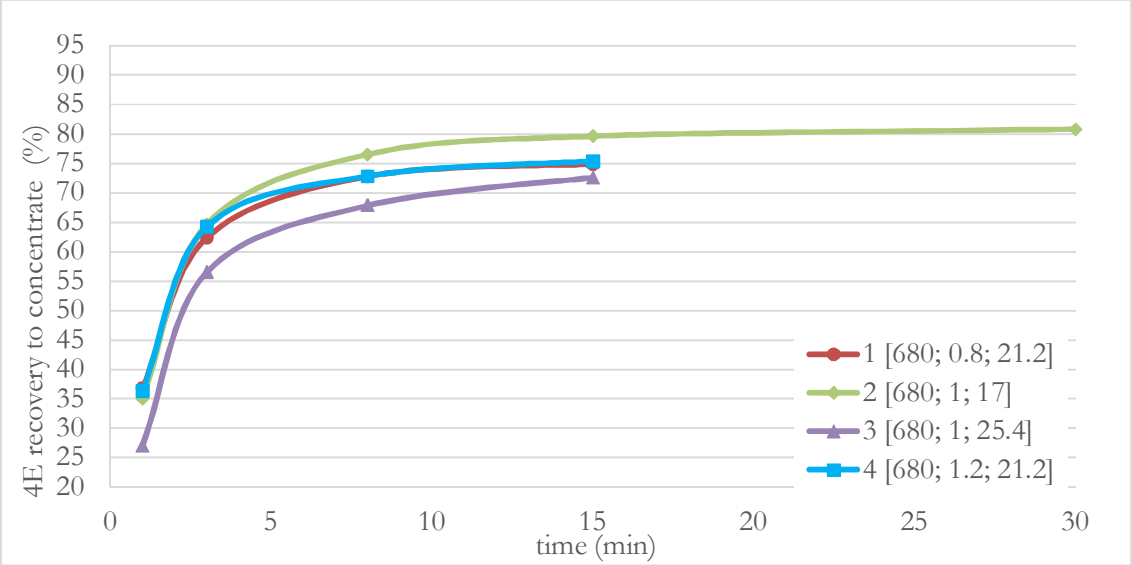

Figure 30: 4E Recovery to concentrate at low mixing intensity while varying superficial gas velocity and recirculation rate. Each run is identified by the run number followed by the mixing intensity (rpm), superficial gas velocity (cm/s) and the recirculation rate (litre/min) given in square brackets.

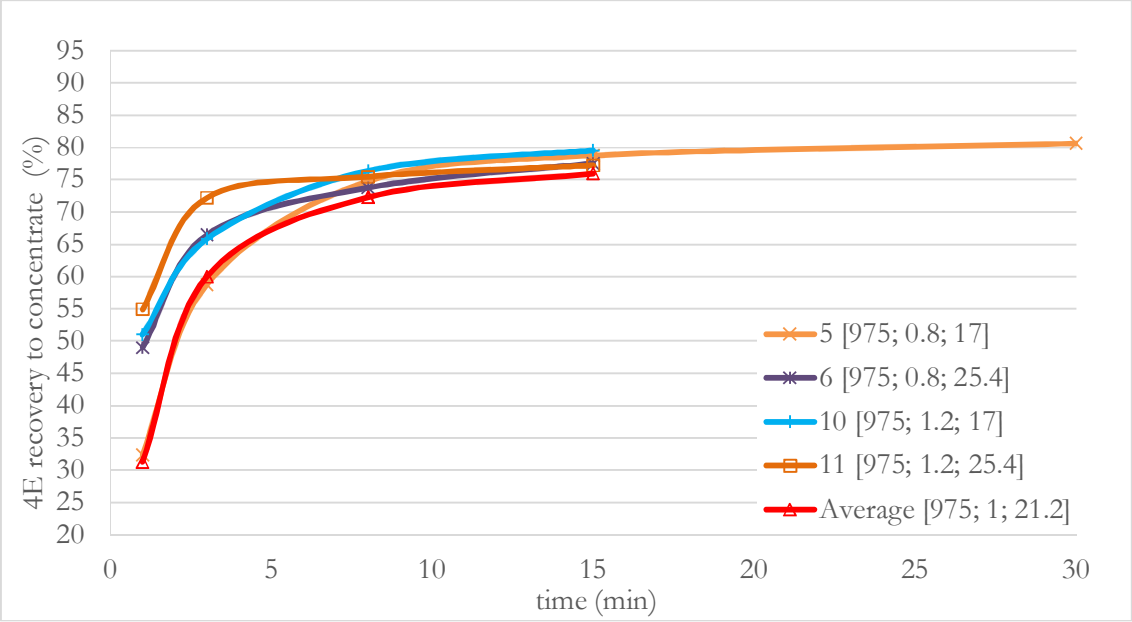

Figure 31: 4E Recovery to concentrate at medium mixing intensity while varying superficial gas velocity and recirculation rate. Each run is identified by the run number followed by the mixing intensity (rpm), superficial gas velocity (cm/s) and the recirculation rate (litre/min) given in square brackets.

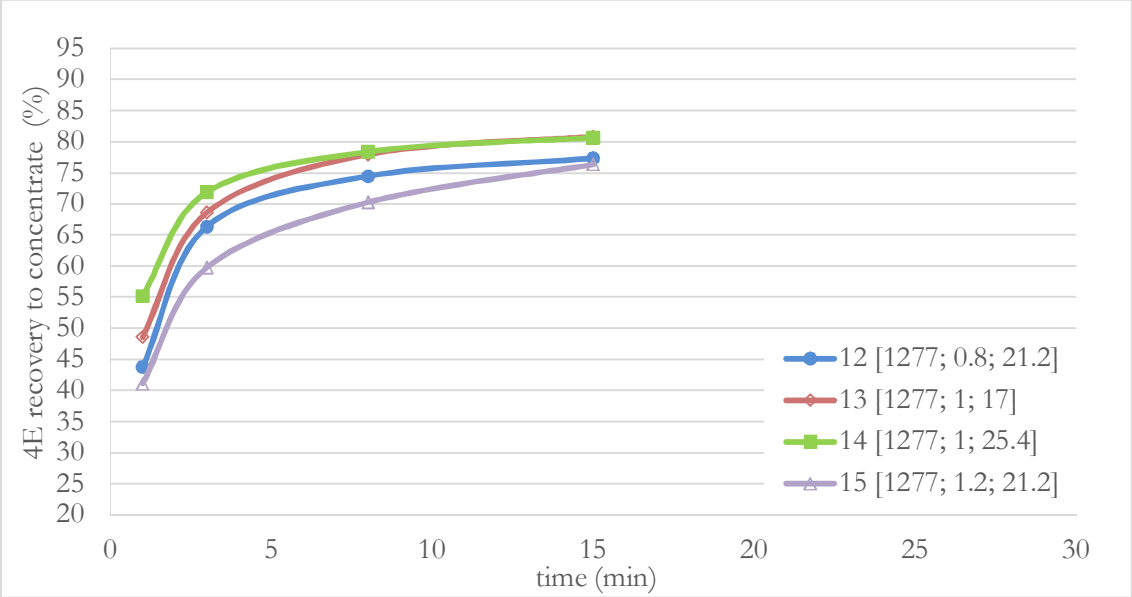

Figure 32: 4E Recovery to concentrate at high mixing intensity while varying superficial gas velocity and recirculation rate. Each run is identified by the run number followed by the mixing intensity (rpm), superficial gas velocity (cm/s) and the recirculation rate (litre/min) given in square brackets.

The highest initial rate of recovery was achieved with a high superficial gas velocity and recirculation rate (run 11) for the three factor analysis. This could possibly be due to smaller bubble creation that created larger available attachment surface for hydrophobic minerals, a more stable froth phase or that the froth phase was better loaded with minerals. The frother increase produced an even higher initial valuable mineral recovery rate, where the bulk of the valuable minerals were recovered before three minutes and the total amount recovered up to eight minutes.

5.4.2. Valuable Metals (4E) Grade Compared to Recovery

At a specific set of operating conditions, increasing the valuable metal recovery to concentrate will decrease the concentrate grade. This grade-recovery relationship is dependent on the liberation characteristics of the mineral slurry treated, as well as the separations efficiency of the flotation cell at the chosen operating conditions. A 100% efficient flotation cell with perfect liberated feed will theoretically be able to recover all the valuable minerals to concentrate while rejecting all the gangue minerals. Completely liberated minerals are more likely to be floated first, followed by partial liberated minerals and hydrophobic gangue minerals that could not be supressed. This confirms the well-known phenomenon that recovery and grade will display an inverse relationship to one another. Plotting the grade against recovery indicates how well the flotation cell performs (if all other factors can be kept constant).

Figure 33, 34 and 35 illustrate 4E mineral concentrate grade against recovery at low, medium and high mixing intensity respectively. At each level of mixing intensity, the superficial gas velocity and the recirculation rate were varied.

The low mixing intensity produced a very high initial grade, but with very low recoveries (Figure 33). Most of the runs had a final recovery around 75% and an increase in recovery resulted in a significant decrease in grade. As such, at low mixing intensity, one will typically run the cell as a concentrate cleaner without forcing recovery.

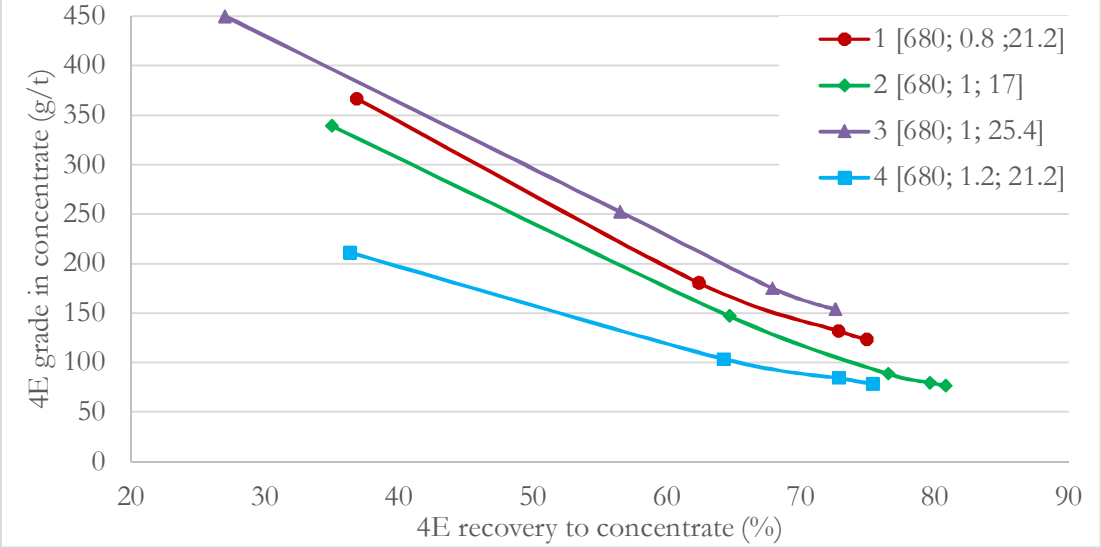

Figure 33: 4E Concentrate grade vs. recovery to concentrate at low mixing intensity while varying the superficial gas velocity and recirculation rate. Each run is identified by the run number followed by the mixing intensity (rpm), superficial gas velocity (cm/s) and the recirculation rate (litre/min) given in square brackets.

At two sets of operating conditions, medium mixing intensity also produced notable high grades (with very low recoveries) in the first minute (Figure 34). The rest of the runs produced significant initial recoveries with lower grades than that obtained with low mixing intensity. However, a further increase in final recovery did not cause such a significant decrease in grade at medium mixing intensity if compared to the low mixing intensity results. The average final recovery from runs with medium mixing intensity was around 78%, which seems to be slightly higher than the average recovery results from Figure 33 (at low mixing intensity), but with slightly lower grades. Notably, runs 13 and 14 (at high mixing intensity – Figure 35) produced recoveries around 80%.

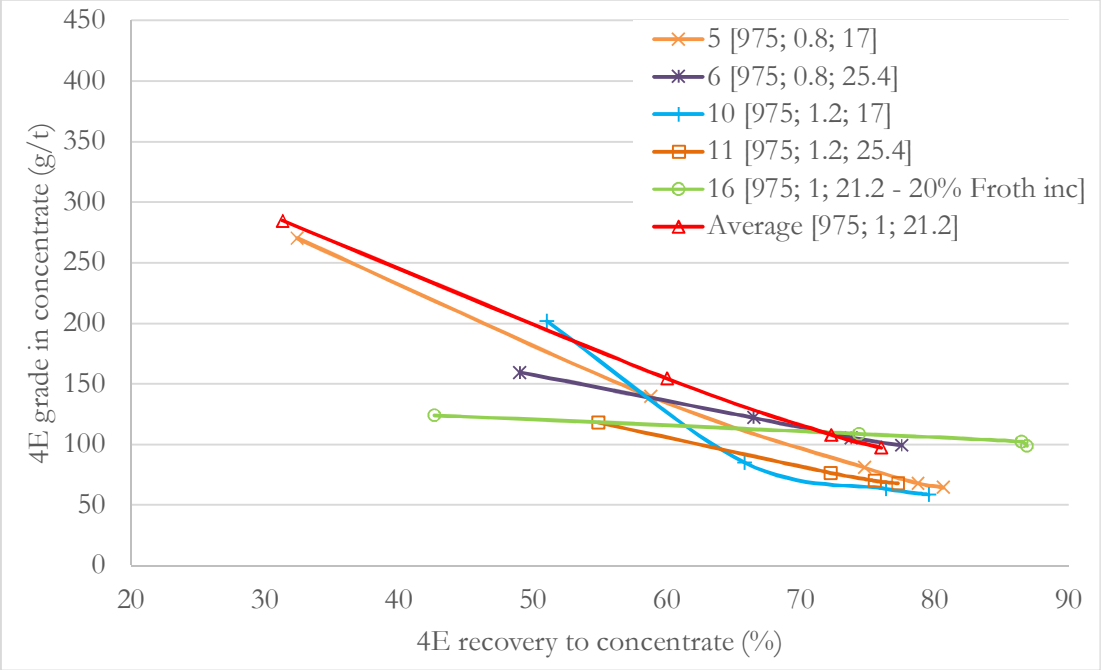

Figure 34: 4E Concentrate grade vs. recovery to concentrate at medium mixing intensity while varying the superficial gas velocity and recirculation rate. Each run is identified by the run number followed by the mixing intensity (rpm), superficial gas velocity (cm/s) and the recirculation rate (litre/min) given in square brackets.

An increase in frother concentration had a positive effect on recovery, with a decrease in the initial grade. The lower initial grade is most likely due to entrainment in the very fine foam created through froth phase establishment. The higher final recovery is most likely due to the increase of available bubble surface area throughout the flotation process, as well as less detachment of valuable minerals from the slower rising bubbles. This indicates that higher recoveries can be achieved if the cell is operating under conditions where the frother concentration is maintained to ensure a stable froth phase throughout. By maintaining the froth concentration, it is possible to increase the recoveries with a slight decrease in grade.

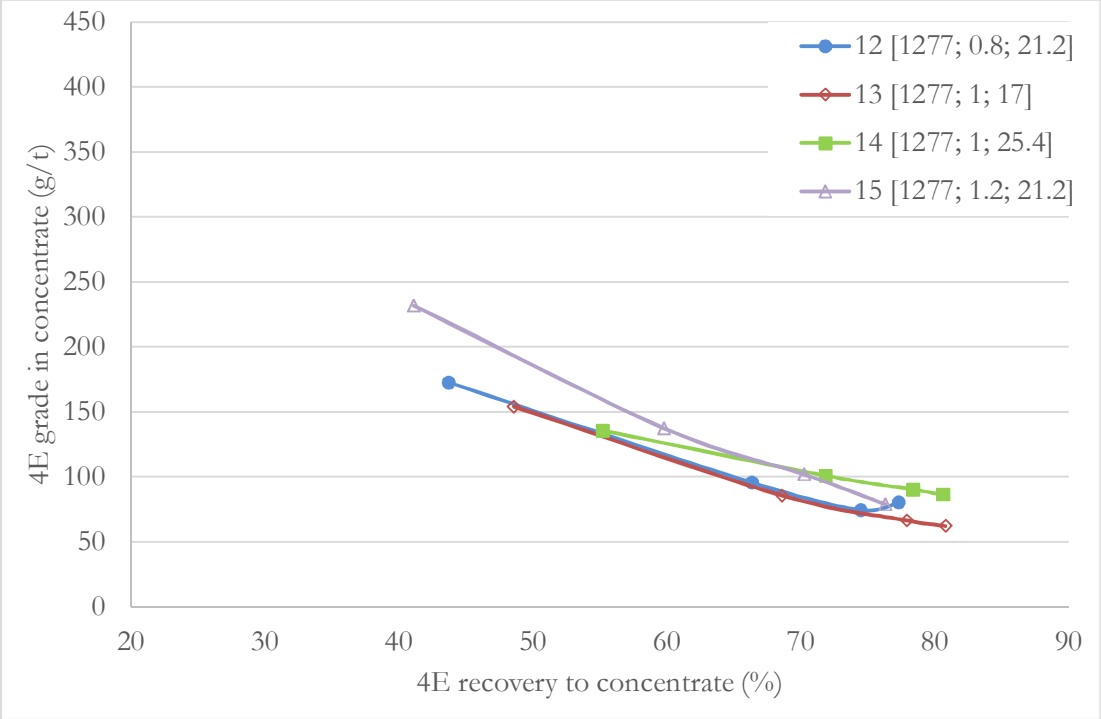

Figure 35:4E Concentrate grade vs. recovery to concentrate for high mixing intensity while varying the superficial gas velocity and recirculation rate. Each run is identified by the run number followed by the mixing intensity (rpm), superficial gas velocity (cm/s) and the recirculation rate (litre/min) given in square brackets.

The high mixing intensity results of Figure 35 were very similar to those presented in Figure 34. This suggests that increasing the mixing intensity above 975 revolutions per minute did not have a significant effect on the separation efficiency of the cell. These results are within experimental error and should be further investigated to ensure that improved repeatability can be obtained.

There are no specific set of operating conditions which had both an exceptional total recovery as well as high final 4E concentrate grade. From Figure 33 to Figure 35 it can be seen that a good 4E concentrate grade result was obtained when the superficial gas velocity was kept at a level below that of recirculation rate (if the recirculation rate was tested at factor level 1, then the superficial gas velocity had to be kept at a factor level of 0 or -1).

It should be noted from the statistical analysis that the 4E grade can be manipulated by varying all three factors (mixing intensity, recirculation rate and superficial gas velocity) where the 4E recovery is only influenced significantly by recirculation rate. As such, recirculation rate can be used to improve recoveries, while the manipulation of the mixing intensity and superficial gas velocity should be utilized to maximize 4E concentrate grade.

5.4.3. Chromite Recovery and Separation Efficiency

Chromite grade is of great concern in the furnace separation process, since a high grade of chromite negatively impacts the furnace refractory material and also produces a layer within the furnace, resulting in a reduction of useable furnace volume. Chromite concentrations can reach 8% in rougher circuits, but the final concentrate stream that leaves the primary separation circuit should be lower than 3% (Ross, 2015). Low recovery of chromite is therefore important in the rougher circuits in order to decrease the amount of chromite that should be removed through downstream processes prior to the smelter.

The statistical evaluation of the final results from the experimental runs indicated that none of the three factors (mixing intensity, recirculation rate or superficial gas velocity) had a statistically significant impact on chromite grade. Some variation in the chromite recovery can be seen between the different runs, but this is considered by the statistical model as normal variability within the data. Noise within the results should be reduced to confirm this observation and other factors should be included to determine which factor(s) have a significant impact on chromite recovery. The discussions that follow discuss the variability in chromite recovery with possible dependence on manipulated variables. Manipulated variables influenced factors such as bubble surface area flux, froth depth and gas dispersion in the cell, but these were not directly measured.

Figure 36 illustrates the chromite recovery to concentrate per time interval for all the runs and it is interesting to see that the lower to medium mixing intensities had lower chrome recoveries except for two significant outliers, run 4 and 5. Runs 10 and 11 had significantly high chromite recoveries, which were possibly due to the increase in superficial gas velocity. Run 4 also had a high superficial gas velocity with medium recirculation that produced slightly elevated chromite recovery.

Figure 37 illustrates chromite recovery against 4E recovery to concentrate at low mixing intensity, Figure 38 at medium mixing intensity and Figure 39 for high mixing intensity. At each mixing intensity the superficial gas velocity and the recirculation rate was varied.

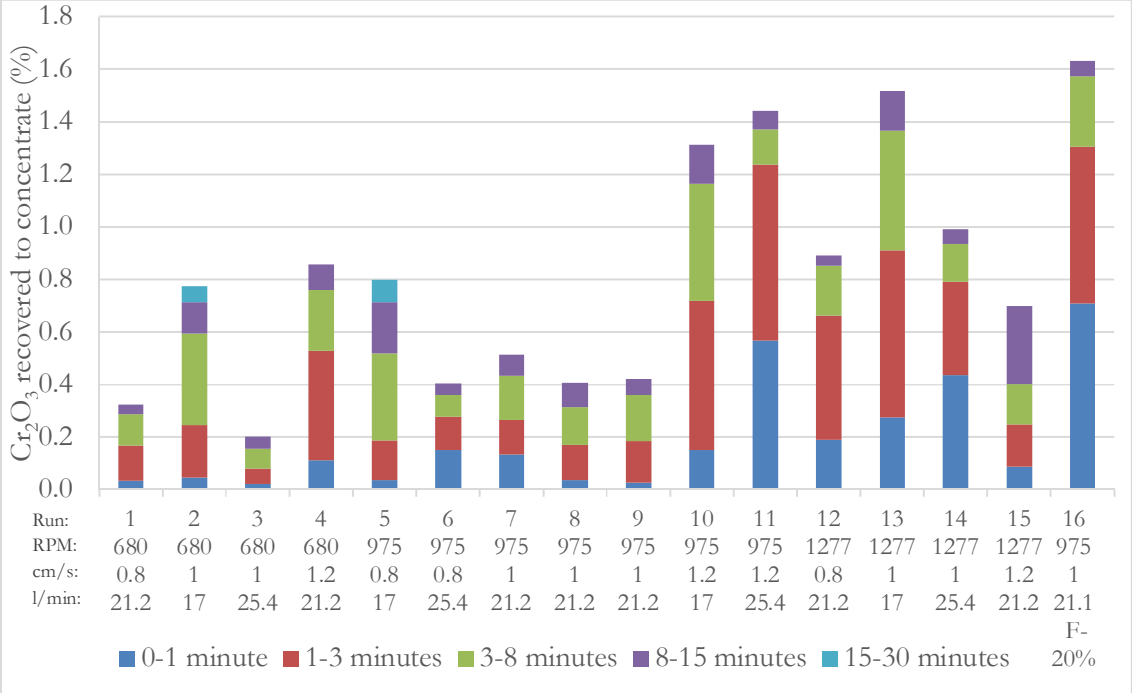

Figure 36: Chrome recovery to concentrate per time interval while varying the mixing intensity (rpm), superficial gas velocity (cm/s) and recirculation rate (litre/min).

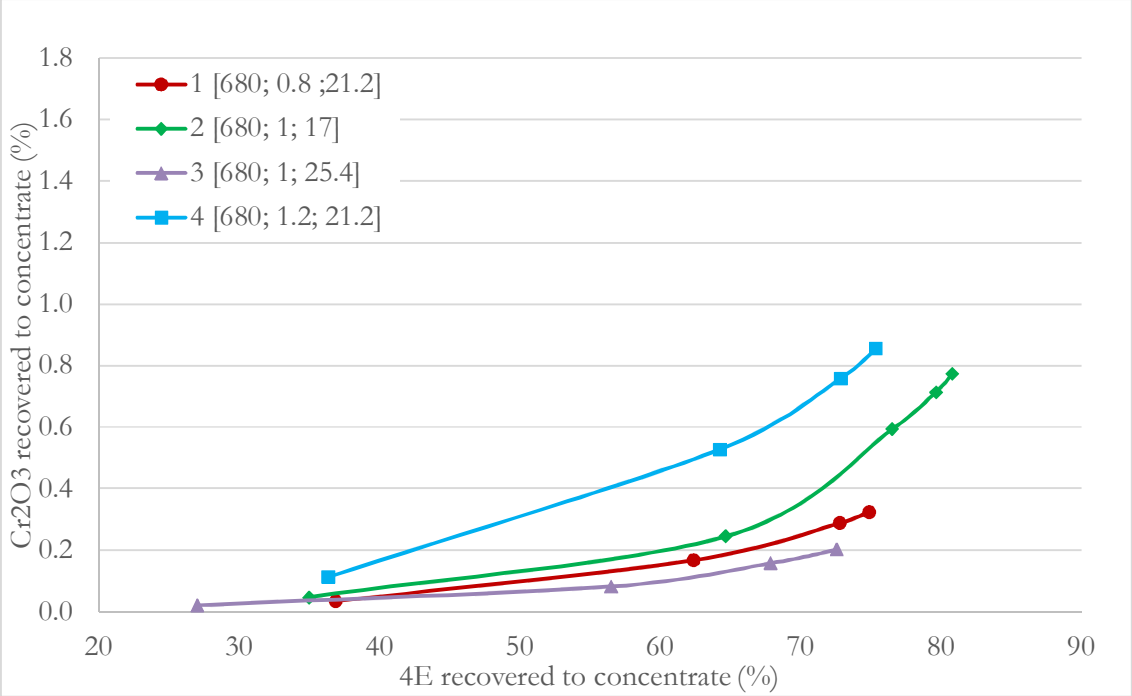

Figure 37: Chromite vs. 4E recovery to concentrate at low mixing intensity while varying superficial gas velocity and recirculation rate. Each run is identified by the run number followed by the mixing intensity (rpm), superficial gas velocity (cm/s) and the recirculation rate (litre/min) given in square brackets.

Runs 10, 11 and 13 had very high water recoveries as well as solids mass pull to concentrate (see Figure 21 and Figure 25), which suggests that the higher chromite content in the concentrate could be due to entrainment. These runs had either relatively high recirculation and aeration rates, or high mixing intensity with low recirculation rates that could have resulted in higher chromite recovery for the following reasons:

- Higher mixing intensity increased the pressure drop over the down-comer, forcing nearly all the slurry and air bubbles out at the top down-comer exit. The lower recirculation rate produced larger bubbles that were more likely to coalesce in the top of the down-comer and leave as a burst of bubbles through the first exit, disturbing the quiet separation zone of the cell and possibly entrain chromite through the froth phase.
- High recirculation rates combined with higher aeration rated and low mixing intensity will force bubbles through more down-comer stations and deeper down the cell, allowing more opportunities for chromite to be entrained.

Figure 37 to Figure 39 compare the separation efficiency of the cell with respect to chromite and the four valuable elements in question. The best selectivities towards the 4E valuable minerals are represented by results farthest to the bottom right of these graphs.

From Figure 37 it is evident that increased chromite recoveries were achieved with increased superficial gas velocity at low recirculation rates (while maintaining low mixing intensity). Run 2 achieved significant 4E recovery while still maintaining a low total chromite recovery, which suggests that low recirculation rates may be advantageous for good separation between chromite and the valuable metals while still achieving high valuable metal recovery. This further suggests that if this flotation cell should ever be used specifically for high chromite rejection, then higher recirculation rates should be utilized with lower superficial gas velocities (if the mixing intensity is kept low).

Run 5 (Figure 38) also achieved good valuable metal recovery with low chromite recovery at low circulation rate, supporting the previous statement. Generally the entrainment of chromite increases over time, but runs 10, 11 and 16 indicates different behaviour compared to the other runs. Figure 25 indicates that runs 10, 11 and 16 had higher water recoveries, indicating that the higher chromite recoveries were possibly due to higher entrainment. Both these runs had high superficial gas velocities, suggesting that the higher water recovery and entrainment of chromite was possible with the shallow froth layers. More experimental data on froth height and chromite are required to confirm this.

Figure 38 shows that although the increase in frother concentration recovered more chromite, the rate of chromite recovery versus the valuable elements recovery was only slightly higher than in runs 5, 6 and the mid-point average. This suggests that the initial high concentration of frother resulted in higher entrainment of chromite, but the higher frother concentration through the middle of the experiment improved the recovery of the valuable elements significantly.

The linear relationship from runs 10 and 11 continues through to runs 12 and 14 that forms part of the high mixing intensity set of runs (see Figure 39). The entrainment of chromite was lower in runs 12 and 14 than in runs 10 and 11 when considering the final chromite and valuable metals recoveries. An interesting shift can also be seen here: the lower mixing intensities produced lower chromite recoveries with a decrease in superficial gas velocity, while the high mixing intensity produced an increase in chromite recovery with a decrease in superficial gas velocity.

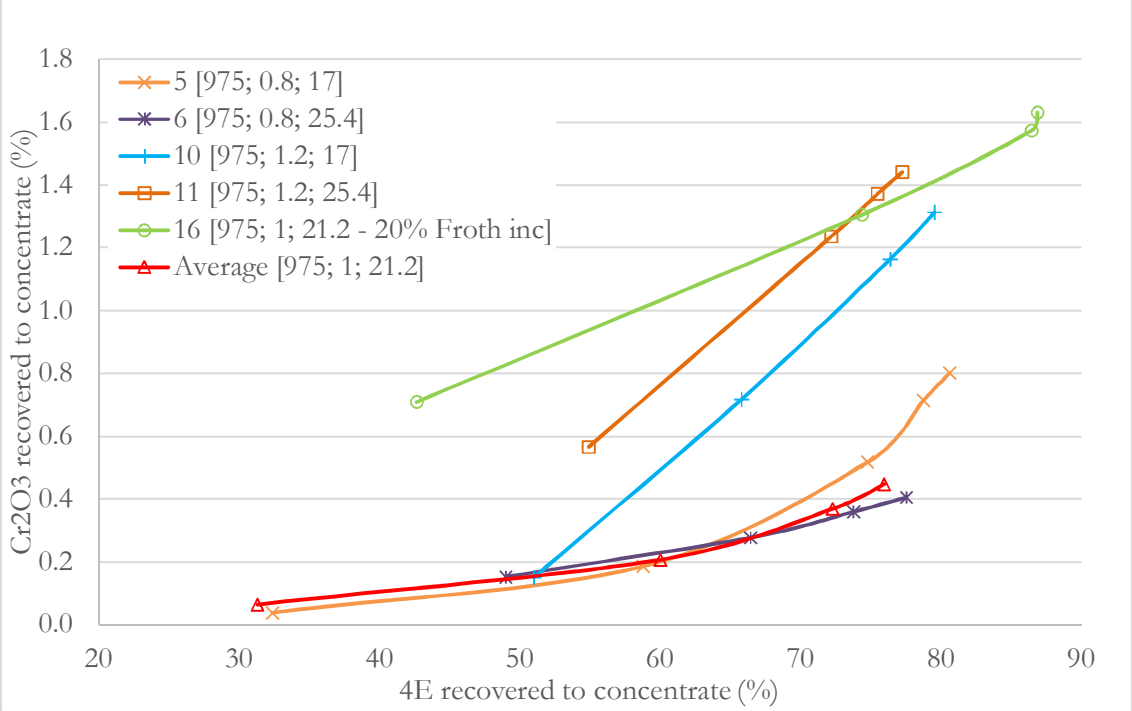

Figure 38: Chromite vs. 4E recovery to concentrate at medium mixing intensity while varying superficial gas velocity and recirculation rate. Each run is identified by the run number followed by the mixing intensity (rpm), superficial gas velocity (cm/s) and the recirculation rate (litre/min) given in square brackets.

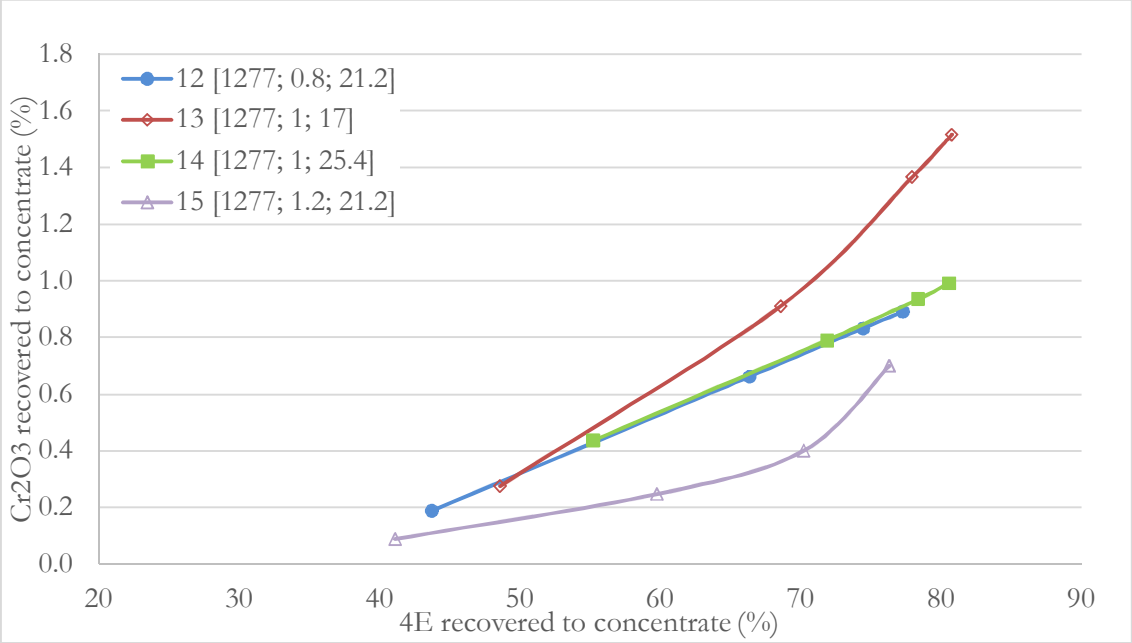

Figure 39: Chromite vs. 4E recovery to concentrate at high mixing intensity while varying superficial gas velocity and recirculation rate. Each run is identified by the run number followed by the mixing intensity (rpm), superficial gas velocity (cm/s) and the recirculation rate (litre/min) given in square brackets.

Operating conditions within the cell should be chosen such to avoid the linear relationship between chromite and valuable metals recovery and should rather show an exponential relationship. This should be done since the linear relationship displays the highest selectivity towards chromite recovery in most cases and should be treated as the worst operating conditions.

5.4.4. Chromite Grade and Entrainment Analysis

Increasing chromite grades would indicate increased chromite entrainment relative to the flotation of valuable minerals. Figure 40 shows the chromite concentrate grade contribution per time interval for all the runs.

A comparison between the results in Figure 40 and the chromite recovery results in Figure 36 shows that the actual amount of chromite recovered to the concentrate was low, but with the corresponding low solids mass pull the chromite content was still relatively high (above the allowable limit of 3% for PGM smelting). The runs that recovered less chromite (Figure 36) also produced the lowest chromite grades in the concentrate, as shown in Figure 40.

In runs 4 and 10-14, the most significant contributions to the final chromite grade occurred in the first three minutes. These runs also produced some of the highest final chromite grades.

Run 15 also showed a noteworthy trend, i.e. the chromite grade contribution up to 8 minutes was relatively low compared to the other runs. The initial froth depth was high (35 mm) where the froth depth was decreased to 10 mm after 3 minutes. Figure 29 shows that the recovery of the valuable metals was not significantly affected by the changes in froth depth. This suggests that chromite recovery can be suppressed by increasing the froth depth in the cell – a well-known flotation phenomenon.

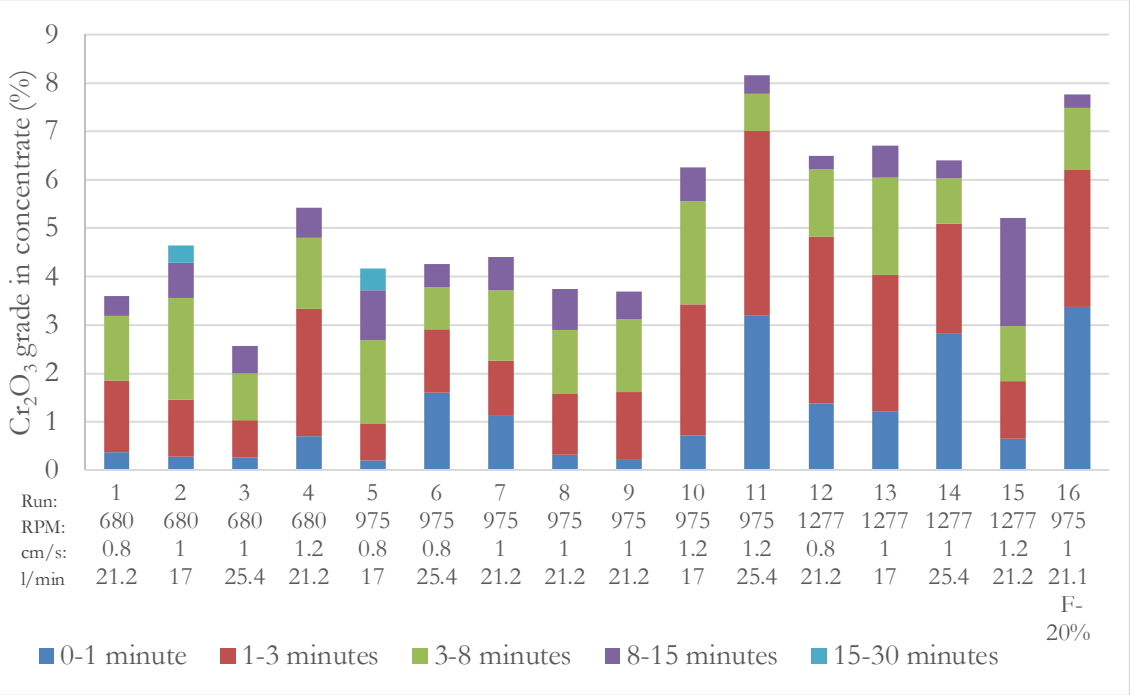

Figure 40: Chromite concentrate grade contribution per time interval while varying mixing intensity, superficial gas velocity and recirculation rate. Each run is identified by the run number, mixing intensity (rpm), superficial gas velocity (cm/s) and recirculation rate (litre/min).

Figure 41, 42 and 43 present chromite recovery against water mass recovery at low, medium and high mixing intensity, respectively. For each level of mixing intensity (rpm), the superficial gas velocity (cm/s) and recirculation rate (litre/min) were varied. The information in these figures can be used to gauge if the chromite content in the concentrate was due to entrainment, or due to true chromite flotation. Entrainment of minerals occurs when they form part of the liquid layer around a bubble passing through the pulp and froth phases and into the concentrate. This phenomena becomes more prominent for the smaller particle sizes (especially the so-called slimes). Mineral entrainment generally has a direct relationship with water recovery, where the mineral versus water recovery graph typically intercepts the origin. If the graph does not intercept the origin, but intersects the ordinate at a positive value, then that percentage recovered can be seen as true flotation of the mineral (Ata, 2012).

The relationship between chromite recovery and water transfer to concentrate would be different for different operating conditions. Figure 41 shows that most of the chromite recovered during the low mixing intensity runs could be attributed to entrainment. It is interesting to see that all these runs produced very similar rates of entrainment and that none produced a true linear relationship between chromite recovery and water mass transfer to concentrate. The systematic decrease in the rate of chromite recovery per time interval is significant as this indicates a decreasing chromite entrainment with time. In further discussions, run 2 will be used as a reference (benchmark) in order to compare the rates of entrainment in all the different mixing intensity runs. Run 2 was specifically chosen as benchmark, since it produced the closest-to-linear relationship between chromite recovery and water transfer, while the total water mass transferred was high.

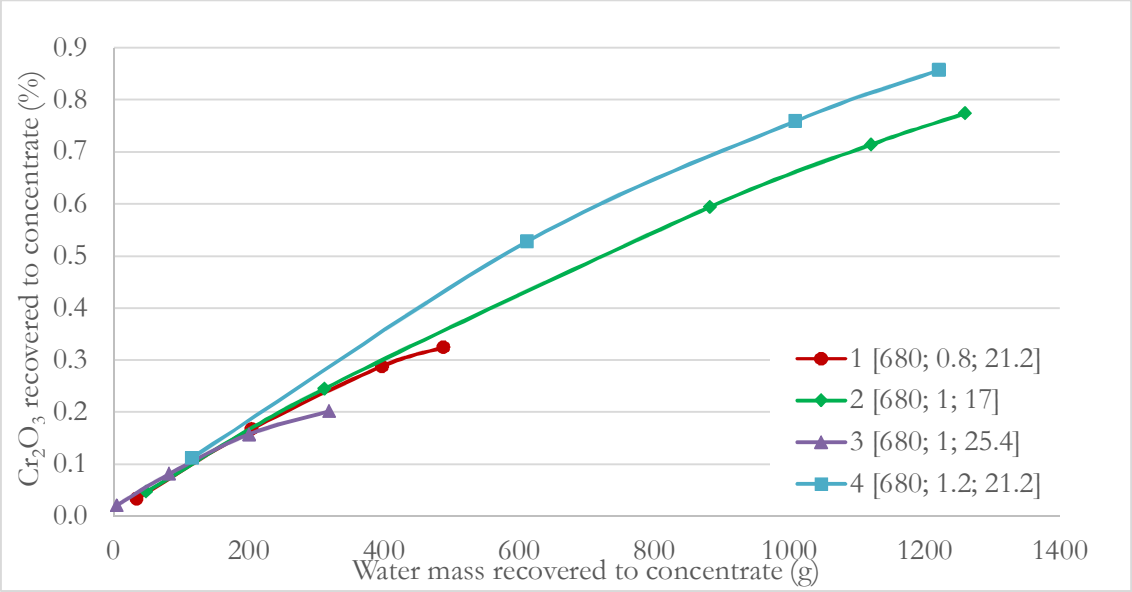

Figure 41: Chromite vs. mass of water recovered to concentrate at low mixing intensity while varying superficial gas velocity and recirculation rate. Each run is identified by the run number followed by the mixing intensity (rpm), superficial gas velocity (cm/s) and the recirculation rate (litre/min) given in square brackets.

From Figure 42, the averaged mid-point results (Average of runs 7-9), as well as runs 5 and 6, had the same recovery rates as the low mixing intensity results. It can be seen that all trend lines from the medium mixing intensity runs should intercept the ordinate close to the origin, if extended. As such, the chromite recovered was in all likelihood mostly entrained. Runs 10 and 11 have increased chromite recovery rates, possibly due to the increased aeration rate during these two runs. This suggests that superficial gas velocities above 1 cm/s should be used with caution to prevent excessive entrainment. These runs still display a decrease in chromite entrainment with an increase in time, which is typical if one assumes that the finer chromite particles (slimes) will be entrained easily and early in the flotation process.

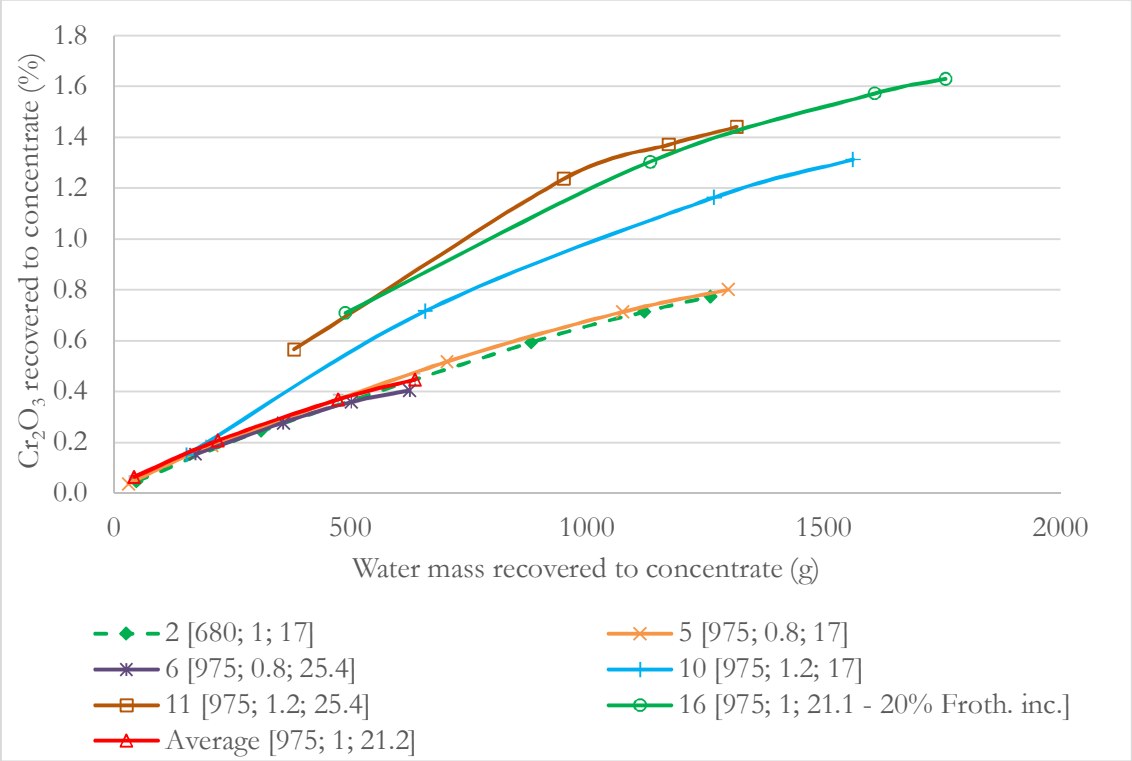

Figure 42: Chromite vs. mass of water recovered to concentrate at medium mixing intensity while varying superficial gas velocity and recirculation rate. Each run is identified by the run number followed by the mixing intensity (rpm), superficial gas velocity (cm/s) and the recirculation rate (litre/min) given in square brackets.

The high mixing intensity results of Figure 43 show that the trend lines of all these runs will also intercept the ordinate very close to the origin if extrapolated. A significant change in the chromite recovery rates can be observed, i.e. at previous mixing intensity levels, an increase in aeration rates resulted in increased chromite recovery; here the trend is not consistent. There are various factors that could affect the chromite recovery that was not directly measured. The statistical analysis of the data indicated that none of the three manipulated variables had a significant impact on chromite recovery. The differences observed in chromite recovery is therefore more likely influenced by an unmeasured variable that is affected by or related to the three manipulated variables in this study.

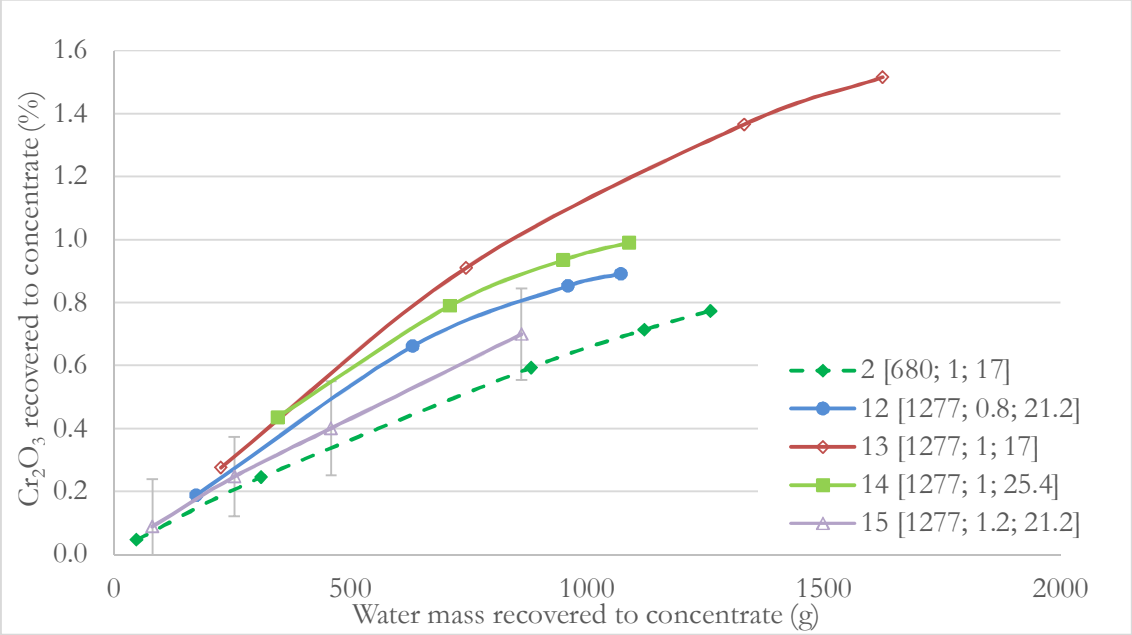

Figure 43: Chromite vs. mass of water recovered to concentrate at high mixing intensity while varying superficial gas velocity and recirculation rate. Each run is identified by the run number followed by the mixing intensity (rpm), superficial gas velocity (cm/s) and the recirculation rate (litre/min) given in square brackets.

5.5. Effect of Recirculation Rate within Size Fractions

The statistical evaluation indicated that recirculation rate had a significant impact (linear and quadratic) on mass pull, as well as a quadratic interaction with the recovery of valuable minerals. A series of experiments were done where the mixing intensity and superficial gas velocity were kept constant while varying the recirculation rate. A mass split was performed according to particle size in the concentrate to determine the percentage of valuable minerals of the concentrate in each size fraction. Four runs had to be replicated for each operating condition set, and these concentrate samples had to be combined in order to obtain enough mass to split them into size fractions for analysis. The experimental confidence should therefore be better than in the previous sections. The results indicate the concentrate size fractions to which most of the valuable minerals reported.

Figure 44 illustrates the mass pull per size fraction for low recirculation rate, Figure 45 for medium recirculation rate and Figure 46 for high recirculation rate, while mixing intensity (975 rpm) and superficial gas velocity (1 cm/s) stayed constant.

The cell recovered about 10 times more of the -38 fraction compared to the other size fractions throughout the experimental process. The fraction above 53 micron is only recovered up to eight minutes (see Figure 44). All the size fractions follow the same curvature which shows that there is

minimal selection towards a specific particle size during an experimental run and that all the particle sizes are subjected to the same change in recovery over time.

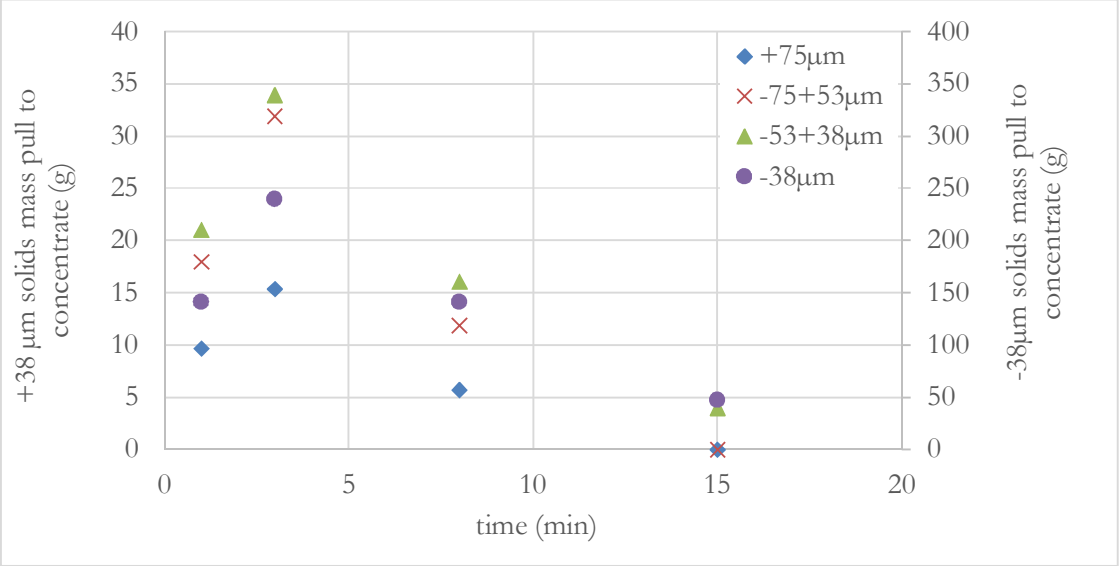

Figure 44: Solids mass pull for 17 L/min recirculation rate separated by particle size interval. All +38 µm fractions are indicated on the left-hand abscissa, while the -38 µm fraction is indicated on the right-hand abscissa.

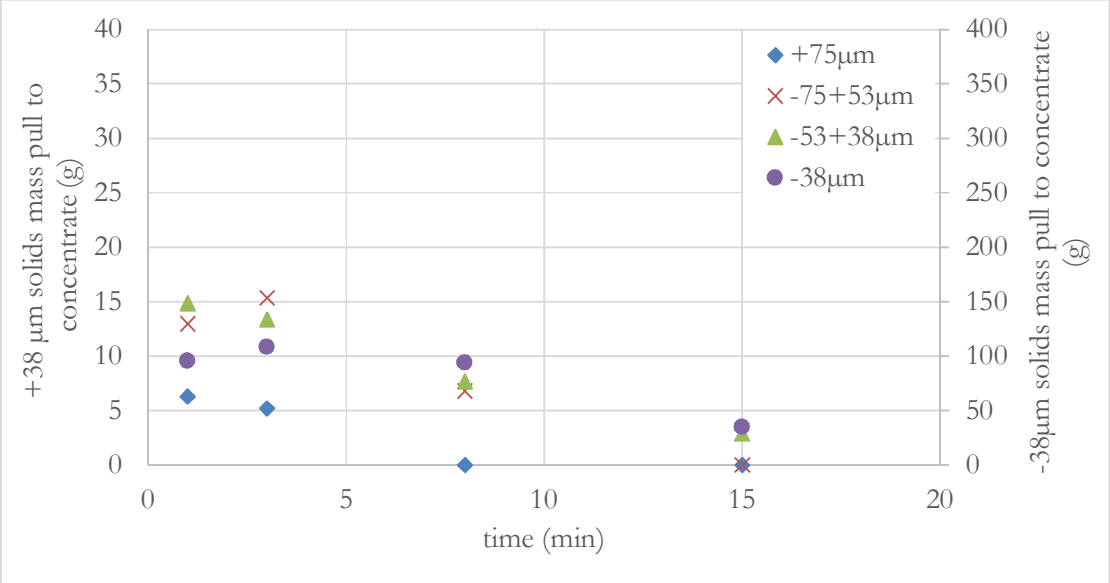

Figure 45: Solids mass pull for 21.2 L/min recirculation rate separated by particle size interval. All +38 µm fractions are indicated on the left-hand abscissa, while the -38 µm fraction is indicated on the right-hand abscissa.

Comparing trends in Figure 44 to Figure 46, it is evident that the solid mass pull decreases – in all size ranges – with an increase in recirculation rate. This effect is significant in the first 8 minutes of the flotation experiments, but not as significant in the 8-15 minutes interval. This could be due

to a decrease in the residence time of particles within the down-comer (and the cell) with an increase in recirculation rate. Increasing the recirculation rate also reduced the bubble size, possibly causing the frother concentration to decrease faster and therefore reducing froth stability later in the run.

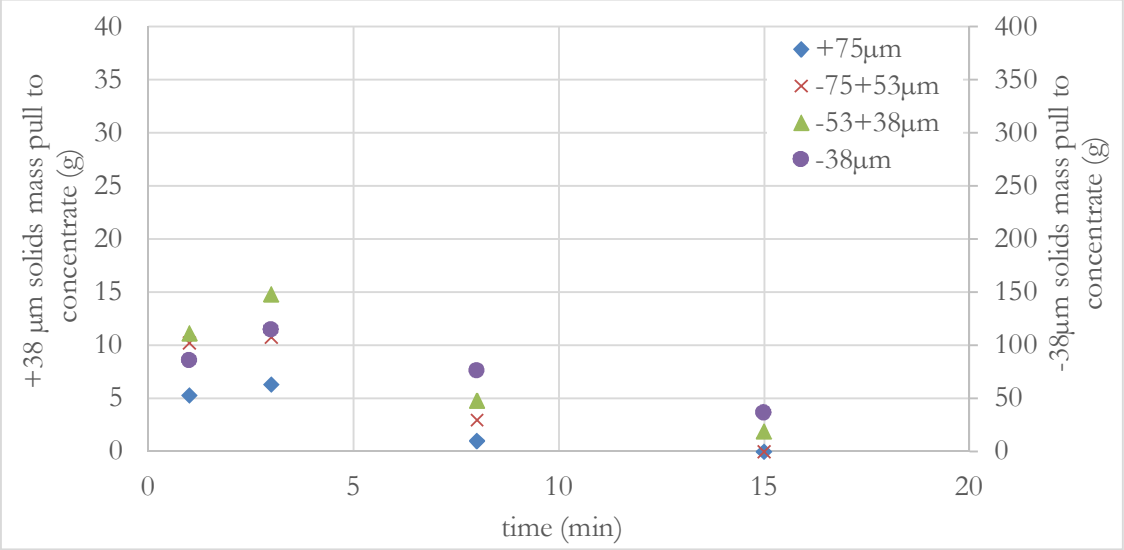

Figure 46: Solids mass pull for 25.4 L/min recirculation rate separated by particle size interval. All +38 µm fractions are indicated on the left-hand abscissa, while the -38 µm fraction is indicated on the right-hand abscissa.

The percentage of valuable metal within each size fraction in the concentrate, as well as the grade of each particle size range are shown in Figure 47. Here the recirculation rate in related runs was varied while the mixing intensity and superficial gas velocity were kept constant at the mid-point conditions. Solid and dashed lines are used to depict the valuable metal split and grade respectively. The valuable metal split is based on the percentage of the valuable metals from the concentrate that reports to a specific particle size range. Therefore, a total of 100% would be obtained if the valuable metal split percentages of the different particle size ranges were added together. This was done in order to identify the size fraction where most of the concentrate valuable metals report to. The grade is displayed as the concentrate grade in the specific particle size fraction. Adding all the grades together over the size fractions will give the total grade of the concentrate for that experimental set.

The valuable metal split percentages for the different runs are very closely related to one another. The difference between the medium and high mixing intensity are so small that the points are on top of one another in Figure 47 and would be within experimental error range. Most of the valuable minerals are within the size fraction below 38 µm. The valuable metals reporting to the -38 µm

size fraction is *ca* 60% higher than the coarser fractions. The trade-off of such improved recoveries is a maximum reduction of 40 g/t (~35%) in concentrate grade compared to the other fractions. The cut sizes in the particle size analysis should have been further reduced to below 10µm, but unfortunately this would have reduced analytical sample sizes again.

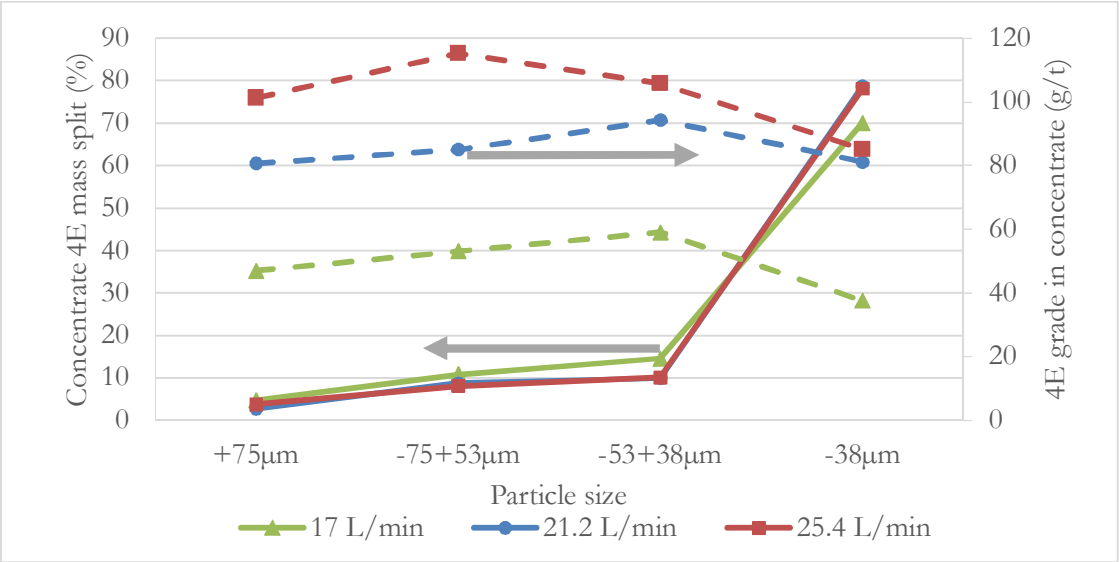

Figure 47: 4E recovery and grade per particle size range for constant mid-point mixing intensity (975 rpm) and superficial gas velocity (1 cm/s) while varying the recirculation rate. The arrows point towards the relevant axis (recovery left and grade right).

The 4E grades produced by varying recirculation rates are significantly different. Grades increase with an increase in recirculation rate, which could be due to lower residence times within the impeller stations, or a decrease in bubble size through the aerator or it could be both. It is also possible that the increase in superficial slurry velocity through the cell aided in the separation efficiency of the cell. Increasing the recirculation rate would reduce the bubble size, increasing the available bubble surface area for attachment. This would increase the recovery rate of hydrophobic minerals if sufficient energy is supplied to the mineral particles. The increase in the recirculation rate through these experiments caused the creation of smaller bubbles that moved further down the down-comer due to the increased superficial slurry velocities in the down-comer and the cell. This increased the gas hold-up within the cell, possibly creating a concentration gradient within the calming zone of the cell that reduced froth contamination. The bubble size reduction with an increase in recirculation rate also caused a more stable froth interface. Furthermore, an observation was made that more bubbles exit through the first down-comer exit port at a recirculation rate of 17 litre/min. This confirms hydrodynamic behaviour in the cell explained in Section 5.3.

The concentrate grades of the different size fractions follow the same trends at the low and medium recirculation rates, but the high mixing intensity seems to produce a higher grade in the 75-53 micron size range. This suggests that the medium mixing intensity and aeration rate, combined with a high recirculation rate, possibly caused some particle-bubble detachment of semi-liberated or weakly hydrophobic particles in that size range, thus mostly allowing the well-liberated valuable minerals to be transferred to the concentrate.

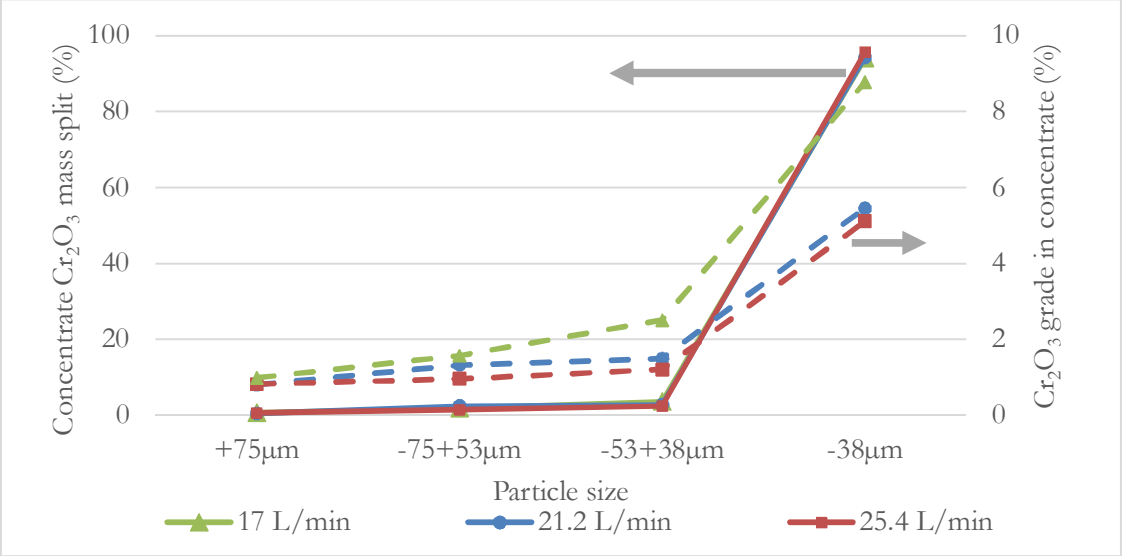

Figure 48: Chromite recovery and grade per particle size range for constant mid-point mixing intensity (975 rpm) and superficial gas velocity (1 cm/s) while varying the recirculation rate. The arrows point towards the relevant axis (recovery left and grade right).

Figure 48 shows concentrate chromite mass split percentage per particle size. Here the chromite mass split percentages are virtually identical at the different recirculation rates. As expected, the highest chromite concentrate mass split is observed in the -38 µm size fraction. The concentrate grades per size fractions vary from one another, suggesting that the recirculation rate had some effect on the selectivity towards chromite (e.g. influencing entrainment). The significant chromite recovery in the -38 µm fraction also reinforces the notion that most of the chromite recovery is due to entrainment (i.e. it is easier to entrain smaller particles). The higher concentrate chromite grade in the -38 µm fraction, at the lowest recirculation rate, was possibly due to disturbances through the calm zone, causing chromite to pass through the froth phase with these disturbances.

From Figure 47 and Figure 48 it is evident that an increase in recirculation rate had a positive effect on the grade of valuable minerals. The recirculation rate also seems to have an effect on the mass split to specific size fractions and this could possibly be used to target specific particle size ranges, depending on the requirements of the specific operation.

5.6. Comparing the Results from the New Cell with Conventional Mechanical Cells

The experimental results will now be compared with results from a PGM plant, as produced during bench cell flotation tests in a Denver cell and a bottom-driven mechanical cell. Unfortunately the exact operating conditions of these cells were not shared due to confidentiality of the plant operating conditions. These tests were performed with Rand water, which contains more dissolved solids than RO permeate, resulting in better froth stability. These runs were completed with froth depths between 20 and 30 millimetre and the volumes of the cells were both 8 litres.

In order to do a comparison, the best experimental runs with the new cell should be identified. Run 2 produced the best results in terms of a combination of final valuable mineral recovery and grade – with adequate chromite rejection. Run 5 can be considered as second best (based on final recovery and grade) and it was also the closest to the predicted optimum of the statistical model. The results of run 3 could also be used sensibly to compare the cell's performance when producing very high grades at lower recoveries.

However, a reliable direct comparison between the mechanical laboratory flotation cells and the new cell can only be done if the feed ore is exactly the same and if the same particle size ranges are used. The water quality, reagent concentrations and conditioning times should also be the same. As some of these factors were different between the cells, the subsequent comparisons only serve as a guide to measure the new cell's performance and to determine of further experiments are justified.

To this end, Figure 49 shows the valuable metal grade against the recovery to concentrate for the two mechanical cells (Twin and Denver) and the new cell. The Twin cell was a conventional bottom-driven flotation cell in which separate tests were performed with two different collectors. The Twin cell outperformed the Denver cell, although the results for both these mechanical cells were relatively close to one another. The new cell achieved very similar final 4E grades and recoveries in run 5, but achieved significantly higher initial 4E grades (i.e. during the initial flotation time intervals). With a decrease in feed water quality and continuous frother addition, such operating performance may prove to be very beneficial.

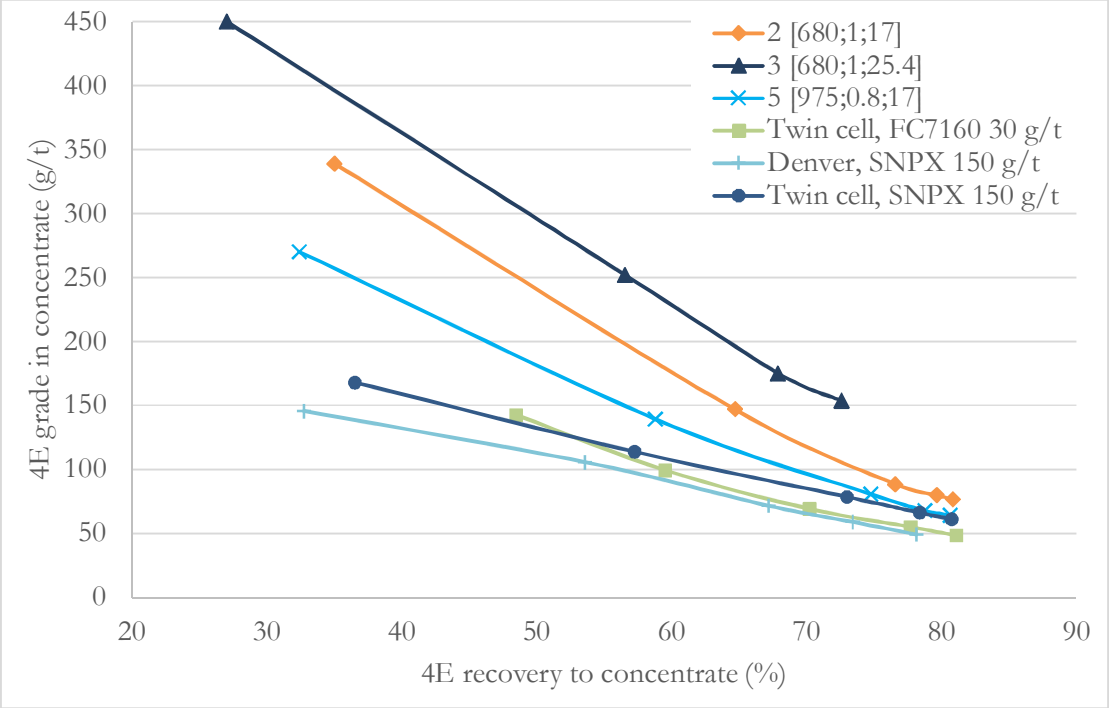

Figure 49: 4E grade vs. recovery comparison between the new cell and mechanical cells.

The performance in run 2 shows significant promise, as the final recovery was the same as with the mechanical cells, but it produced a 4E grade of 76.4 g/t, which was 15 g/t higher than with the mechanical cells. The higher grade of run 2 was achieved at shallower froth depths than the mechanical cells, and could still be improved with an increase in froth depth. The recovery rate in run 2 was faster than with the mechanical cells, where run 2 obtained a 64% recovery in three minutes against the 53% of the Denver cell. Run 2 maintained the faster recovery up to 15 minutes, after which the decrease in recovery caused the mechanical cells to catch up. This may be the result of frother depletion or froth depth in the new cell which suggests that the recovery may even be higher if the frother concentration was maintained.

It should be noted that the froth depth in the new cell was maintained closely around 10mm (except for the one initial excursion in run 15) while the mechanical cells had froth depths twice to three times as deep (Ross, 2015). An increased froth depth generally increases the concentrate grade, sometimes with no significant reduction in recovery of valuable minerals (Corin and Wiese, 2014). Increasing the forth depth also improves the chromite rejection, which is very important for downstream processes.

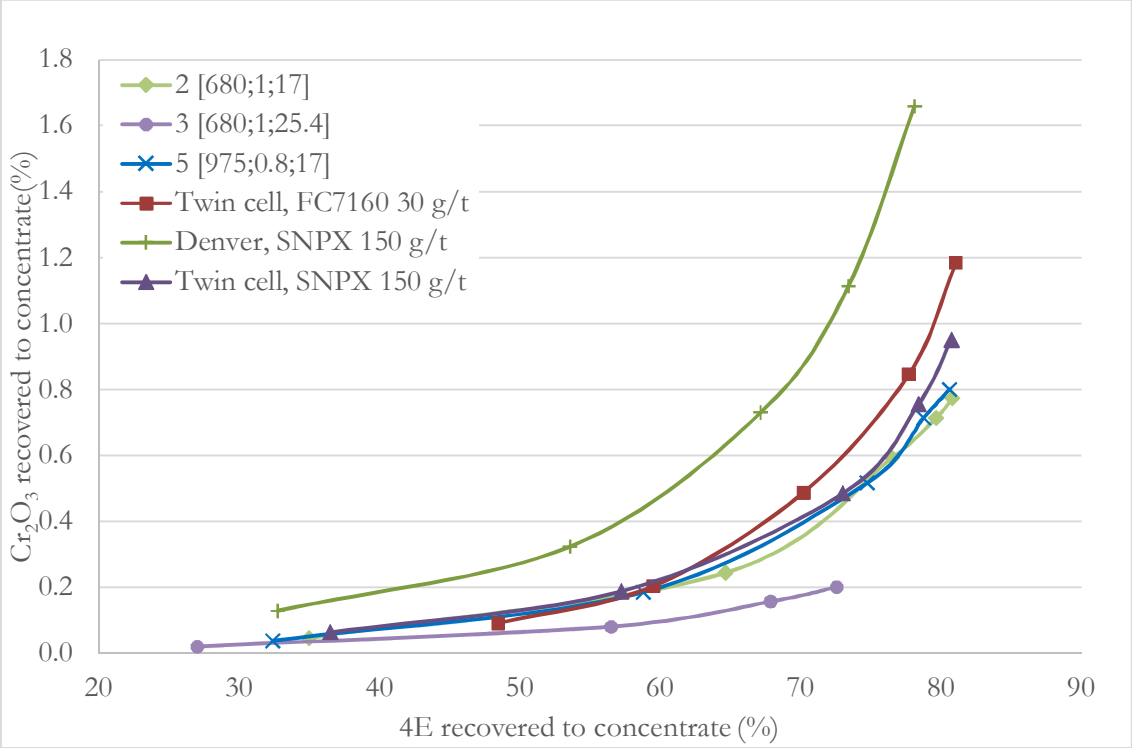

Figure 50: Chromite vs. 4E recovery comparison between the new cell and mechanical cells.

Comparing the chromite recovery with the recovery of valuable minerals in Figure 50 shows that run 5 performed very similar to the twin cell and SNPX collector within the first 8 minutes. Run 5 shows a slight decrease in chromite recovery after 8 minutes if compared to the mechanical cell. Run 2 showed very similar results to run 5 in the recovery of chromite, which serves as early indication that the cell may have good chromite rejection abilities that may be improved further by increasing froth depth. Run 3, with its high-grade concentrate, shows a significant reduction in chromite recovery compared to the mechanical cells.

Chapter 6 – Conclusions and Recommendations

This study combined design features from column and conventional mechanical flotation cells in an attempt to improve the recovery and separation of fine PGE minerals. Sequential release of aerated slurry (into a calm froth separation zone) from a down-comer with built-in agitation, attempted to achieve the following:

- High-intensity, confined mixing during aeration to maximise particle-bubble interaction and attachment.
- The creation of a concentration gradient within the calming (froth) zone of the cell in order to improve concentrate grade.

After a systematic design and construction exercise, the baseline performance of the cell was evaluated and compared to the performance of standard mechanically agitated cells at a PGM plant. Three independent factors that could affect the hydrodynamics within the cell were varied, viz. mixing intensity (rpm), recirculation rate (l/min) and superficial gas velocity (cm/s). The total mass pull to concentrate varied between 2-6% while final (overall) valuable metal (4E) recovery varied between 70% and 85%. Within the first 1-minute time interval, the recovery of valuable minerals to concentrate varied between 27% and 55% - depending on the hydraulic operating conditions. Final concentrate grades varied between 50 and 150 g/t, while chromite recoveries to the concentrate could be maintained between 0.2 and 1.6%.

6.1. Primary Design Features of the Cell

The cell was designed to provide the following operational features:

- The slurry feed is aerated through an external (sintered medium, 5µm pore size) aerator before flowing downwards through the vertical down-comer of the cell. The down-comer incorporates three stator-impeller stations, creating high mixing intensity zones to facilitate bubble-particle attachment.
- Aerated slurry can escape from the down-comer into a calming zone (froth separation zone) through exit ports below each stator-impeller station. These exit ports in the down-comer facilitate a stratified release of aerated slurry. In concept, the idea is to enable the most floatable and strongly attached particles to be released first (close to the pulp-froth interface). Less floatable (un-attached) hydrophobic minerals can then pass through another stator-impeller station to facilitate further bubble-particle attachment and subsequent release into the calming zone (further below the pulp-froth interface).

- Conceptually and due to the stratification approach, the calming zone should allow for proper rejection of gangue minerals. The calming zone exist in a cylinder with a diameter of 143 mm and a length of 490 mm.

As provided in Table 13, the hydraulic design and operating features of the cell are as follows:

Parameter	**Range**
Superficial gas velocity, J_g (cm/s)	0.8 – 1.2
Down-comer superficial slurry velocity, $J_{s,down\text{-}comer}$ (cm/s)	27.8 – 41.6
Cell superficial slurry velocity, J_s (cm/s)	1.8 – 2.6
Down-comer max. velocity ($J_g + J_s$: cm/s)	39.4 – 59.1
Theoretical Power (W, equation 4)	0.06 – 0.41
Theoretical impeller specific energy input (J/kg)	0.17 – 0.76
Total theoretical impeller power input (Wh/kg)	0.0052-0.0343
Impeller tip speed (m/s)	1.14 – 2.14
Aeration rate (L/min)	7.1 – 10.7
Recirculation rate (L/min)	17 – 25.4
Tank volume replacement time (s)	19 – 28
Mixing intensity (rpm)	680 – 1277

6.2. General Performance of the Cell

The results indicate that the cell may either be used in rougher or cleaner duties by only manipulating the hydrodynamic environment within the cell.

The recirculation rate and superficial gas velocity can be used to manipulate ore- and water mass-pull, where the recirculation rate is the only manipulated variable with statistically significant (quadratic relationship) impact on 4E recovery. The 4E grade can be manipulated by all of the following three variables: mixing intensity, recirculation rate and superficial gas velocity. Evidence exists that there is a combined effect of mixing intensity and recirculation rate on 4E grade. Chromite rejection appears to be affected slightly by mixing intensity, and chromite recovery tends to decrease with an increase in mixing intensity.

A low recirculation rate (17 l/min) should typically be used to achieve high recoveries in rougher applications. A high recirculation rate (25.4 l/min), medium superficial gas velocity (1 cm/s) and low mixing intensity (680 RPM) should typically be used to achieve high grades in cleaner applications. The effect of other factors such as (but not limited to) chemical suite used, bubble

surface area flux and froth depth on valuable metal grade and recovery, as well as on chromite rejection, should be investigated further.

A direct and accurate comparison between the new cell design and conventional flotation cells could not be completed, since these cells could not be operated side by side. However, typical laboratory results were obtained from an operating PGM plant and useful preliminary comparisons could be made, as follows: The new cell could achieve similar valuable (4E) mineral recoveries, while simultaneously achieving higher final grades. The new cell also showed better initial 4E grades at similar recoveries compared to the conventional cells. The selectivity towards the valuable minerals was higher in the new cell.

Due to potential differences in chemical and ore conditions, these observations are qualified and are shared with due caution. As such, it is recommended that the new cell should be operated in parallel (side by side) to an actual plant – with the same conditioned feed – to enable a more accurate comparison.

This cell design shows promise, but it should be optimized further for specific applications and conditions.

6.3. Recommendation on Scale-up Possibilities

Some design difficulties were experienced due to the size limitations of the design. One obvious limitation was the minimal equipment options. For example, there are not many small sized slurry pumps available on the market.

The radial distribution of the down-comer exit ports was poor due to the lower size limit on the holes and the maximum allowable exit area at each station (to ensure aerated slurry flow throughout the down-comer). Radial distribution of exits will be improved through scale-up, since the lower limit of the hole size would not increase in the same ratio as the open-size requirement after each impeller station.

Pressure drop through the down-comer would also be reduced through scale up. The shaft diameter used was quite large compared to the down-comer diameter. With the small scale it is impossible to install shaft stabilizers throughout the down-comer and therefore the shaft diameter had to be large enough to prevent buckling, which contributed to vibrations through the down-comer.

Mounting the impellers to the shaft with grub screws also required a material thickness of at least three millimetres around the shaft, which decreased the available area for slurry to flow through

the impellers. On this scale the enlarged impeller core had a significant effect on the flow of the slurry through the down-comer, which added to the pressure drop through the cell.

The down-comer diameter can be decreased through scale-up due to the scale improvements mentioned above. Decreasing the down-comer diameter will reduce the recirculation rate requirements and therefore increase the residence times within the cell.

In larger cells the aerator could be integrated into the down-comer, which would reduce the distance between the aerator and the first impeller station. This would reduce the chances of coalescence before the aerated slurry reach the first station. Coalescence would also be reduced as the aerated slurry would flow straight down the down-comer instead of making sharp turns as it exits the aerator. This would ultimately allow a reduced pressure drop through the down-comer, which would also reduce the recirculation rate requirements needed to prevent coalescence and air build-up in the top section of the down-comer.

With larger cells the motor could possibly be integrated into the down-comer, which would reduce the shaft length needed. Mechanical seals could be mounted around the shaft throughout the down-comer, which makes the use of bearings possible to stabilise the shaft throughout. This would open up the top of the cell to install froth scrapers, which would move the froth to the launder around the cell.

All these changes, with an increased scale, may have a significant benefit in the operation conditions of the cell as well as possible improvements in the cell performance.

Chapter 7 – References

AHMED, N. and JAMESON, G.J., 1985. The effect of bubble size on the rate of flotation of fine particles. *International Journal of Mineral Processing,* **14**(3), pp. 195-215.

ARBITER, N., HARRIS, C.C. and YAP, R.F., 1976. *The air flow number in flotation machine scale-up.*

ARBITER, N., 2000. Development and scale-up of large flotation cells. *Mining Engineering,* **52**(3), pp. 28.

ATA, S., 2012. *Phenomena in the froth phase of flotation — A review.*

ATKINSON, B. and CONWAY, C., 1993. Fundamentals of Jameson Cell operation including size-yield response, *Proceedings of the 6th Australian Coal Preparation Conference* 1993, Australian Coal Prep. Soc. Mackay, pp. 401-417.

BARNES, A. and NEWALL, A., 2006. Spinel removal from PGM smelting furnaces, R.T. JONES, ed. In: *Southern African Pyrometallurgy*, 5-8 March 2006 2006, South African Institute of Mining and Metallurgy, pp. 77.

CAWTHORN, R.G., 1999. The platinum and palladium resources of the Bushveld Complex. *South African Journal of Science,* **95**(11), pp. 481-489.

ÇENGEL, YUNUS A., CIMBALA,JOHN M., 2010. *Fluid mechanics : fundamentals and applications.* Boston: McGraw-Hill Higher Education.

ÇINAR, M., SAHBAZ, O., ÇINAR, F., KELEBEK, S. and ÖTEYAKA, B., 2007. Effect of Jameson cell operating variables and design characteristics on quartz-dodecylamine flotation system. *Minerals Engineering,* **20**(15), pp. 1391-1396.

COLLINS, G.L. and JAMESON, G.J., 1977. Double-layer effects in the flotation of fine particles. *Chemical Engineering Science,* **32**(3), pp. 239-246.

COLLINS, G.L. and JAMESON, G.J., 1976. Experiments on the flotation of fine particles. The influence of particle size and charge. *Chemical Engineering Science,* **31**(11), pp. 985-991.

CORIN, K.C., REDDY, A., MIYEN, L., WIESE, J.G. and HARRIS, P.J., 2011. The effect of ionic strength of plant water on valuable mineral and gangue recovery in a platinum bearing ore from the Merensky reef. *Minerals Engineering,* **24**(2), pp. 131-137.

CORIN, K.C. and WIESE, J.G., 2014. Investigating froth stability: A comparative study of ionic strength and frother dosage. *Minerals Engineering,* **66**, pp. 130-134.

DAI, Z., DUKHIN, S., FORNASIERO, D. and RALSTON, J., 1998. The Inertial Hydrodynamic Interaction of Particles and Rising Bubbles with Mobile Surfaces. *Journal of colloid and interface science,* **197**(2), pp. 275-292.

DE F. GONTIJO, C., FORNASIERO, D. and RALSTON, J., 2007. The Limits of Fine and Coarse Particle Flotation. *The Canadian Journal of Chemical Engineering,* **85**(5), pp. 739-747.

DEGLON, D.A., EGYA-MENSAH, D. and FRANZIDIS, J.P., 2000. Review of hydrodynamics and gas dispersion in flotation cells on South African platinum concentrators. *Minerals Engineering,* **13**(3), pp. 235-244.

DERJAGUIN, B.V. and DUKHIN, S.S., 1993. Theory of flotation of small and medium-size particles. *Progress in Surface Science,* **43**(1–4), pp. 241-266.

GAUDIN, A. M., SCHUHMANN, R., SCHLECHTEN,A.W., 1942. Flotation Kinetics. II. The Effect of Size on the Behavior of Galena Particles. *J.Phys.Chem.The Journal of Physical Chemistry,* **46**(8), pp. 902-910.

GAUDIN, A.M., 1957. *Flotation.* New York: McGraw-Hill.

GLEMBOT□ S□ KIŤ, V.A. and RABINOVICH, H.S., 1963. *Flotation.* New York : Primary Sources,.

GORAIN, B., FRANZIDIS, J. and MANLAPIG, E., 2000. Flotation Cell Design: Application of Fundamental Principles.

HACIFAZLIOGLU, H. and TOROGLU, I., 2007. Optimization of design and operating parameters in a pilot scale Jameson cell for slime coal cleaning. *Fuel Processing Technology,* **88**(7), pp. 731-736.

HARBORT, G.J., MANLAPIG, E.V. and DEBONO, S.K., 2002. Particle collection within the Jameson cell downcomer. *Transactions of the Institutions of Mining and Metallurgy, Section C: Mineral Processing and Extractive Metallurgy,* **111**(JAN./APR.), pp. C1-C10.

JOWETT, A., 1980. FORMATION AND DISRUPTION OF PARTICLE-BUBBLE AGGREGATES IN FLOTATION. *Proceedings - IEEE Computer Society's International Computer Software & Applications Conference,* , pp. 720-754.

KYZAS, G.Z. and MATIS, K.A., 2016. Electroflotation process: A review. *Journal of Molecular Liquids,* **220**, pp. 657-664.

LIU, Q., WANNAS, D. and PENG, Y., 2006. Exploiting the dual functions of polymer depressants in fine particle flotation. *International Journal of Mineral Processing,* **80**(2–4), pp. 244-254.

MATIS, K.A., GALLIOS, G.P. and KYDROS, K.A., 1993. Separation of fines by flotation techniques. *Separations Technology,* **3**(2), pp. 76-90.

MATIS, K.A. and PELEKA, E.N., 2010. Alternative flotation techniques for wastewater treatment: Focus on electroflotation. *Separation Science and Technology,* **45**(16), pp. 2465-2474.

MIETTINEN, T., RALSTON, J. and FORNASIERO, D., 2010. The limits of fine particle flotation. *Minerals Engineering,* **23**(5), pp. 420-437.

NELSON, M.G. and LELINSKI, D., 2000. Hydrodynamic design of self-aerating flotation machines. *Minerals Engineering,* **13**(10–11), pp. 991-998.

NGUYEN, ANH V., GEORGE, PETER, JAMESON, GRAEME J., 2006. Demonstration of a minimum in the recovery of nanoparticles by flotation: Theory and experiment. *CES Chemical Engineering Science,* **61**(8), pp. 2494-2509.

PEASE, J.D., YOUNG, M.F., CURRY, D. and JOHNSON, N.W., 2010. Improving fines recovery by grinding finer. *Transactions of the Institutions of Mining and Metallurgy, Section C: Mineral Processing and Extractive Metallurgy,* **119**(4), pp. 216-222.

RALSTON, J. and DUKHIN, S.S., 1999. The interaction between particles and bubbles. *Colloids and Surfaces A: Physicochemical and Engineering Aspects,* **151**(1–2), pp. 3-14.

RALSTON, J., DUKHIN, S.S. and MISHCHUK, N.A., 2002. Wetting film stability and flotation kinetics. *Advances in Colloid and Interface Science,* **95**(2–3), pp. 145-236.

REAY, D. and RATCLIFF, G.A., 1975. Experimental testing of the hydrodynamic collision model of fine particle flotation. *The Canadian Journal of Chemical Engineering,* **53**(5), pp. 481-486.

REAY, D. and RATCLIFF, G.A., 1973. Removal of fine particles from water by dispersed air flotation: Effects of bubble size and particle size on collection efficiency. *The Canadian Journal of Chemical Engineering,* **51**(2), pp. 178-185.

ROSS, V., 2015.

RUBIO, J., CAPPONI, F. and MATIOLO, E., 2006. Flotation of sulphides ore fines and ultrafines particles, *IMPC 2006 - Proceedings of 23rd International Mineral Processing Congress* 2006, pp. 587-592.

RULYOV, N.N., 2008. Turbulent microflotation of ultrafine minerals. *Transactions of the Institutions of Mining and Metallurgy, Section C: Mineral Processing and Extractive Metallurgy,* **117**(1), pp. 32-37.

RULYOV, N.N., 2001. Turbulent microflotation: theory and experiment. *Colloids and Surfaces A: Physicochemical and Engineering Aspects,* **192**(1–3), pp. 73-91.

RULYOV, N.N., 1999. Application of ultra-flocculation and turbulent micro-flotation to the removal of fine contaminants from water. *Colloids and Surfaces A: Physicochemical and Engineering Aspects,* **151**(1–2), pp. 283-291.

SCHULZE, H.J., 1992. Probability of particle attachment on gas bubbles by sliding. *Advances in Colloid and Interface Science,* **40**, pp. 283-305.

SONG, S., LOPEZ-VALDIVIESO, A., REYES-BAHENA, J.L. and LARA-VALENZUELA, C., 2001. Floc flotation of galena and sphalerite fines. *Minerals Engineering,* **14**(1), pp. 87-98.

SUBRAHMANYAM, T.V. and FORSSBERG, K.S.E., 1990. Fine particles processing: shear-flocculation and carrier flotation — a review. *International Journal of Mineral Processing,* **30**(3–4), pp. 265-286.

SUTHERLAND, K.L., 1948. Physical Chemistry of Flotation. XI. Kinetics of the Flotation Process. *J.Phys.Chem.The Journal of Physical and Colloid Chemistry,* **52**(2), pp. 394-425.

VERMAAK, C.F. and VAN DER MERWE, M.J., 19uu. *The platinum mines and deposits of the Bushveld Complex, South Africa*. Randburg : Mintek,.

VON GRUENEWALDT, G., 1985. *Platinum-chromitite associations in the Bushveld Complex*. Pretoria : Institute for Geological Research on the Bushveld Complex, University of Pretoria,.

WARREN, L.J., 1975. Shear-flocculation of ultrafine scheelite in sodium oleate solutions. *Journal of colloid and interface science,* **50**(2), pp. 307-318.

WIESE, J. and HARRIS, P., 2012. The effect of frother type and dosage on flotation performance in the presence of high depressant concentrations. *Minerals Engineering,* **36-38**, pp. 204-210.

WIESE, J., HARRIS, P. and BRADSHAW, D., 2011. The effect of the reagent suite on froth stability in laboratory scale batch flotation tests. *Minerals Engineering,* **24**(9), pp. 995-1003.

YANG, SEUNG-MAN, HAN, SANG PHIL, HONG,JEONG JIN, 1995. Capture of Small Particles on a Bubble Collector by Brownian Diffusion and Interception. *YJCIS Journal of Colloid And Interface Science,* **169**(1), pp. 125-134.

YOON, R.H. and LUTTRELL, G.H., 1989. The Effect of Bubble Size on Fine Particle Flotation. *Mineral Processing and Extractive Metallurgy Review,* **5**(1-4), pp. 101-122.

Appendices

8.1. Appendix A – Raw Data

Table 13: Raw data 1

Run	Time (min)	Sample Mass (g)	Water Recovered (g)	Sample Grade				
				Cr2O3 (%)	Au (g/t)	Pd (g/t)	Pt (g/t)	Rh (g/t)
1 680 0.8 21.2	1	12.8	34.1	2.24	1.94	133.00	194.00	37.70
	3	31.2	169.2	3.67	0.61	30.50	61.00	12.10
	8	26.3	193.5	3.95	0.36	14.30	29.70	6.09
	15	7.1	90.4	4.42	0.49	11.00	23.10	3.14
	T	2879.6		29.70	0.05	0.32	0.69	0.05
2 680 1 17	1	13.4	48.1	2.88	3.08	100.00	203.00	33.00
	3	43.8	263.3	3.73	0.84	21.50	56.60	9.16
	8	55.1	570.3	5.22	0.52	4.67	19.80	3.00
	15	17.3	238.4	5.72	0.48	5.40	15.60	1.86
	30	7.8	139.4	6.37	0.47	5.22	12.00	2.05
	T	2831.6	0.0	28.90	0.05	0.22	0.56	0.05
3 680 1 25.4	1	7.0	4.8	2.29	3.84	144.00	269.00	45.80
	3	21.2	77.3	2.18	1.47	48.60	113.00	19.50
	8	20.9	117.9	2.77	0.89	16.90	46.50	6.95
	15	10.9	118.5	3.11	0.96	13.30	37.40	5.15
	T	2907.5	0.0	26.20	0.10	0.37	0.83	0.05
4 680 1.2 21.2	1	22.0	115.8	3.98	2.50	68.25	122.50	17.85
	3	57.3	495.7	5.64	0.78	16.20	39.00	6.29
	8	31.2	397.3	5.77	0.63	6.01	24.80	3.84
	15	12.5	212.2	6.10	0.89	6.61	15.80	2.52
	T	2847.9	0.0	27.10	0.05	0.28	0.73	0.05
5 975 0.8 17.0	1	13.8	31.0	2.08	1.55	94.80	145.00	28.80
	3	34.8	175.4	3.20	0.58	26.60	49.70	10.50
	8	58.1	496.9	4.28	0.29	8.87	18.90	3.57
	15	27.2	371.9	5.44	0.19	5.32	9.53	1.90
	30	10.6	222.8	6.18	0.56	5.56	13.00	1.13
	T	2825.0	0.0	26.40	0.05	0.22	0.47	0.05

Table 14: Raw data 2

Run	Time (min)	Sample Mass (g)	Water Recovered (g)	Sample Grade				
				Cr2O3 (%)	Au (g/t)	Pd (g/t)	Pt (g/t)	Rh (g/t)
6 975 0.8 25.4	1	31.2	172.1	4.09	1.08	54.40	87.30	16.70
	3	24.2	186.2	4.31	0.51	21.20	42.70	8.84
	8	15.7	143.7	4.35	0.48	14.50	25.80	6.45
	15	8.2	122.3	4.59	0.41	9.59	32.30	4.38
	T	2887.5	0.0	28.80	0.05	0.21	0.48	0.05
7 975 1.0 21.2	1	17.0	87.7	6.27	1.44	86.2	131	25.7
	3	26.8	156.8	3.87	0.77	34.85	67.55	13.45
	8	35.5	266.4	3.79	0.35	11.6	26.8	5.03
	15	13.6	169.5	4.74	0.34	8.53	19.6	3.37
	T	2867.1	0.0	27.6	0.05	0.24	0.52	0.05
8 975 1.0 21.2	1	12.2	23.6	2.23	1.63	99.90	162.00	32.70
	3	30.4	166.8	3.56	0.55	30.10	60.90	12.30
	8	28.5	217.5	3.99	0.32	11.80	29.10	5.74
	15	14.7	177.9	4.92	0.33	8.35	19.60	3.39
	T	2878.1	0.0	27.40	0.05	0.26	0.62	0.05
9 975 1.0 21.2	1	9.7	17.2	2.06	2.24	111.00	167.00	33.30
	3	38.7	204.6	3.30	0.51	28.20	53.80	10.80
	8	33.0	281.6	4.22	0.29	10.80	24.60	4.96
	15	10.2	139.0	4.96	0.43	10.50	22.70	3.57
	T	2872.1	0.0	27.70	0.05	0.28	0.66	0.05
10 975 1.2 17.0	1	29.4	153.4	3.88	1.56	59.70	121.00	19.30
	3	60.7	505.1	7.05	0.23	7.92	16.70	3.42
	8	50.3	609.9	6.69	0.21	6.44	14.90	2.88
	15	18.0	293.0	6.27	0.30	5.64	12.10	2.41
	T	2811.9	0.0	26.50	0.05	0.23	0.52	0.05
11 975 1.2 25.4	1	57.7	380.7	7.86	0.54	36.60	67.90	12.80
	3	59.4	569.6	9.05	0.25	10.65	21.00	4.20
	8	16.7	222.2	6.45	0.25	6.75	14.70	2.62
	15	7.6	143.1	7.37	0.55	8.08	17.30	2.55
	T	2819.7	0.0	28.00	0.05	0.29	0.61	0.05

Table 15: Raw data 3

Run	Time (min)	Sample Mass (g)	Water Recovered (g)	Sample Grade				
				Cr2O3 (%)	Au (g/t)	Pd (g/t)	Pt (g/t)	Rh (g/t)
12 1277 0.8 21.2	1	31.1	173.8	5.21	0.98	62.50	91.00	18.10
	3	54.1	458.0	7.53	0.35	14.90	29.90	6.21
	8	26.7	326.9	6.15	0.11	1.85	4.04	0.56
	15	6.1	112.4	5.45	1.38	51.60	116.00	23.00
	T	2842.7	0.0	30.00	0.05	0.28	0.60	0.05
13 1277 1.0 17.0	1	40.5	226.5	5.03	0.83	52.60	85.10	15.60
	3	62.3	517.7	7.52	0.50	9.84	26.90	4.07
	8	47.9	587.1	7.01	0.20	6.84	14.90	3.15
	15	16.0	293.0	6.91	0.31	6.40	13.60	2.53
	T	2806.5	0.0	25.90	0.05	0.24	0.54	0.05
14 1277 1.0 25.4	1	50.8	346.0	6.45	1.47	39.70	81.50	13.00
	3	38.1	364.1	6.98	0.68	13.80	34.50	5.65
	8	19.4	238.6	5.61	0.59	10.20	27.20	3.84
	15	8.1	140.2	5.24	0.68	8.74	21.30	3.63
	T	2849.2	0.0	26.10	0.05	0.21	0.54	0.05
15 1277 1.2 21.2	1	20.6	81.2	3.60	1.35	78.50	127.00	25.00
	3	29.9	173.5	4.44	0.46	21.60	41.80	8.71
	8	29.5	204.3	4.35	0.31	11.00	24.90	5.03
	15	32.3	402.4	7.74	0.23	5.98	13.20	2.48
	T	2853.5	0.0	29.10	0.05	0.28	0.59	0.05
16 975 1.0 21.2 +20% F	1	66.7	489.5	8.64	0.51	34.50	75.60	13.30
	3	66.0	643.4	7.34	0.46	30.60	52.20	9.91
	8	31.4	474.4	6.94	0.25	19.40	47.80	7.27
	15	6.6	149.7	7.11	0.36	3.45	7.18	1.24
	T	2796.3	0.0	28.60	0.05	0.26	0.55	0.05

8.2. Appendix B – Sample Calculations

The following calculations can be used in order to evaluate the results. These calculations are all for one experimental run only where Experimental Run 1 will be used to do the calculations. Therefore there are a maximum of five concentrate samples and one tailings sample. First the actual sample mass need to be calculated which gives the sample mass in Table 13 through to Table 15:

$$m_{sample,i} = m_{dry\ tray\ with\ sample,i} - m_{tray,i}$$

$$m_{sample,1} = 12.8$$

$$m_{sample,2} = 31.2$$

$$m_{sample,3} = 26.3$$

$$m_{sample,4} = 7.1$$

$$m_{sample,T} = 2879.6$$

The water carried over to the concentrate tray can be estimated as follow which can be seen in Table 13 through to Table 15 as the water recovery:

$$m_{sprayed} = \frac{m_{spray\ bottle\ before\ experiment} - m_{spray\ bottle\ after\ experiment}}{number\ of\ sample\ trays}$$

$$m_{water\ collected,i} = m_{wet\ sample\ tray,i} - m_{dry\ tray\ with\ sample,i} - m_{sprayed}$$

$$m_{water\ collected,1} = 34.1$$

$$m_{water\ collected,2} = 169.2$$

$$m_{water\ collected,3} = 193.5$$

$$m_{water\ collected,4} = 90.4$$

This can then be used to calculate the cumulative mass pull percentage to the concentrate according to the sample number i:

$$m_{experiment,k} = m_{tailings,k} + \sum_{i=1}^{i=5} m_{sample\ k,i}$$

$$X_{k,i}(\%) = \frac{0.01 \times X_{k,i-1} \times m_{experiment,k} + m_{sample\ k,i}}{m_{experiment}} \times 100$$

$$m_{experiment,1} = 2879.6 + \ 12.8 + 31.2 + 26.3 + 7.1 = 2957$$

$$X_{1,1}(\%) = \frac{0.01 \times 0 \times 2957 + 12.8}{2957} \times 100 = 0.43\%$$

$$X_{1,2}(\%) = \frac{0.01 \times 0.43 \times 2957 + 31.2}{2957} \times 100 = 1.49\%$$

$$X_{1,3}(\%) = \frac{0.01 \times 1.49 \times 2957 + 26.3}{2957} \times 100 = 2.37\%$$

$$X_{1,4}(\%) = \frac{0.01 \times 2.37 \times 2957 + 7.1}{2957} \times 100 = 2.61\%$$

The cumulative mass pull of water collected can also be calculated according to the sample number i:

$$m_{water\ k,i} = \sum_{j=1}^{j=i} m_{water\ collected,j}$$

$$m_{water\ 1,1} = 34.1$$

$$m_{water\ 1,2} = 34.1 + 169.2 = 203.3$$

$$m_{water\ 1,3} = 203.3 + 193.5 = 396.8$$

$$m_{water\ 1,3} = 396.8 + 90.4 = 487.2$$

The total grade of the experimental ore mass has to be calculated back from the analysis grades of the concentrate and the tailings. For the valuable metals platinum, palladium, rhodium, gold and chrome as the gangue, the following equation can be used where k denotes the specific metal in question:

$$x_{k,total} = \frac{\sum_{i=1}^{i=5}\left(x_{k,i} \times m_{sample,i}\right) + x_{k,tailings} \times m_{tailings}}{m_{experiment}}$$

Gold will be calculated as an example:

$$x_{Au,total\ 1} = \frac{1.94 \times 12.8 + 0.61 \times 31.2 + 0.36 \times 26.3 + 0.49 \times 7.1 + 0.05 \times 2957}{2957}$$

$$x_{Au,total\ 1} = 0.07$$

Here the grade of the valuable minerals is in grams per tonne (g/t) and chrome is in percentage. The combined grades and recovery of all four valuable metals will be used to compare different runs from one another. Therefore:

$$x_{4E,i} = \sum_{k=1}^{k=4} x_{k,i}$$

This will be done for the first sample:

$$x_{4E,1} = 1.94 + 133 + 194 + 37.7 = 366.64\ g/t$$

Recovery percentages can also be calculated for the different metals for the different samples:

$$r_{k,i}(\%) = \frac{x_{k,i} \times m_{sample,i}}{x_{k,total} \times m_{experiment}} \times 100$$

As an example the recovery of gold will be calculated:

$$r_{Au,1}(\%) = \frac{1.94 \times 12.8}{0.07 \times 2957} \times 100 = 12.37\%$$

$$r_{Au,2}(\%) = \frac{0.61 \times 31.2}{0.07 \times 2957} \times 100 = 9.48\%$$

$$r_{Au,3}(\%) = \frac{0.36 \times 26.3}{0.07 \times 2957} \times 100 = 4.72\%$$

$$r_{Au,4}(\%) = \frac{0.49 \times 7.1}{0.07 \times 2957} \times 100 = 1.73\%$$

The cumulative recovery percentages can then be calculated:

$$R_k(\%) = \sum_{i=1}^{i=5} r_{k,i}$$

$$R_{Au}(\%) = 12.37 + 9.48 + 4.72 + 1.73 = 28.29\%$$

The cumulative recovery of the gangue metal, chrome can also be calculated with the equations shown above. The following equation can then be used to calculate the cumulative recoveries for the four metals (platinum, palladium, rhodium and gold):

$$R_{4E}(\%) = \frac{\sum_{k=1}^{k=4} x_{4E,i} \times m_{sample,i}}{x_{4E,total\ i} \times m_{experiment,i}} \times 100$$

That is all the calculations needed in order to analyse the results. The following two point equation can also be used to verify that the recoveries obtained are correct:

$$R_k(\%) = \frac{x_k \times (x_{k,total} - x_{k,tailings})}{x_{k,total} \times (x_k - x_{k,tailings})} \times 100$$

The recovery results can be seen in the following table:

Table 16: Experiment 1 recovery

	Recovery %					
Sample	**Cr2O3%**	**Au**	**Pd**	**Pt**	**Rh**	**4E**
1	0.03	12.37	42.25	33.93	40.67	36.85
2	0.13	9.48	23.61	26.01	31.82	25.53
3	0.12	4.72	9.33	10.67	13.50	10.42
4	0.04	1.73	1.94	2.24	1.88	2.10
T	99.68	71.71	22.87	27.15	12.13	25.10

Table 17: Experiment 1 cumulative recovery

	Cumulative Recovery %					
Sample	**Cr2O3%**	**Au**	**Pd**	**Pt**	**Rh**	**4E**
1	0.03	12.37	42.25	33.93	40.67	36.85
2	0.17	21.85	65.86	59.94	72.49	62.38
3	0.29	26.56	75.19	70.61	85.99	72.80
4	0.32	28.29	77.13	72.85	87.87	74.90
T	100.00	100.00	100.00	100.00	100.00	100.00

Table 18: Experiment 1 cumulative grade

	Cum Grade					
Sample	**Cr2O3%**	**Au (g/t)**	**Pd (g/t)**	**Pt (g/t)**	**Rh (g/t)**	**4E (g/t)**
1	2.235	1.94	133.00	194.00	37.70	366.64
2	3.25	1.00	60.32	99.69	19.55	180.55
3	3.51	0.76	43.10	73.51	14.51	131.88
4	3.60	0.73	40.16	68.88	13.47	123.24
T	28.92	0.07	1.36	2.47	0.40	4.31

8.3. Appendix C – Statistical Analysis

The statistical analysis was completed using Statistica as the computational package. The raw input and results can be seen below.

Table 19: Raw information entered into Statistica for statistical analysis of the design

	3 factor Box-Behnken design, 1 block , 15 runs (3 factor Box-Behnken design, 1 block , 15 runs in Box Behnken Design)							
Standard Run	Mixing RPM	Superficial Gas Velocity (cm/s)	Recirculation Rate (l/min)	Mass Pull	Water Rec	Chromite Recovery	4E Recovery	4E Grade
1	680	1	21	2.61	487.30	3.60	74.90	123.24
2	1277	1	21	3.98	1071.00	6.50	77.310	80.44
3	680	1	21	4.15	1220.80	5.42	75.381	78.34
4	1277	1	21	3.79	861.20	5.21	76.309	78.98
5	680	1	17	4.64	1259.70	4.65	80.824	76.44
6	1277	1	17	5.63	1624.10	6.71	80.785	62.29
7	680	1	25	2.03	318.30	2.57	72.593	153.62
8	1277	1	25	3.93	1088.90	6.40	80.602	86.45
9	975	1	17	4.88	1298.10	4.17	80.617	64.24
10	975	1	17	5.35	1561.30	6.26	79.543	58.33
11	975	1	25	2.68	624.40	4.26	77.534	99.28
12	975	1	25	4.77	1315.60	8.16	77.234	67.65
13	975	1	21	3.14	680.30	4.41	78.983	99.75
14	975	1	21	2.90	585.70	3.75	75.249	99.94
15	975	1	21	3.09	642.50	3.68	73.707	91.41

8.3.1. Model effect estimates with linear interactions

The following model effects estimates were determined while acknowledging that linear interactions may exist between the manipulated variables.

Table 20: Effect of the manipulated variables on Mass Pull

	Effect Estimates; Var.:Mass Pull; R-sqr=0.94135; Adj:0.83577 3 3-level factors, 1 Block, 15 Runs; MS Residual=.1908436 DV: Mass Pull									
Factor	Effect	Std.Err.	t(5)	p	-95.%	+95.%	Coeff.	Std.Err.	-95.%	+95.%
Mean/Interc.	4.038	0.126	32.022	0.000	3.714	4.362	4.038	0.126	3.714	4.362
(1)Mixing RPM(L)	0.975	0.309	3.157	0.025	0.181	1.769	0.488	0.154	0.091	0.885
Mixing RPM(Q)	-0.109	0.227	-0.479	0.652	-0.693	0.475	-0.054	0.114	-0.347	0.238
(2)Superficial Gas Velocity (cm/s)(L)	0.974	0.309	3.151	0.025	0.179	1.768	0.487	0.154	0.090	0.884
Superficial Gas Velocity (cm/s)(Q)	-0.479	0.227	-2.105	0.089	-1.063	0.106	-0.239	0.114	-0.531	0.053
(3)Recirculation Rate (l/min)(L)	-1.768	0.309	-5.723	0.002	-2.562	-0.974	-0.884	0.154	-1.281	-0.487
Recirculation Rate (l/min)(Q)	-0.898	0.227	-3.952	0.011	-1.483	-0.314	-0.449	0.114	-0.741	-0.157
1L by 2L	-0.869	0.437	-1.990	0.103	-1.992	0.253	-0.435	0.218	-0.996	0.127
1L by 3L	0.454	0.437	1.039	0.346	-0.669	1.577	0.227	0.218	-0.335	0.788
2L by 3L	0.813	0.437	1.861	0.122	-0.310	1.936	0.406	0.218	-0.155	0.968

Table 21: Effect of manipulated variables on water recovery

Factor	Effect Estimates; Var.:Water Rec; R-sqr=0.9263; Adj:0.79364 3 3-level factors, 1 Block, 15 Runs; MS Residual=33947.06 DV: Water Rec									
	Effect	Std.Err.	t(5)	p	-95.%	+95.%	Coeff.	Std.Err.	-95.%	+95.%
Mean/Interc.	1061.56	53.19	19.96	0.00	924.83	1198.28	1061.56	53.19	924.83	1198.28
(1)Mixing RPM(L)	339.78	130.28	2.61	0.05	4.87	674.68	169.89	65.14	2.44	337.34
Mixing RPM(Q)	-71.41	95.89	-0.74	0.49	-317.90	175.08	-35.71	47.94	-158.95	87.54
(2)Superficial Gas Velocity (cm/s)(L)	366.75	130.29	2.81	0.04	31.84	701.67	183.38	65.14	15.92	350.83
Superficial Gas Velocity (cm/s)(Q)	-200.50	95.89	-2.09	0.09	-446.99	45.98	-100.25	47.94	-223.49	22.99
(3)Recirculation Rate (l/min)(L)	-597.82	130.29	-4.59	0.01	-932.73	-262.91	-298.91	65.14	-466.37	-131.45
Recirculation Rate (l/min)(Q)	-363.18	95.89	-3.79	0.01	-609.66	-116.70	-181.59	47.94	-304.83	-58.35
1L by 2L	-472.88	184.24	-2.57	0.05	-946.49	0.73	-236.44	92.12	-473.24	0.36
1L by 3L	201.45	184.24	1.09	0.32	-272.15	675.06	100.73	92.12	-136.08	337.53
2L by 3L	214.00	184.25	1.16	0.30	-259.62	687.62	107.00	92.12	-129.81	343.81

Table 22: Effect of manipulated variables on 4E recovery

Factor	Effect Estimates; Var.:4E Recovery; R-sqr=0.81969; Adj:0.49514 3 3-level factors, 1 Block, 15 Runs; MS Residual=3.743013 DV: 4E Recovery									
	Effect	Std.Err.	t(5)	p	-95.%	+95.%	Coeff.	Std.Err.	-95.%	+95.%
Mean/Interc.	77.808	0.559	139.316	0.000	76.373	79.244	77.808	0.559	76.373	79.244
(1)Mixing RPM(L)	2.827	1.368	2.066	0.094	-0.690	6.343	1.413	0.684	-0.345	3.172
Mixing RPM(Q)	0.034	1.007	0.034	0.974	-2.554	2.622	0.017	0.503	-1.277	1.311
(2)Superficial Gas Velocity (cm/s)(L)	-0.478	1.368	-0.350	0.741	-3.995	3.039	-0.239	0.684	-1.997	1.519
Superficial Gas Velocity (cm/s)(Q)	-0.014	1.007	-0.014	0.990	-2.602	2.575	-0.007	0.503	-1.301	1.287
(3)Recirculation Rate (l/min)(L)	-3.428	1.368	-2.505	0.054	-6.944	0.089	-1.714	0.684	-3.472	0.045
Recirculation Rate (l/min)(Q)	-2.739	1.007	-2.720	0.042	-5.327	-0.151	-1.369	0.503	-2.664	-0.075
1L by 2L	-0.738	1.935	-0.381	0.719	-5.711	4.235	-0.369	0.967	-2.855	2.118
1L by 3L	4.015	1.935	2.075	0.093	-0.958	8.988	2.008	0.967	-0.479	4.494
2L by 3L	0.387	1.935	0.200	0.849	-4.586	5.360	0.193	0.967	-2.293	2.680

Table 23: Effect of manipulated variables on chromite recovery

Factor	Effect Estimates; Var.:Chromite Recovery; R-sqr=0.75766; Adj:0.32145 3 3-level factors, 1 Block, 15 Runs; MS Residual=1.542379 DV: Chromite Recovery									
	Effect	Std.Err.	t(5)	p	-95.%	+95.%	Coeff.	Std.Err.	-95.%	+95.%
Mean/Interc.	5.329	0.359	14.864	0.000	4.407	6.250	5.329	0.359	4.407	6.250
(1)Mixing RPM(L)	2.146	0.878	2.444	0.058	-0.111	4.404	1.073	0.439	-0.056	2.202
Mixing RPM(Q)	-0.289	0.646	-0.448	0.673	-1.951	1.372	-0.145	0.323	-0.975	0.686
(2)Superficial Gas Velocity (cm/s)(L)	1.625	0.878	1.850	0.124	-0.633	3.882	0.812	0.439	-0.316	1.941
Superficial Gas Velocity (cm/s)(Q)	-0.934	0.646	-1.446	0.208	-2.596	0.727	-0.467	0.323	-1.298	0.364
(3)Recirculation Rate (l/min)(L)	-0.093	0.878	-0.106	0.920	-2.351	2.164	-0.047	0.439	-1.175	1.082
Recirculation Rate (l/min)(Q)	-0.832	0.646	-1.288	0.254	-2.494	0.829	-0.416	0.323	-1.247	0.415
1L by 2L	-1.573	1.242	-1.266	0.261	-4.765	1.620	-0.786	0.621	-2.383	0.810
1L by 3L	0.870	1.242	0.700	0.515	-2.323	4.062	0.435	0.621	-1.161	2.031
2L by 3L	0.907	1.242	0.731	0.498	-2.285	4.100	0.454	0.621	-1.143	2.050

Table 24: Effect of manipulated variables on 4E grade

Factor	Effect Estimates; Var.:4E Grade; R-sqr=0.92495; Adj:0.78985 3 3-level factors, 1 Blocks, 15 Runs; MS Residual=132.9332 DV: 4E Grade									
	Effect	Std.Err.	t(5)	p	-95.%	+95.%	Coeff.	Std.Err.	-95.%	+95.%
Mean/Interc.	85.714	3.328	25.753	0.000	77.158	94.270	85.714	3.328	77.158	94.270
(1)Mixing RPM(L)	-30.869	8.153	-3.786	0.013	-51.826	-9.912	-15.435	4.076	-25.913	-4.956
Mixing RPM(Q)	-7.953	6.000	-1.325	0.242	-23.378	7.471	-3.977	3.000	-11.689	3.736
(2)Superficial Gas Velocity (cm/s)(L)	-20.848	8.153	-2.557	0.051	-41.806	0.110	-10.424	4.076	-20.903	0.055
Superficial Gas Velocity (cm/s)(Q)	14.554	6.000	2.426	0.060	-0.870	29.978	7.277	3.000	-0.435	14.989
(3)Recirculation Rate (l/min)(L)	36.275	8.153	4.449	0.007	15.317	57.233	18.137	4.076	7.658	28.616
Recirculation Rate (l/min)(Q)	10.106	6.000	1.684	0.153	-5.318	25.531	5.053	3.000	-2.659	12.765
1L by 2L	21.695	11.529	1.882	0.119	-7.942	51.332	10.847	5.765	-3.971	25.666
1L by 3L	-26.338	11.529	-2.284	0.071	-55.975	3.299	-13.169	5.765	-27.988	1.649
2L by 3L	-12.858	11.530	-1.115	0.315	-42.496	16.780	-6.429	5.765	-21.248	8.390

8.3.2. ANOVA analysis with linear interactions

ANOVA analysis of the data was done while acknowledging that linear interactions may exist.

Table 25: ANOVA analysis on mass pull with linear interactions

Factor	ANOVA; Var.:Mass Pull; R-sqr=0.94135; Adj:0.83577 3 3-level factors, 1 Block, 15 Runs; MS Residual=.1908436 DV: Mass Pull				
	SS	df	MS	F	p
(1)Mixing RPM L+Q	1.95068	2	0.975340	5.11067	0.061843
(2)Superficial Gas Velocity (cm/s) L+Q	2.74098	2	1.370490	7.18122	0.033886
(3)Recirculation Rate (l/min) L+Q	9.23174	2	4.615872	24.18667	0.002686
1*2	0.75606	1	0.756059	3.96167	0.103198
1*3	0.20602	1	0.206019	1.07952	0.346416
2*3	0.66067	1	0.660670	3.46184	0.121876
Error	0.95422	5	0.190844		
Total SS	16.26918	14			

Table 26: ANOVA analysis on water recovery with linear interactions

Factor	ANOVA; Var.:Water Rec; R-sqr=0.9263; Adj:0.79364 3 3-level factors, 1 Block, 15 Runs; MS Residual=33947.06 DV: Water Rec				
	SS	df	MS	F	p
(1)Mixing RPM L+Q	250789	2	125394.4	3.69382	0.103503
(2)Superficial Gas Velocity (cm/s) L+Q	417434	2	208717.2	6.14831	0.044928
(3)Recirculation Rate (l/min) L+Q	1201738	2	600869.0	17.70018	0.005388
1*2	223631	1	223630.9	6.58764	0.050240
1*3	40586	1	40586.0	1.19557	0.324067
2*3	45796	1	45796.0	1.34904	0.297874
Error	169735	5	33947.1		
Total SS	2303064	14			

Table 27: ANOVA analysis on 4E recovery with linear interactions

Factor	ANOVA; Var.:4E Recovery; R-sqr=0.81969; Adj:0.49514 3 3-level factors, 1 Block, 15 Runs; MS Residual=3.743013 DV: 4E Recovery				
	SS	df	MS	F	p
(1)Mixing RPM L+Q	15.9810	2	7.99049	2.134774	0.213687
(2)Superficial Gas Velocity (cm/s) L+Q	0.4579	2	0.22895	0.061167	0.941359
(3)Recirculation Rate (l/min) L+Q	51.1929	2	25.59647	6.838466	0.037082
1*2	0.5442	1	0.54419	0.145388	0.718647
1*3	16.1231	1	16.12308	4.307513	0.092595
2*3	0.1496	1	0.14960	0.039968	0.849420
Error	18.7151	5	3.74301		
Total SS	103.7947	14			

Table 28: ANOVA analysis on chromite recovery with linear interactions

Factor	ANOVA; Var.:Chromite Recovery; R-sqr=0.75766; Adj:0.32145 3 3-level factors, 1 Block, 15 Runs; MS Residual=1.542379 DV: Chromite Recovery				
	SS	df	MS	F	p
(1)Mixing RPM L+Q	9.55045	2	4.775223	3.096011	0.133399
(2)Superficial Gas Velocity (cm/s) L+Q	8.50216	2	4.251079	2.756183	0.156018
(3)Recirculation Rate (l/min) L+Q	2.57442	2	1.287211	0.834562	0.486691
1*2	2.47348	1	2.473476	1.603676	0.261173
1*3	0.75612	1	0.756117	0.490228	0.515056
2*3	0.82316	1	0.823159	0.533695	0.497837
Error	7.71189	5	1.542379		
Total SS	31.82284	14			

Table 29: ANOVA analysis on 4E grade with linear interactions

Factor	ANOVA; Var.:4E Grade; R-sqr=.92495; Adj:0.78985 3 3-level factors, 1 Block, 15 Runs; MS Residual=132.9332 DV: 4E Grade				
	SS	df	MS	F	p
(1)Mixing RPM L+Q	2128.860	2	1064.430	8.00726	0.027614
(2)Superficial Gas Velocity (cm/s) L+Q	1651.283	2	825.641	6.21095	0.044125
(3)Recirculation Rate (l/min) L+Q	3008.684	2	1504.342	11.31653	0.013927
1*2	470.695	1	470.695	3.54084	0.118616
1*3	693.755	1	693.755	5.21882	0.071139
2*3	165.325	1	165.325	1.24367	0.315476
Error	664.666	5	132.933		
Total SS	8855.732	14			

8.3.3. ANOVA analysis with quadratic interactions

ANOVA analysis on the data was done while acknowledging that higher order (quadratic) interactions may exist.

Table 30: ANOVA analysis on mass pull with quadratic interactions

Factor	ANOVA; Var.:Mass Pull; R-sqr=0.998; Adj:0.98602 3 3-level factors, 1 Block, 15 Runs; MS Residual=.0162452 DV: Mass Pull				
	SS	df	MS	F	p
(1)Mixing RPM L+Q	1.25297	2	0.626483	38.5642	0.025275
(2)Superficial Gas Velocity (cm/s) L+Q	2.20931	2	1.104653	67.9987	0.014493
(3)Recirculation Rate (l/min) L+Q	9.43840	2	4.719202	290.4978	0.003431
1*2	1.37880	3	0.459601	28.2914	0.034333
1*3	0.50500	2	0.252502	15.5431	0.060448
2*3	0.66067	1	0.660670	40.6686	0.023718
Error	0.03249	2	0.016245		
Total SS	16.26918	14			

Table 31: ANOVA analysis on water recovery with quadratic interactions

Factor	ANOVA; Var.:Water Rec; R-sqr=0.99803; Adj:0.98622 3 3-level factors, 1 Block, 15 Runs; MS Residual=2267.373 DV: Water Rec				
	SS	df	MS	F	p
(1)Mixing RPM L+Q	144897	2	72448.5	31.9526	0.030347
(2)Superficial Gas Velocity (cm/s) L+Q	344605	2	172302.6	75.9921	0.012988
(3)Recirculation Rate (l/min) L+Q	1231395	2	615697.5	271.5466	0.003669
1*2	349359	3	116453.0	51.3603	0.019159
1*3	80059	2	40029.3	17.6545	0.053606
2*3	45796	1	45796.0	20.1978	0.046113
Error	4535	2	2267.4		
Total SS	2303064	14			

Table 32: ANOVA analysis on 4E recovery with quadratic interactions

Factor	ANOVA; Var.:4E Recovery; R-sqr=0.85817; Adj:0.00717 3 3-level factors, 1 Block, 15 Runs; MS Residual=7.360749 DV: 4E Recovery				
	SS	df	MS	F	p
(1)Mixing RPM L+Q	10.7221	2	5.36106	0.728331	0.578593
(2)Superficial Gas Velocity (cm/s) L+Q	0.2964	2	0.14819	0.020132	0.980265
(3)Recirculation Rate (l/min) L+Q	52.0311	2	26.01555	3.534361	0.220538
1*2	3.3234	3	1.10779	0.150500	0.920961
1*3	17.3375	2	8.66873	1.177696	0.459201
2*3	0.1496	1	0.14960	0.020324	0.899701
Error	14.7215	2	7.36075		
Total SS	103.7947	14			

Table 33: ANOVA analysis on chromite recovery with quadratic interactions

Factor	ANOVA; Var.:Chromite Recovery; R-sqr=0.98995; Adj:0.92968 3 3-level factors, 1 Block, 15 Runs; MS Residual=.1598513 DV: Chromite Recovery				
	SS	df	MS	F	p
(1)Mixing RPM L+Q	6.68841	2	3.344203	20.92071	0.045619
(2)Superficial Gas Velocity (cm/s) L+Q	5.66596	2	2.832980	17.72259	0.053411
(3)Recirculation Rate (l/min) L+Q	2.90972	2	1.454860	9.10133	0.098997
1*2	7.43550	3	2.478499	15.50502	0.061195
1*3	3.18629	2	1.593144	9.96641	0.091188
2*3	0.82316	1	0.823159	5.14953	0.151318
Error	0.31970	2	0.159851		
Total SS	31.82284	14			

Table 34: ANOVA analysis on 4E grade with quadratic interactions

Factor	ANOVA; Var.:4E Grade; R-sqr=0.99465; Adj:0.96252 3 3-level factors, 1 Block, 15 Runs; MS Residual=23.70788 DV: 4E Grade				
	SS	df	MS	F	p
(1)Mixing RPM L+Q	1596.868	2	798.434	33.67799	0.028837
(2)Superficial Gas Velocity (cm/s) L+Q	1617.671	2	808.836	34.11674	0.028476
(3)Recirculation Rate (l/min) L+Q	3409.487	2	1704.743	71.90618	0.013716
1*2	673.233	3	224.411	9.46566	0.097052
1*3	1108.468	2	554.234	23.37761	0.041021
2*3	165.325	1	165.325	6.97342	0.118456
Error	47.416	2	23.708		
Total SS	8855.732	14			

8.4. Appendix D – Experimental Procedures

The experimental procedures can be divided into the preparation for the experiment, the actual experiment and sample preparation.

8.4.1. Experimental Preparation

The experimental preparation involves milling the sample to the correct particle size, preparing the equipment for the experiment, preparing the reagents added during the experiment as well as the sample containers that will be used through the experiment.

The laboratory mills available had only one opening on the one end and this made it difficult to effectively remove all the milled minerals without adding too much water. Another mill was built with similar dimensions as the laboratory mills so the same milling rods could be used in the milling process. The mill was designed so one end could be completely removed for cleaning while the other end consist of a cone to channel the mill content into a funnel and hose for loading directly into the cell. This design ensured that all the rods and the entire mill body could be washed without diluting the mill contents below 30% solids per weight.

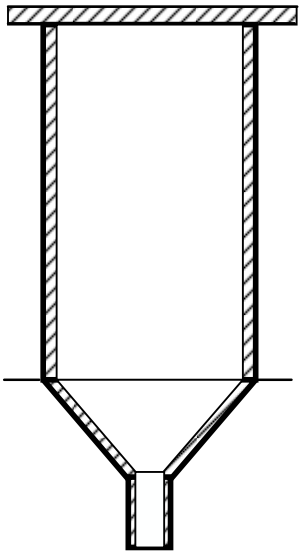

Figure 51: Shape of the Rod Mill body specifically built for the test work

The outer shell of the mill was made from stainless steel plate and the inside was protected by a layer of urethane. The urethane was chosen with a shore hardness of 70A to prevent mineral particles to be impounded into the rubber. It also has high abrasion resistance which will ensure longevity of the mill liner. The liner was cast inside the mill by spinning the mill vertically at a constant speed to cover the cone section with Urethane while it sets. This resulted in a parabolic finish which was not perfect, but still fitted the purpose for which it was intended. The whole mill was then spun horizontally in order to cast the outer shell of the mill to ensure its capacity to handle the impact of the rods. A liner of around five millimetres was created which was sufficient for this mill.

Milling Preparation

Milling the sample involves the following procedure for an experiment with 30% solids loading:

1. Ensure the mill outer and milling rods are dry and clean to start the milling procedure.
2. Weigh off 2961 grams of sample for the run.
3. Measure off 1400 ml water in a measuring flask for the mill.
4. Ensure the bottom of the mill is sealed and add the water into the mill with the top open.
5. Slowly add the ore sample into the mill to avoid creating dust which will be lost to the surroundings.
6. Place the milling rods into the mill according to Figure 52 to ensure good repeatability.

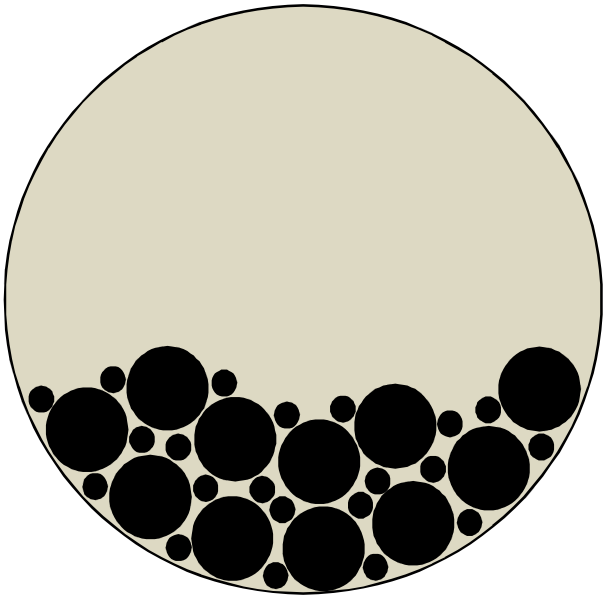

Figure 52: Mill packing

7. Attach the top lid and ensure that a good seal is achieved.
8. Place the mill on the roller and record the time when the roller is started.
9. When three hours and 45 minutes have passed, switch off the roller and transfer mill to the experimental setup.

Equipment Preparation

Equipment preparation should be done prior to every run. Reagents can be mixed once a day, but should not be used for longer than a day. The following method was used to prepare the reagent dilutions.

1. Discard all the remaining reagents of the previous day into a waste container.
2. Rinse reagent vials thoroughly with tap water and dry the containers completely.
3. Place the copper sulphate vial on the scale and tare the scale to ensure correct measurement will occur.
4. Use a small stainless steel spatula to transfer the copper sulphate into the designated vial.
5. Continue until the correct amount has been transferred.
6. Repeat steps three to five for the Norilose and SNPX.
7. Use a pipette to accurately measure the correct amount of frother into the designated vial.
8. Fill all the vials with 20 millilitres of reversed osmosis water to make up the solutions.
9. Allow sufficient time for solids to dissolve and shake the vials to ensure that the reagents are thoroughly dissolved.

Table 35: Reactant mass for 20ml solutions

CuSO4 (grams)	Norilose (grams)	SNPX (grams)	Frother (ml)
0.4739	0.7108	1.7770	0.4066

The experimental setup should be further prepared as follows:

1. Open the water feed to the flotation cell and fill the cell with water.
2. Ensure that the electrical supply to the setup is switched on.
3. Adjust the frequency of the impeller drive to the required setting for the run.
4. Open the air supply valve to the setup.
5. Open the air feed to the diaphragm pump to circulate water through the system.
6. Adjust the air flow and pressure to obtain the correct recirculation rate.
7. Start the mixing motor and look for any abnormalities in its functioning.
8. Push the sintered metal into the water stream flowing through the aerator body.
9. Open up the air flow to the aerator and adjust the flow rate to the required flow setting.
10. Ensure that the air flow gauge of the aerator is functioning at the calibrated pressure, if not, adjust the chocking valve accordingly.
11. Check that the operating conditions are all maintained at the correct settings for the experiment.
12. Close the air supply to the aerator as well as the slurry pump.
13. Switch off the impeller motor.
14. Drain the system to ensure that any surfactants and particles are removed.
15. Pull the sinter back, out of the aeration chamber in order to protect it during the loading process.

Flush the aerator sinter with water after every second run to see if blockage becomes excessive. If the sinter seems blocked, clean the sinter as follows:

1. Remove the sinter from its housing.
2. Submerge the sinter into acetone in a 100 ml beaker in order to dissolve the organic compounds.
3. Place the beaker into a sonic bath and add enough water to the bath so it reaches just below the level of the acetone in the beaker.
4. Switch the sonic bath on and allow running for twenty minutes before switching it off again.
5. Drain the beaker's content into a waste container.
6. Rinse the sinter and the beaker with tap water.

7. Submerge the sinter in two percent nitric acid in the 100 ml beaker and place back into the sonic bath.
8. Switch the sonic bath on and allow running for another 20 minutes before switching it off again.
9. Drain the beakers contents into an acid waste container.
10. Rinse the sinter and beaker thoroughly with water.
11. Submerge the sinter in tap water in the 100 ml beaker and place back into the sonic bath.
12. Switch the sonic bath on and allow running for five minutes before switching it off again.

The sample trays should be prepared as follows:

1. Ensure that at least six non – stick baking trays are free of mineral content to be used in the experiment as sample trays.
2. Wash each tray thoroughly with tap water and a soft cloth to ensure that the non–stick surface of the trays won't scratch.
3. Place all the trays in the oven to ensure that they are completely dry.
4. Record the dry mass of each tray in the experiment logbook.
5. Fill the collection trough spray bottle with water and record the full mass in the logbook.

The following check list can be completed to ensure that everything is in order to do the experimental run:

1. Check that reverse osmosis water, electricity and compressed air are available for the duration of the experimental run.
2. Ensure that the experimental setup is correctly set up in terms of mixing intensity, recirculation rate and aeration rate.
3. Ensure that the reagents are completely dissolved and that there are four 5 ml syringes available for the reagent injection into the flotation cell.
4. Ensure that the sample trays are clean and dry and that each one's empty mass is recorded into the logbook.
5. Ensure that the collection trough spray bottle is filled with water and that the total weight is recorded in the logbook.
6. Ensure that an extra tray is available to place the milling rods in.
7. Switch the drying oven on to warm it up.
8. Make sure that a stop watch is available to take the time.
9. If all the above points are checked, the experiment can be done when the mill is finished with the milling process.

Everything should now be in order to complete the experimental run.

8.4.2. Experimental Run

The actual experiment can be divided into loading of the flotation cell with the slurry, reagent addition, collection of concentrate and drainage of the cell. The following steps can be followed when the milling is done in order to load the flotation cell:

1. Open the reverse osmosis water feed to the flotation cell and add sufficient water to circulate through the system.
2. Open the air feed to the circulation pump to circulate the water through the system.
3. Check that the loading hose is placed completely into the flotation cell.
4. Turn the mill upside down (onto the big lid) and remove the plug out of the protruding tube at the end of the conical section.
5. Lift the mill slowly and empty the contents into the loading funnel by resting the protruding tube of the mill on the funnel edge.
6. When all the slurry is drained, tip the mill over into a vertical position so it rests on the funnel.
7. Loosen the wing nuts and open the top cover of the mill.
8. Use the spray nozzle from the reverse osmosis water feed and gently rinse all the slurry from the top cover into the mill.
9. Rinse all visible slurry through the mill.
10. Remove all the small diameter rods one by one and wash them clean with the spray nozzle while making sure all the slurry runs through the mill and don't get splashed away.
11. Place the rods into the extra tray reserved for the milling rods.
12. Remove all the large diameter rods and wash them with the spray nozzle and place them into the milling rods tray as well.
13. Wash the inside of the mill body when all the rods are removed.
14. Close the water supply to the spray nozzle.
15. Place the milling rods tray into the oven to dry the rods.
16. Remove the mill body from the flotation cell loading funnel.
17. Open the water supply to the spray nozzle.
18. Rinse all minerals out of the flotation cell loading funnel and tube.
19. Close the supply to the spray nozzle.
20. Remove the loading funnel tube from the flotation cell and move it out of the way.

The slurry is now loaded into the flotation cell and the following steps can be used to add the reagents and increase the slurry volume to the required volume.

1. Open the reverse osmosis water to the slurry level (froth depth) control vessel.

2. Ensure that the pipe flowing towards the cell is not blocked and that the flotation volume is increasing.
3. Continuously monitor the slurry level within the flotation cell and close the feed water the moment the slurry level reaches 7.8 litres.
4. Use the syringes to suck up 5ml from each reagent solution, each into a separate syringe.
5. Suck up extra air into the syringe after each syringe was correctly filled with 5 ml of a specific reagent.
6. Increase the circulation rate to 20 l/min by increasing the air pressure supplied to the circulation diaphragm pump.
7. Switch the mixing drive on.
8. Remove the stopper from the reagent dosage point and attach the copper sulphate solution syringe to the dosage point.
9. Inject the solution into the recirculation pipe and start the timer.
10. Remove the copper sulphate syringe after two minutes and 45 seconds and attach the Norilose syringe to the reagent dosage point.
11. Inject the Norilose solution into the recirculation pipe.
12. Immediately remove the Norilose syringe and attach the SNPX syringe to the reagent dosage point.
13. Inject the SNPX solution into the slurry circulation pipe (by now it should be three minutes).
14. Fill another syringe with water.
15. Remove the SNPX syringe and attach the frother syringe to the reagent dosage point after three minutes and 45 seconds.
16. Inject the frother into the slurry circulation pipe after four minutes have passed.
17. Remove the frother syringe and attach the syringe filled with clean water.
18. Inject the clean water to wash out any frother solution that might be present within the reagent dosage point.
19. Place the collection trays under the concentrate trough in the same order as the numbers are recorded in the logbook.

Reagent addition is now complete and the froth collection part of the experiment will be completed now.

1. Allow the reagent dosage time of five minutes to pass and clear the timer.
2. Open the air supply to the aerator as small as possible, only to produce a positive pressure within the sintered metal of the aerator.

3. Reduce the circulation rate to five litres per minute by reducing the air feed pressure to the diaphragm pump.
4. Introduce the sintered metal of the aerator into the slurry by pushing it into the aerator housing.
5. Slightly increase the air feed to the sintered metal to three litres per minute.
6. Increase the air supply pressure to the diaphragm pump to obtain the required circulation flow rate for the specific experimental run.
7. Increase the air flow rate to the aerator to the required flow rate for the specific experimental run.
8. Make fine adjustments to the air feed to the aerator to ensure the correct flow rate while maintaining a one bar pressure through the flow meter.
9. Open the water feed to the slurry level control vessel to fill the flotation cell to the correct experimental volume.
10. Start the timer the moment the froth starts to overflow to the first concentrate tray.
11. Continuously scrape any froth that rise above the cell wall into the collection launder.
12. Use the spray bottle to wash away any mineral still in the launder at 55 seconds after the froth collection time started.
13. Remove the first tray at one minute.
14. Continue to scrape off any excess froth into the collection launder.
15. Monitor the cell performance throughout to see any irregularities in terms of froth stability, froth height, recirculation rate as well as aeration rate.
16. Use the spray bottle to rinse away any minerals in the collection launder after two minutes 55 seconds.
17. Remove the second tray after three minutes.
18. Continue to scrape off any excess froth into the collection launder.
19. Use the spray bottle to wash away any minerals in the collection launder after seven minutes and 55 seconds.
20. Remove the third tray after eight minutes.
21. Continue to scrape of any excess froth into the collection launder.
22. If changes occur with regard to froth depth, aeration and recirculation rates make the necessary adjustments to rectify the deviances.
23. Reduce the aeration and recirculation rate after 15 minutes and close off the water feed to the level control vessel.
24. Switch off the mixing motor drive.

25. Close off the recirculation pump's air supply to stop slurry circulation.
26. Remove the drainage plug in the circulation system to drain all the slurry into a ten litre bucket.
27. When the system finished draining, remove the bucket and place another ten litre bucket under the drainage exit.
28. Clean the collection launder from any minerals by using the water spray bottle.
29. Remove the last tray from under the collection launder exit.
30. Open the water supply to the level controlling vessel.
31. Open the water supply to the spray nozzle and rinse out the cell's inside.
32. Ensure that the slurry runs out smoothly into the tailings bucket without any splashing.
33. When the water leaving the drainage point clears, block the drainage point.
34. Open the air supply to the circulation pump to circulate clean water through the system.
35. When circulation was established within the system, wait another minute before opening the drainage point again to drain the remaining minerals out of the system.
36. Close the water supply to the spray nozzle as well as the supply to the level controlling vessel.
37. Close the air supply to the pump and the aerator.
38. Close the main water and air supply valves to the setup.
39. Remove the milling rods from the oven in order to cool for the next experiment.

This is the complete methodology for the froth collection phase. The samples now need to be prepared for analysis.

8.4.3. Sample Preparation

The samples first need to be dried after froth the froth collection phase of the experiment completes. The samples can then be bagged and labelled for analysis. The following steps should be followed in order to prepare the samples for analysis:

1. Weigh each of the concentrate collection trays and record the wet mass of each in the experiment logbook.
2. Place all the concentrate collection trays into the oven to dry for 24 hours at 105 degrees Celsius.
3. Place a filter paper with aperture size of 5-10 microns in the bottom of the dewatering press.
4. Attach the body of the press before emptying the contents of the 10 litre rinse bucket into the dewatering press.
5. Add more slurry water from the 10 litre drainage bucket to fill the dewatering press completely.

6. Place the 10 litre rinse bucket below the exit of the dewatering press in order to collect the first run off of water.
7. Attach the lid of the dewatering press and open the air supply to the press slowly.
8. Collect the first run off water into the 10 litre rinse bucket until the water becomes visibly clear of any minerals.
9. Wait for all the water to be pressed out before closing the air supply to the dewatering press.
10. Open the pressure relieve valve of the dewatering press to release the pressure before opening the lid.
11. Rinse out any minerals left in the 10 litre drainage bucket as well as the 10 litre rinse bucket into the dewatering press.
12. Attach the lid and close the pressure relieve valve.
13. Open the air supply to the dewatering press slowly so that the pressure builds up gradually inside.
14. Wait for all the water to be pressed out before closing the air supply to the dewatering press.
15. Relieve the pressure to the dewatering press before opening the lid.
16. Remove the body of the dewatering press and empty the contents into another sample collection tray.
17. Place the tailings tray into the oven and wait for 48 hours in order to completely dry the contents.

After 24 hours the concentrate samples are dried and can be bagged and labelled by following the procedure laid out below:

1. Remove the concentrate collection trays from the oven.
2. Weigh each tray and record the dry sample tray mass in the experiment logbook according to the sample number.
3. Wait for the samples to completely cool.
4. Label ziplock bags with the experiment date as well as the sample identifier for each of the samples from the experimental run.
5. Start with the last sample and empty the contents of the collection tray into the designated ziplock bag by using a stiff haired brush.
6. After the sample is completely transferred into the sample bag, use compressed air to clean the brush as well as the gloves used.

7. Follow the same experimental procedure of point five and six as shown above for each of the remaining samples by working from the second last sample to the first sample to ensure that any possible contamination will only reduce the bagged sample's grade.
8. Place all the concentrate samples into a bigger ziplock bag in order to ensure that the samples are protected.

The concentrate samples are now ready to be packed with other samples to ship them for analysis. After another 24 hours the tailing sample can also be bagged by following the procedure below:

1. Remove the tailings sample from the oven.
2. Weigh and record the dry tailings tray mass in the experimental logbook.
3. Label a ziplock bag with the experiment date as well as the sample identifier for the tailings of the experiment.
4. Thoroughly break up the tailings filter cake by hand in order to minimize sample losses through a mill.
5. Spread the whole sample over a 1000x840 mm piece of brown paper.
6. Use a folding technique to thoroughly mix the sample by folding the paper over from one side to the other.
7. Repeat the folding technique until the sample seems thoroughly mixed through.
8. Use a stainless steel spatula and collect tailings portions from eight randomized positions throughout the tailings mass.
9. Ensure that enough mineral is taken in order to have a combined mass of 200–300 grams.
10. Place these portions into the tailings sample ziplock bag to send for analysis.
11. Transfer the rest of the tailings into another bag with the sample date and identifier for storage.

The whole experimental procedure concludes with sending the samples through for analysis.

8.5. Appendix E – Design Drawings

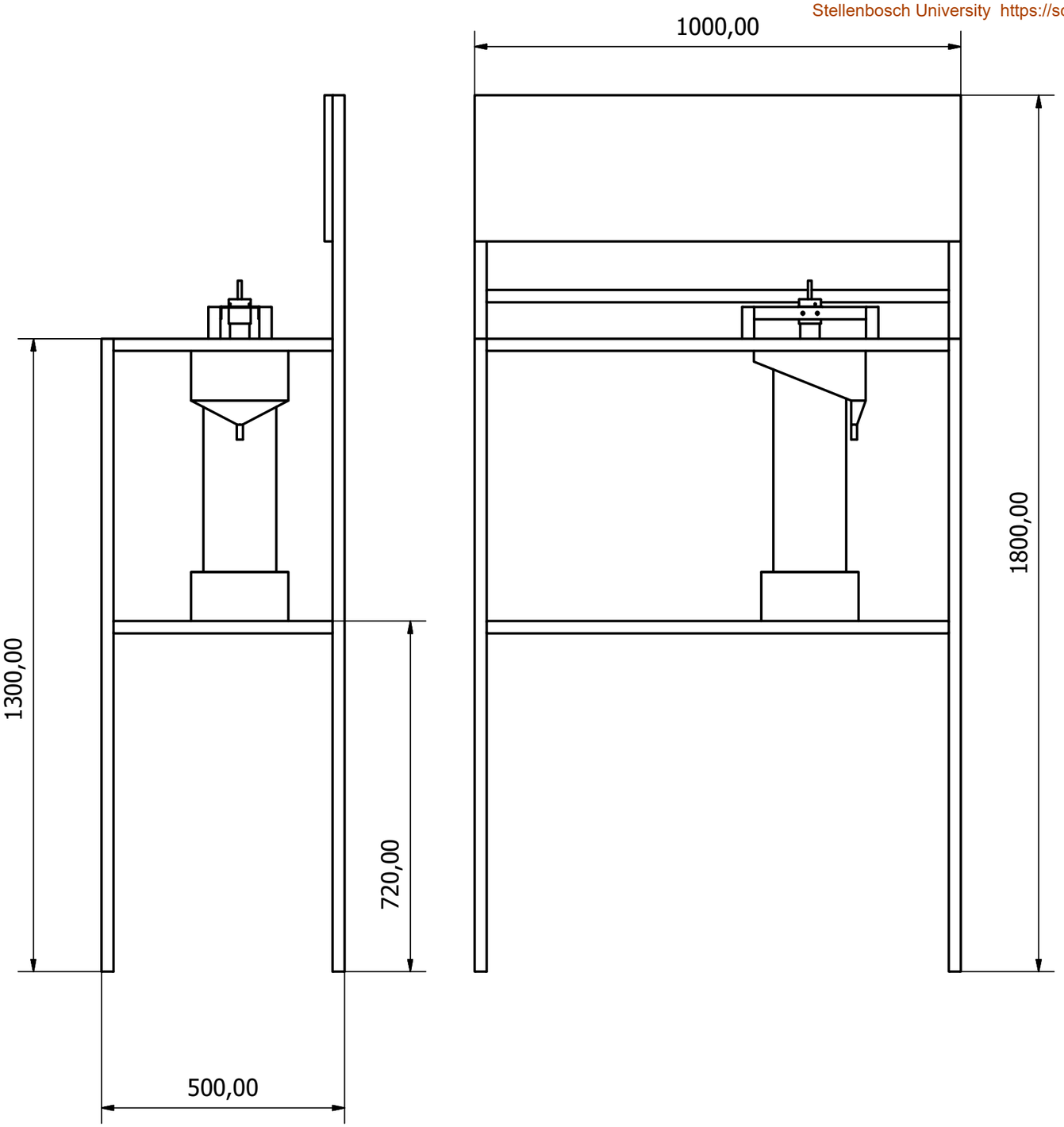

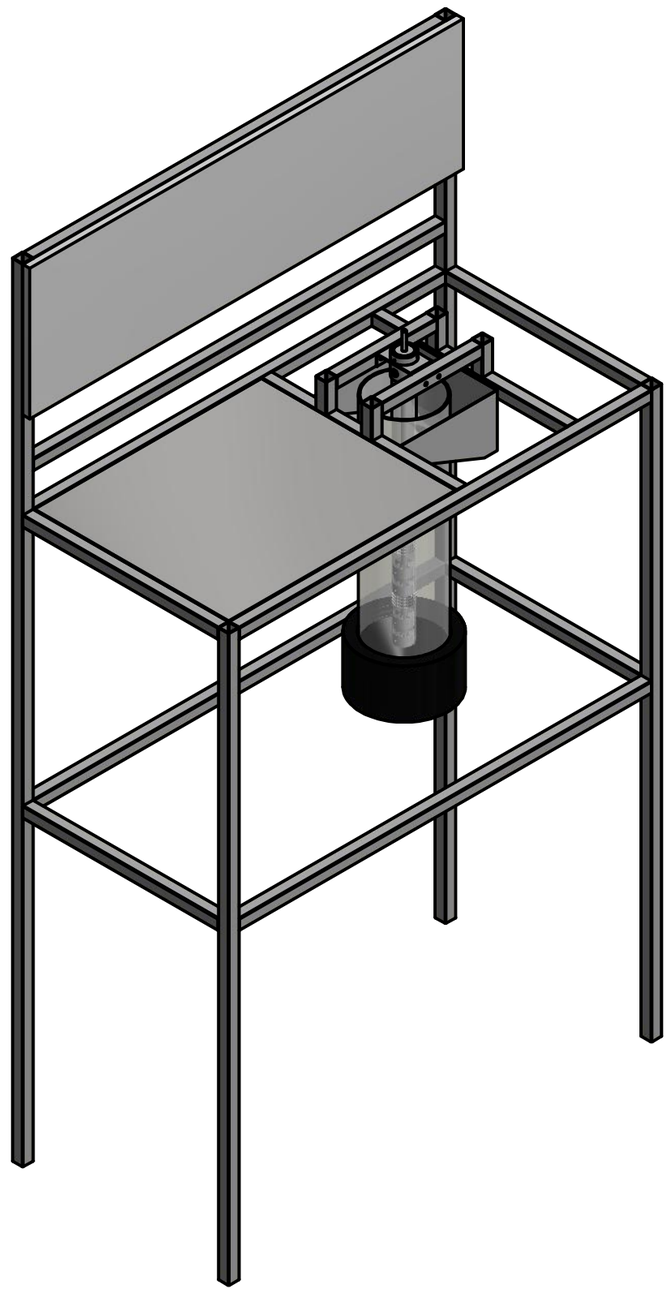

Designed by	Checked by	Approved by	Date		Date	
Nardus					7/28/2014	

complete Assembly PVC	Edition	Sheet 1 / 1	

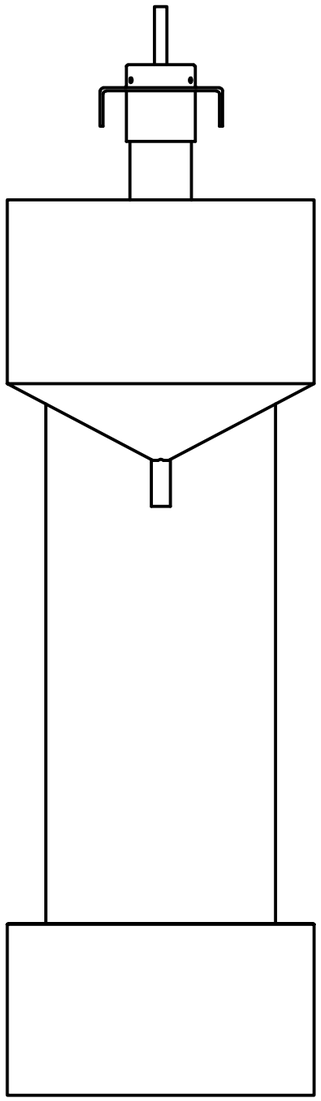

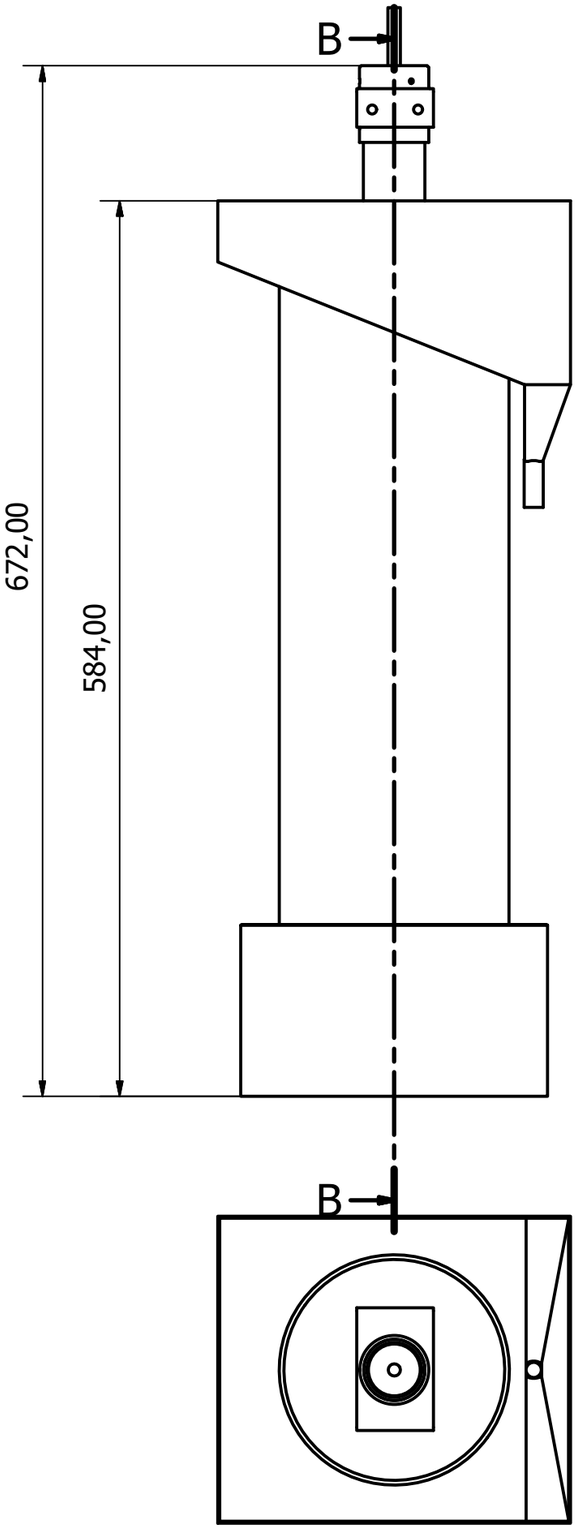

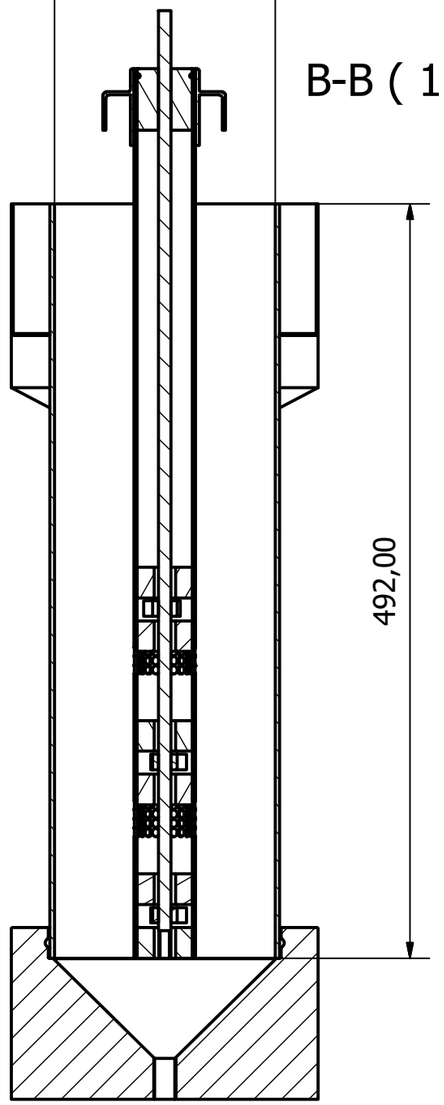

B-B (1:4)

Designed by	Checked by	Approved by	Date		Date	
Nardus					5/15/2014	

Flotation cell assembled	Edition	Sheet 1 / 1

B-B (1 : 1)

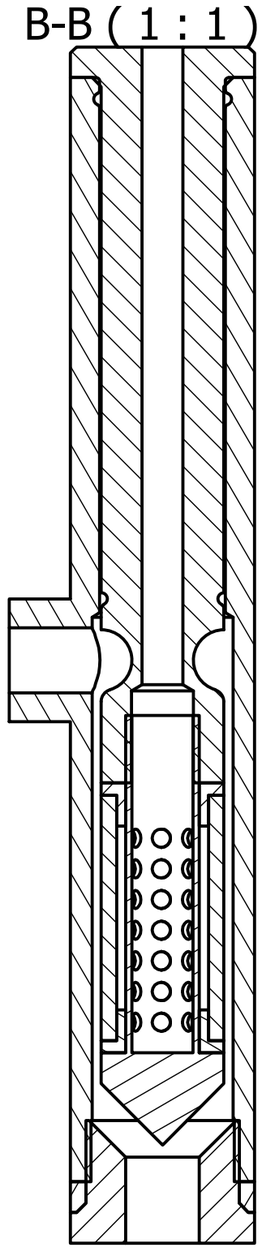

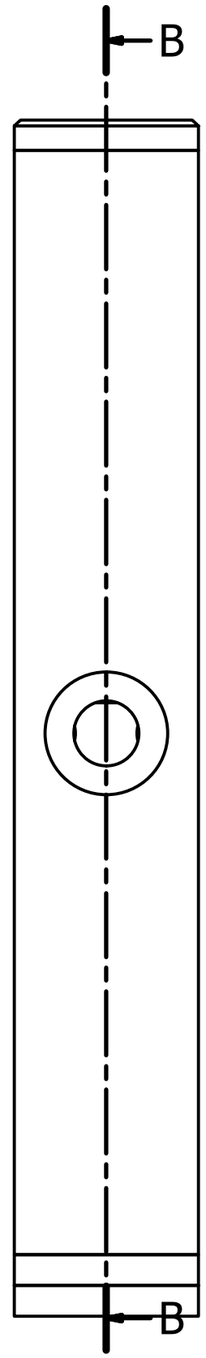

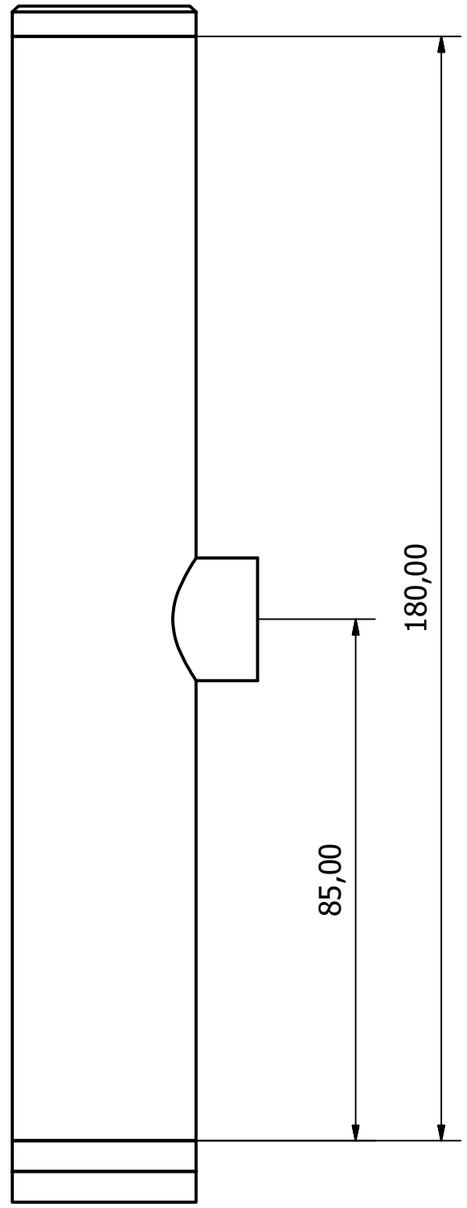

Designed by	Checked by	Approved by	Date		Date	
Nardus					7/3/2014	

Bubble pull out assembly	Edition	Sheet 1 / 1	

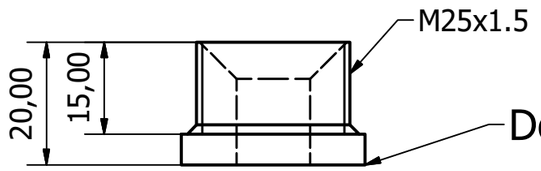

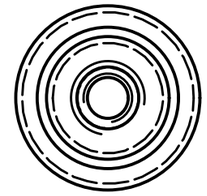

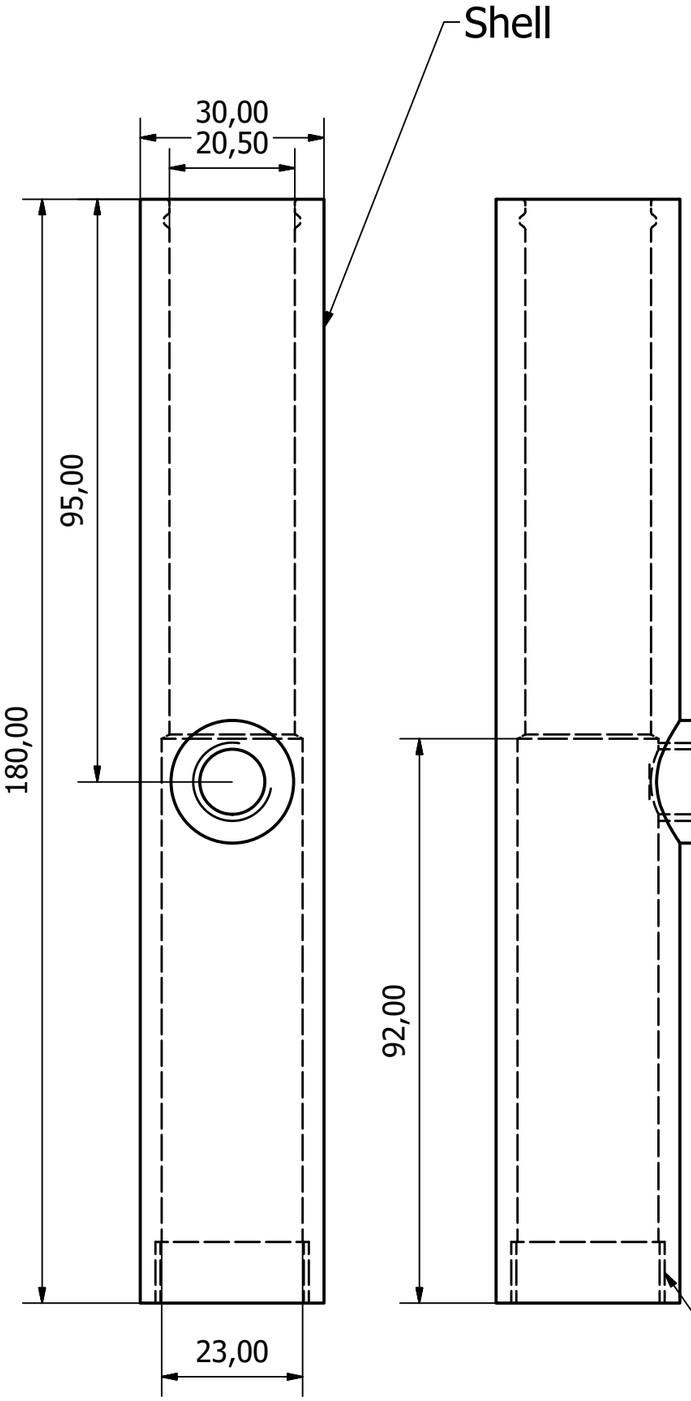

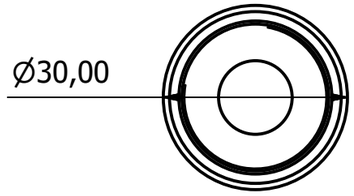

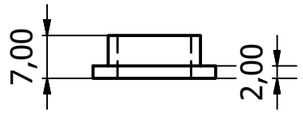

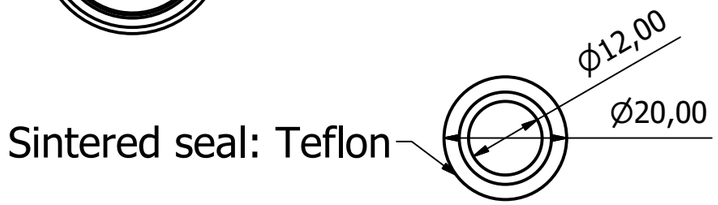

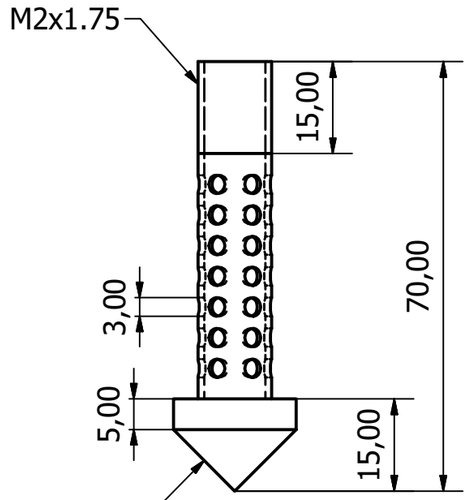

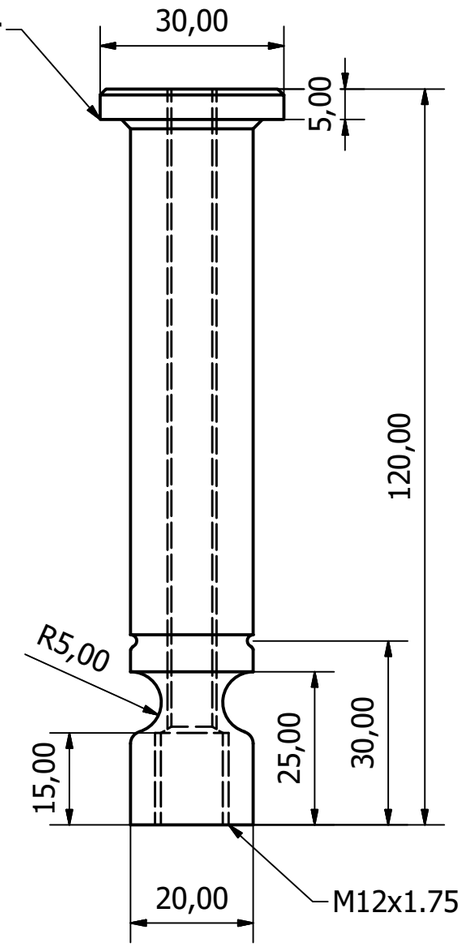

Designed by	Checked by	Approved by	Date		Date	
Nardus					7/16/2014	

bubble pull out parts 1		Edition	Sheet 1 / 1

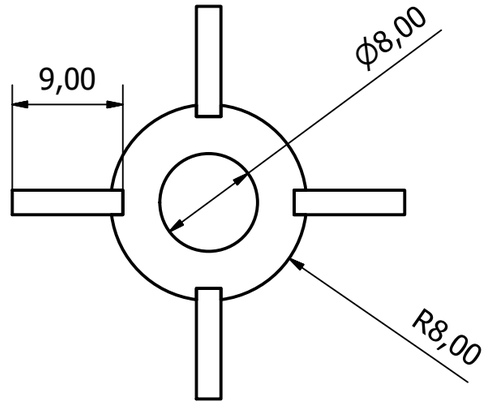

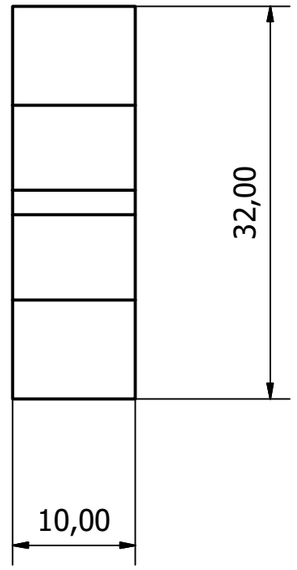

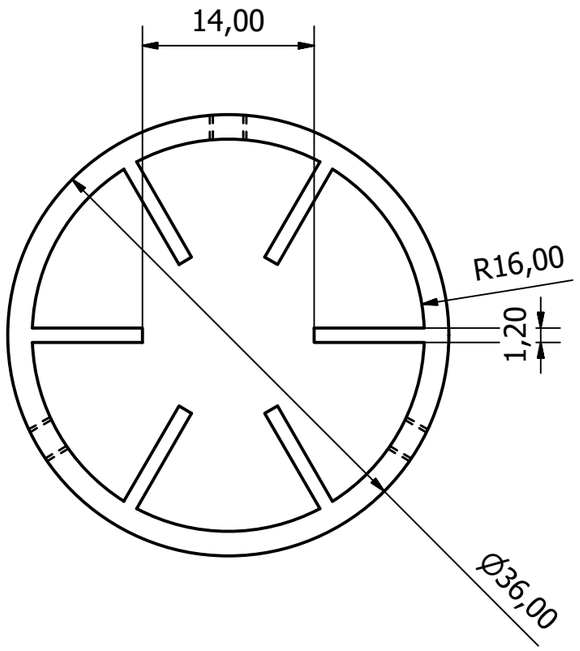

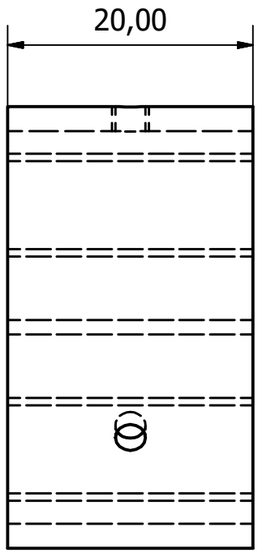

Designed by	Checked by	Approved by	Date		Date	
Nardus					7/22/2014	

Mixer parts 1	Edition	Sheet 1 / 1	

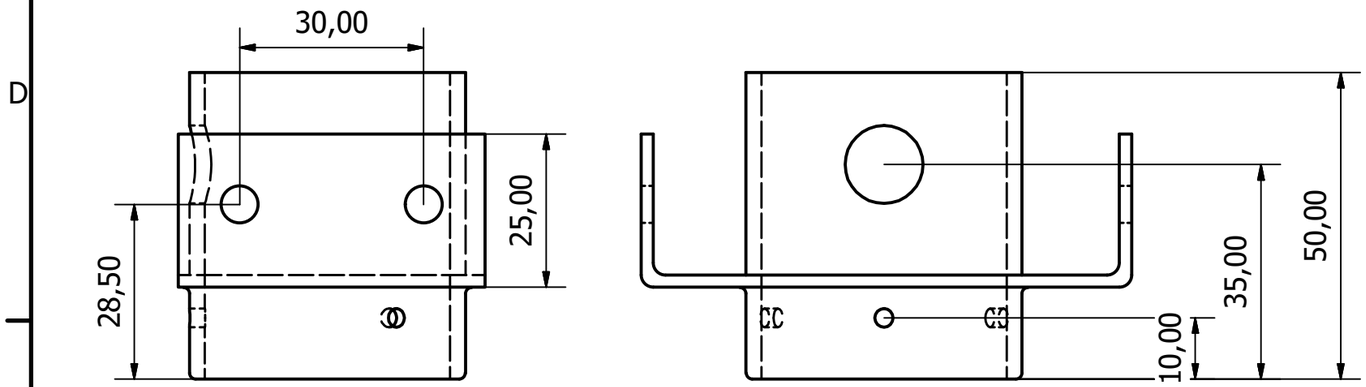

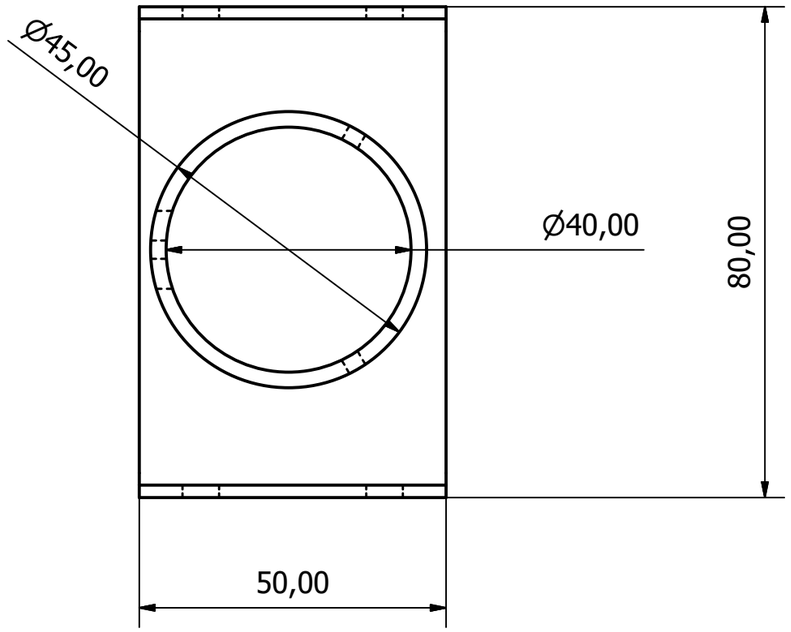

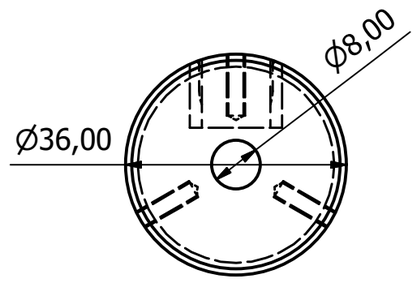

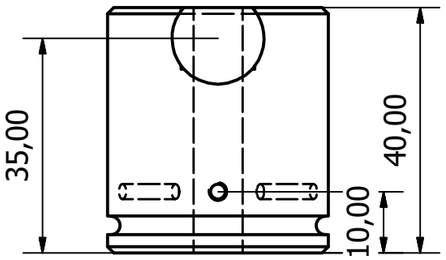

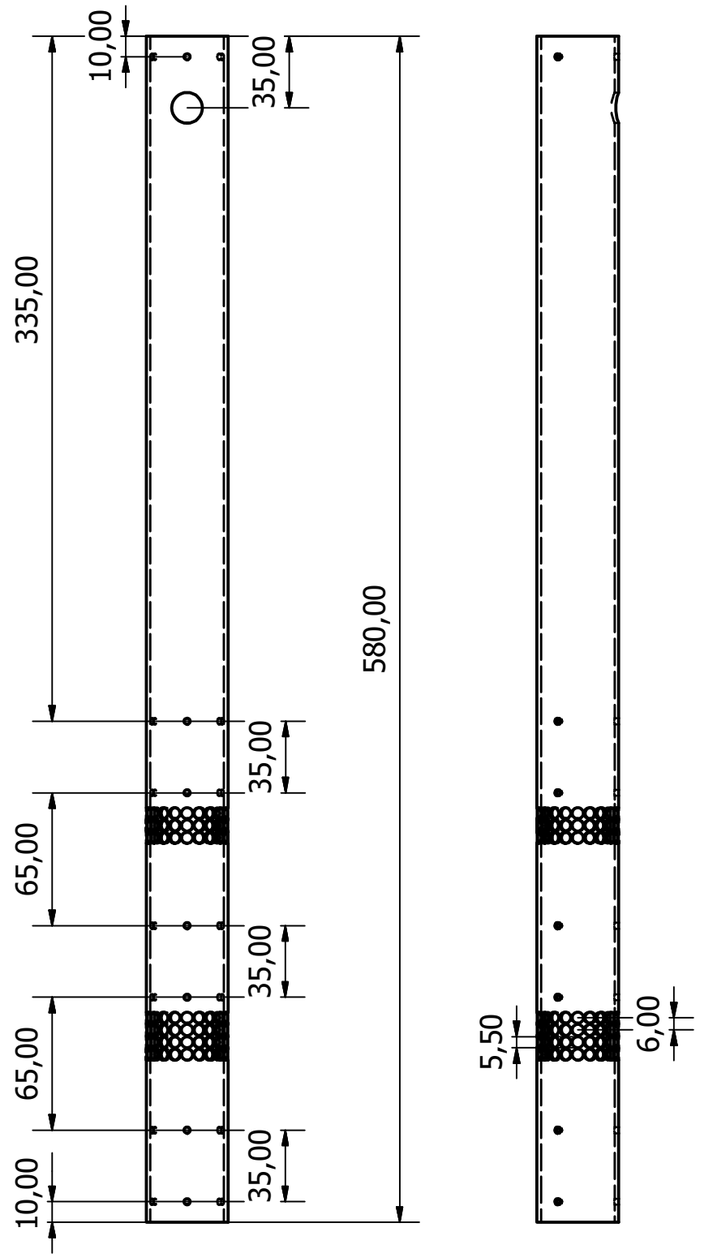

Designed by	Checked by	Approved by	Date		Date	
Nardus					7/28/2014	

mixer parts 2		Edition	Sheet 1 / 1

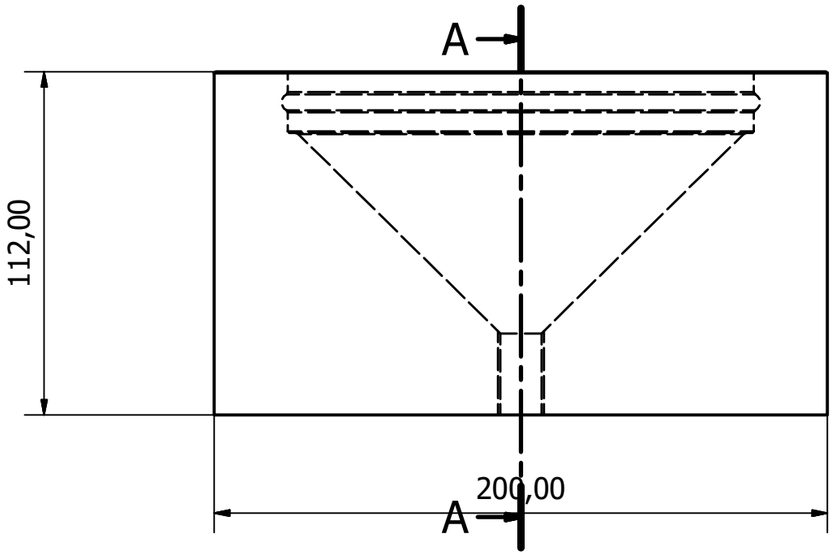

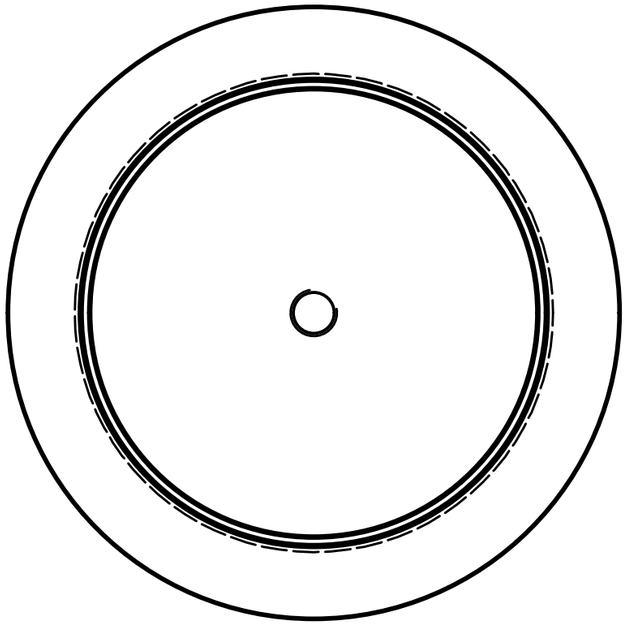

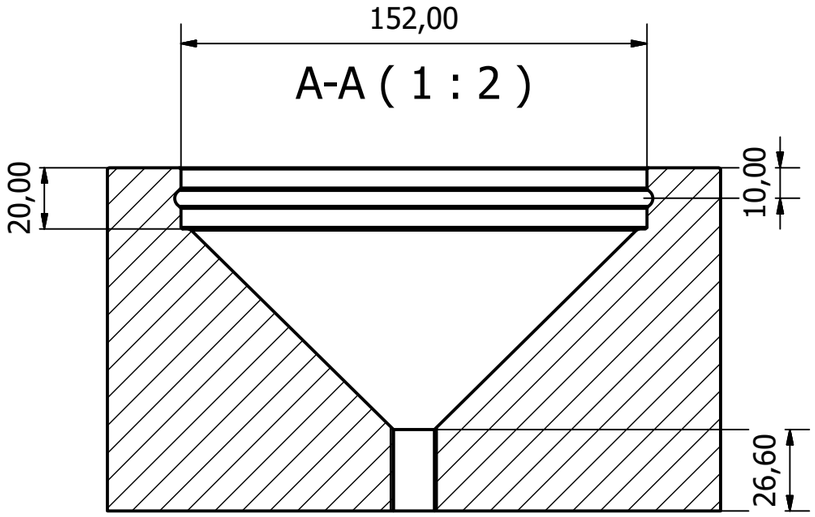

Designed by Nardus	Checked by	Approved by	Date	Date 7/28/2014	
		conical bottom		Edition	Sheet 1 / 1

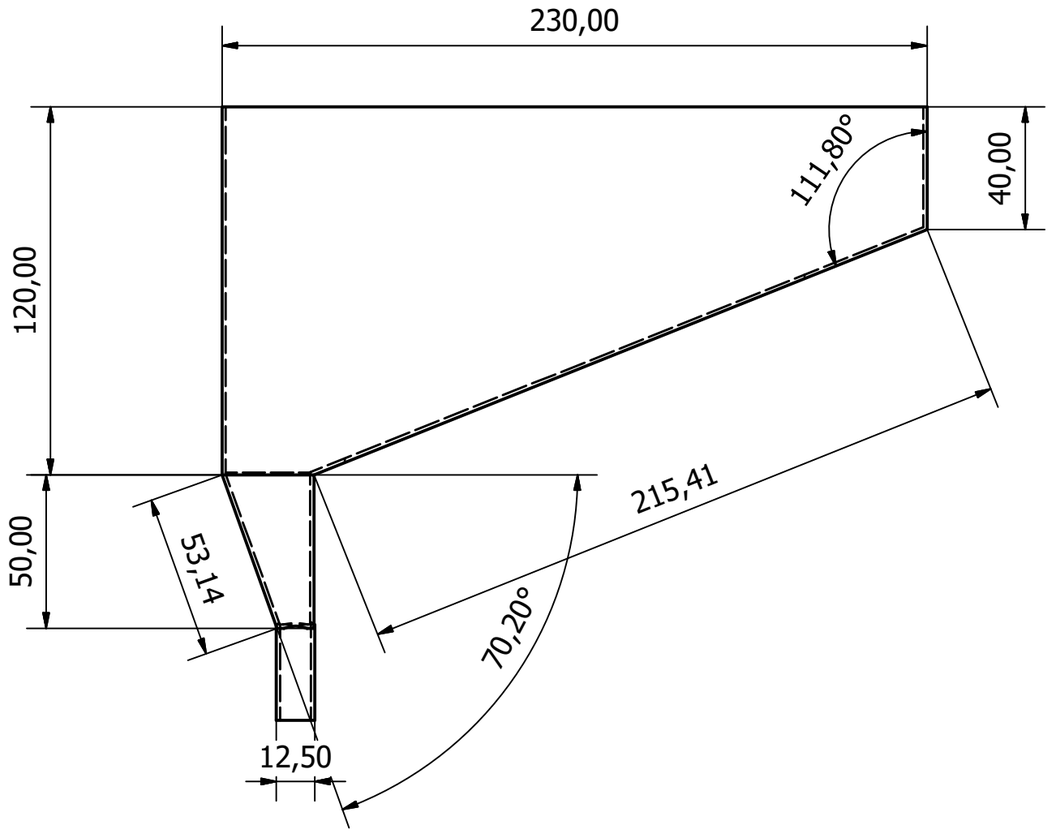

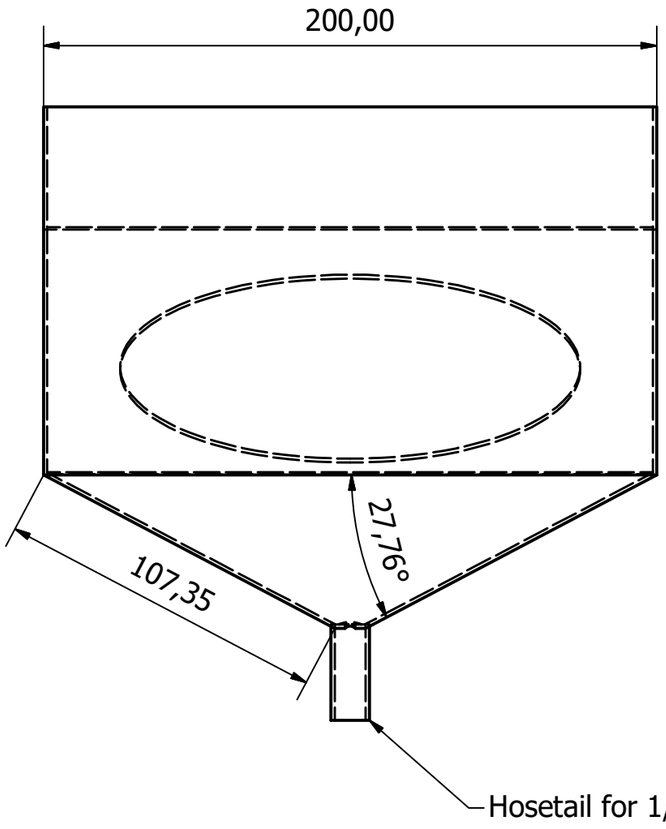

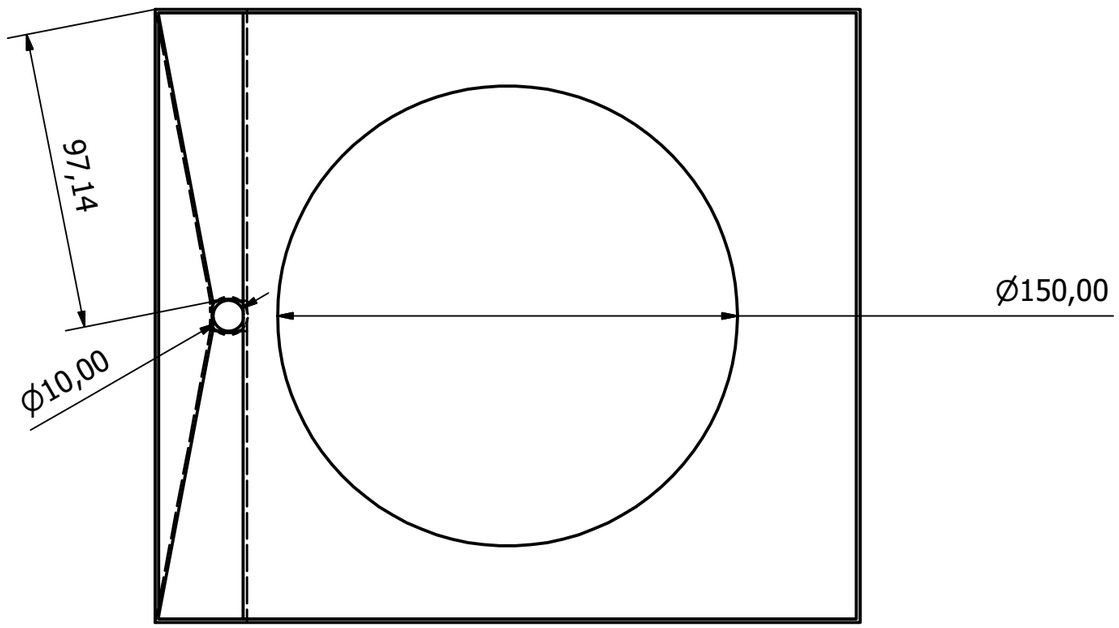

Designed by	Checked by	Approved by	Date		Date	
Nardus					7/22/2014	

PVC trough (made from Stainless) | Edition 1 | Sheet 1 / 1